UNIVERSITY OF ALBERTA

Numerical Modelling of Hailstone Growth in Alberta Storms

by

Julian Charles Brimelow ©

A thesis submitted to the Faculty of Graduate Studies and Research in partial fulfillment of the requirements for the degree of Master of Science

Department of Earth and Atmospheric Sciences

Edmonton, Alberta

Fall 1999

National Library of Canada
Acquisitions and Bibliographic Services
395 Wellington Street
Ottawa ON K1A 0N4
Canada

Bibliothèque nationale du Canada
Acquisitions et services bibliographiques
395, rue Wellington
Ottawa ON K1A 0N4
Canada

Your file Votre référence

Our file Notre référence

The author has granted a non-exclusive licence allowing the National Library of Canada to reproduce, loan, distribute or sell copies of this thesis in microform, paper or electronic formats.

L'auteur a accordé une licence non exclusive permettant à la Bibliothèque nationale du Canada de reproduire, prêter, distribuer ou vendre des copies de cette thèse sous la forme de microfiche/film, de reproduction sur papier ou sur format électronique.

The author retains ownership of the copyright in this thesis. Neither the thesis nor substantial extracts from it may be printed or otherwise reproduced without the author's permission.

L'auteur conserve la propriété du droit d'auteur qui protège cette thèse. Ni la thèse ni des extraits substantiels de celle-ci ne doivent être imprimés ou autrement reproduits sans son autorisation.

0-612-47010-5

Canada

UNIVERSITY OF ALBERTA

LIBRARY RELEASE FORM

Name of Author: Julian Charles Brimelow

Title of Thesis: Numerical Modelling of Hailstone Growth in Alberta Storms

Degree: Master of Science

Year this Degree Granted: 1999

Permission is hereby granted to the University of Alberta Library to reproduce single copies of this thesis, and to lend or sell such copies for private, scholarly, or scientific purposes only.

The author reserves all other publication and other rights in association with the copyright in the thesis, and except as hereinbefore provided, neither the thesis nor any substantial portion thereof may be printed or otherwise reproduced in any material form whatever without the author's prior written permission.

3 June 1999

11164 78 Ave.
Edmonton, AB, T6G 0M6

UNIVERSITY OF ALBERTA

FACULTY OF GRADUATE STUDIES AND RESEARCH

The undersigned certify that they have read, and recommend to the Faculty of Graduate Studies and Research for acceptance, a thesis entitled *Numerical modelling of hailstone growth in Alberta storms* submitted by Julian Charles Brimelow in partial fulfillment of the requirements for the degree of Master of Science.

G.W. Reuter

B.R. Sutherland

E.P. Lozowski

Approved: 2 June 1999

DEDICATION

For my mother and all those who believed in me.

ABSTRACT

A one-dimensional, steady-state cloud model is combined with a time-dependent hail growth model, to predict maximum hailstone diameter at the ground. Sensitivity experiments, using a severe hailstorm sounding, indicated that the forecast hailstone diameter was controlled primarily by the maximum updraft velocity, the temperature at which it occurred and the updraft duration. Other finding were: (1) Small variations (~1 °C) in surface temperature and dew-point changed the forecast diameter by about 50%. (2) Reducing the heat transfer from growing hail, decreased the final diameter by as much as 60%. (3) A 10% reduction in the liquid water content, reduced the final diameter by about 40%. (4) Increasing the hailstone embryo diameter led to larger hail and decreased the hail growth time.

The forecast hailstone diameters were compared against daily observations of maximum hail size within the Alberta Hail Project area, for 160 days between 1983 and 1985. The model displayed significant skill when forecasting hail (Heidke Skill Score: HSS=64%, Probability of Detection: POD=85%, False Alarm Rate: FAR=26%) and performed even better (HSS=67%, POD=89%, FAR=40%) on days with hail larger than 2 cm in diameter. Moreover, the model showed significantly more skill than a nomogram technique developed to forecast hail size in Alberta.

ACKNOWLEDGEMENTS

I am greatly indebted to the many individuals who provided encouragement and guidance to me during this undertaking. In particular I wish to thank:

- Dr Gerhard Reuter, my thesis supervisor. His comments, suggestions and guidance were invaluable and very much appreciated.
- Mr Brian Crenna for his invaluable assistance with the computer programming and many hours spent helping me modify the model, as well as his numerous comments and suggestions.
- Mr Neil Taylor for his support, suggestions and valuable comments when reading drafts of the thesis.
- Mr Russ Sampson for his helpful suggestions and advice.
- Dr Geoff Strong for preparing and providing the upper-air data that formed an integral part of this study.
- Mr. T. Thompson and Mrs. L. Smith for their assistance in collecting meteorological data and literature.

TABLE OF CONTENTS

		Page
1	INTRODUCTION	1
	1.1 Background	1
	1.2 Alberta Hailstorms	2
	1.3 Theory of Hail Growth	5
	1.4 Review of Hail Forecasting Techniques	12
	1.5 Statement of Research Problems	16
2	THE HAILCAST MODEL	19
	2.1 The Cloud Model	20
	2.2 The Hail Model	23
	2.3 Hail Growth Cycle	30
	2.4 Comments on Numerical Methods	32
3	MODEL CASE STUDIES OF HAIL GROWTH	33
	3.1 Synoptic Situation and Observed Weather Conditions	34
	3.2 Forecast Cloud Profiles and Hail Growth	36
	3.3 Discussion and Conclusions	41
4	MODEL SENSITIVITY EXPERIMENTS	44
	4.1 Sensitivity Experiments- Cloud Model	43
	4.2 Sensitivity Experiments- Hail Model	49
	4.3 Summary and Conclusions	57
5	ALBERTA HAIL PROJECT DATA SET	60
	5.1 Problems Intrinsic to Evaluating Model Forecast Hail Size	60
	5.2 Alberta Hail Project Hail Data	63
	5.3 AHP Upper-air and Surface Data	64
	5.4 Hail Classification used During the AHP	67
	5.5 Hailfall Activity During the 1983-1985 Summer Seasons	68

6 EVALUATION OF HAILCAST AGAINST OTHER FORECASTING TECHNIQUES 69

6.1 Forecast Skill Scores 69
6.2 HAILCAST Model Evaluation 70
6.3 Comparison Between HAILCAST, SkyWatch and RAM Hail Forecasts 74
6.4 Discussion and Conclusions 77

7 CONCLUSIONS AND SUGGESTIONS FOR FUTURE WORK 83

7.1 Conclusions 83
7.2 Suggestions for Future Work 88

REFERENCES 92

APPENDIX A: ESI and Storm Type 106

APPENDIX B: Days Excluded from the Data Set 109

APPENDIX C: Contingency Tables 111

APPENDIX D: Hail Size Category Forecasts 113

APPENDIX E: Absolute Diameter Errors 116

APPENDIX F: Improvements to the SkyWatch Model 119

FIGURES 121

TABLES 144

LIST OF FIGURES

Figure		Page
1.1	Kinetic energy (dashed line) and terminal velocity (solid line) versus hailstone diameter.	121
1.2	Schematic indicating the primary growth mechanisms from cloud droplet to hail. Coalescence refers to the collision and merging of two water droplets, accretion refers to an ice particle collecting supercooled water droplets or small ice crystals, and riming refers to the accretion of supercooled droplets in the form of a low density ice deposit. Adapted from Knight and Knight, (1998).	121
1.3	Cross-section of a multi-cell hailstorm showing the embryo formation region (EFR), hail growth zone (HGZ) and hail cascade. The radar reflectivity factors are indicated by dashed lines (in dBZ) and airflow by arrows (Adapted from K.C. Young, 1977).	122
1.4	Nomogram developed for forecasting maximum hail size in Alberta. Numbers 1 to 6 (shot through greater than golfball) correspond to the maximum observed hail size at the surface, versus the forecast maximum updraft velocity and temperature at the updraft maximum. Adapted from Renick and Maxwell (1977).	123
2.1	Maximum hail growth duration as a function of the Energy Shear Index (ESI).	124
3.1	500 hPa analysis for 1800 LDT on 11 July 1985. Solid contours represent the 500 hPa height (in gpm), and dashed isopleths the 1000-500 hPa thickness. Wind speeds are in knots with a full barb equivalent to 10 knots and a flag 50 knots.	125
3.2	Upper-air sounding released from Penhold at 1715 LDT on 11 July 1985 plotted on a skew T-log P diagram. The dashed line represents the dew-point profile, the solid line the environmental temperature and the curved solid line the pseudoadiabat. The boundary layer has been mixed out based on the maximum temperature of 28 °C.	125
3.3	Same as Figure 3.1 except for 24 August 1983.	126
3.4	Same as Figure 3.2, except for 24 August 1983. The boundary layer has been mixed out based on the maximum temperature of 22 °C.	126

3.5 Model derived profiles of (a) Updraft velocity and (b) Liquid water content (LWC) for 11 July 1985 (solid lines) and 24 August 1983 (dashed lines). 127

3.6 Growth time history of a hailstone simulated by HAILCAST for 11 July 1985. Depicted are (a) Height (Z); (b) In-cloud (TC) and hailstone temperature (TS); (c) Ground relative (VR) and updraft velocity (VU); (d) Growth rate (dD/dt); (e) Diameter (D) and (f) Fractional liquid water content (F_w). 128

3.7 Same as Figure 3.6 except for 24 August 1983. 130

4.1 Maximum updraft velocity (ms^{-1}) contoured on a surface temperature and surface dew-point diagram. Points A, B and C correspond to sensitivity experiments discussed in section 4.1.1. 132

4.2 Temperature (°C) at the level of maximum updraft velocity contoured on a surface temperature and surface dew-point diagram. Points A, B and C correspond to sensitivity experiments discussed in section 4.1.1. 133

4.3 Maximum forecast hail diameter at the ground (in cm) contoured on a surface temperature and surface dew-point diagram. Points A, B and C correspond to sensitivity experiments discussed in section 4.1.1. 134

4.4 Hail growth time series for 3 hailstones A, B and C determined using different surface temperature and dew-points. Hailstone B denotes the control. Depicted are (a) Height (Z), (b) Hailstone temperature (T) and (c) Diameter (D). 135

4.5 Hail growth time series for 3 hailstones A, B and C determined using hail embryo diameters of 100 μm (C), 300 μm (B) and 1000 μm (A). Variables are the same as shown in Figure 4.4. 136

4.6 Hail growth time series for 3 hailstones using E_i of 0.15 (hailstone A), 0.21 (hailstone B) and 0.25 (hailstone C) respectively. 137

4.7 Ventilation coefficient versus Reynolds number calculated using the scheme of PAR79 (Pruppacher and Rasmussen, 1979) and that of RAH87 (Rasmussen and Heymsfield, 1987a). 138

4.8 Hail growth time series for 2 hailstones using the ventilation coefficient scheme of RAH87 (Rasmussen and Heymsfield, 1987a) and PAR79 (Pruppacher and Rasmussen, 1979). 139

5.1 The Alberta Hail Project's principal target area between Edmonton and Calgary and centred on the radar site located at the Red Deer Industrial Airport. 140

5.2 Example of a hail card completed each summer by volunteer observers within the Alberta Hail Project area. (From Renick, 1984). 141

5.3 Sounding released from Penhold on 21 August 1983. Solid line depicts the environmental temperature profile, dashed line the dew-point and the dot-dashed depicts line the pseudo-adiabat. (Adapted from Renick, 1983). 142

6.1. 1800 LDT surface analysis and 1400 LDT sounding released from Penhold on 1 August 1985. 143

6.2 Same as for Figure 6.1 except for 2 August 1985. 143

LIST OF TABLES

Table		Page
2.1	Entrainment mechanism and amount as determined by the ESI.	144
3.1	Thermodynamic and wind derived parameters calculated using the HAILCAST model for 1800 LDT on 11 July 1985 and 24 August 1983.	144
3.2	Environmental and model parameters utilised in model runs for 11 July 1985 and 24 August 1983.	144
4.1	Updraft and hail growth statistics for hailstone trajectories A, B and C. Note the time in the supercooled region refers only to the downward pass through the cloud.	145
4.2	Updraft and hail growth statistics for lateral entrainment sensitivity experiments. D represents the forecast hailstone diameter at the ground and τ the time taken for the hailstone to reach the ground.	145
4.3	Same as Table 4.2, except for cloud top entrainment.	145
4.4	Environmental, updraft and hailstone statistics for vertical wind shear sensitivity experiments. Values in parentheses indicate the updraft duration (maximum hail growth time).	146
4.5	Same as Table 4.4, except for 1985-08-02.	146
4.6	Hailstone statistics for hail embryo diameter sensitivity experiments.	146
4.7	Hailstone diameter (D) and the time taken for the hailstone to reach the ground (τ) for ice collection efficiency sensitivity experiments.	147
4.8	Hailstone diameter (D) and the time taken for the hailstone to reach the ground (τ) for liquid water content (LWC) sensitivity experiments.	147
4.9	Hailstone diameter (D) and the time taken for the hailstone to reach the ground (τ) for ventilation coefficient sensitivity experiments.	147

4.10 Hailstone diameter (D) and the time taken for the hailstone to reach the ground (t) for terminal velocity scheme sensitivity experiments. 148

5.1 Time frame during which upper-air soundings were conducted at Penhold from 1983-1985. 148

5.2 Time frame during which upper-air soundings were conducted at Penhold from 1983-1985. 148

5.3 Number of hail days and reports recorded in the AHP area from 1 June to 31 August for 1983-1985 compared with the 1974-1985 means. 148

5.4 Categories used to classify hail size during the Alberta Hail Project (AHP). 149

6.1 2x2 Contingency table used in calculation of forecast skill statistics. 149

6.2 Summary of skill scores used to evaluate hail forecasts. 149

6.3 Summary of forecast skill scores for HAILCAST from 1983-1985. 150

6.4 HAILCAST Forecast hail size category evaluation. 150

6.5 Summary of hail category forecasts for HAILCAST from 1983-1985. 150

6.6 Summary of mean absolute hail diameter errors (cm) for HAILCAST from 1983-1985. 151

6.7 Summary of forecast skill scores for HAILCAST, SkyWatch and RAM from 1983-1985. 151

6.8 Forecast hail category evaluation for no-hail days for HAILCAST, SkyWatch and RAM from 1983-1985. 151

6.9 Forecast hail category evaluation for all hail days for HAILCAST, SkyWatch and RAM from 1983-1985. 152

6.10 Forecast hail category evaluation for non-severe hail days for HAILCAST, SkyWatch and RAM from 1983-1985. 152

6.11 Forecast hail category evaluation for severe hail days for HAILCAST, SkyWatch and RAM from 1983-1985. 152

6.12 Summary of hail category forecasts for HAILCAST, SkyWatch and RAM from 1983-1985. 152

6.13 Mean maximum surface temperature, dew-point and CAPE observed at Penhold for severe hail days from 1983-1985. 153

6.14 Forecast maximum hail size and upper-air conditions over the AHP area for 17 days when HAILCAST forecast hail and none was observed. UAR denotes upper-air ridge. 153

1. INTRODUCTION

1.1 Background

Hailstorms occur frequently in central Alberta during the summer months, with hail observed an average of 51 days between 1 June and 31 August (Deibert, 1985). On average, 20 of these are severe hail days (maximum hailstone diameter larger than 2 cm). Hailstorms cause millions of dollars damage annually in the agriculture sector alone. Further, the Edmonton hailstorm of 31 July 1987 was responsible for an insured loss of $250 million (Charlton et al., 1998), while the Calgary hailstorm of 7 September 1991 set a record (at that time) for the most expensive natural disaster in Canadian history at $400 million (Charlton et al., 1995).

Hail is frequently observed in the so-called "Alberta Hail Belt", which is bounded in the west by the foothills of the Rockies and stretches in a NNW-SSE direction from Edmonton to Lethbridge. The hail belt is some 100-130 km wide and 400 km long (Aktary, 1993).

The damage inflicted by a falling hailstone is determined primarily by its kinetic energy (E_k) upon impact. The E_k for a spherical hailstone of radius r, is proportional to r^4 (mass and terminal fall speed are proportional to r^3 and $r^{0.5}$ respectively). Figure 1.1 shows the increase in the kinetic energy and terminal fall speed with increasing hailstone diameter.

In light of the destructive capability of severe hailstorms, it is important to issue timely warnings for the occurrence of severe hail. Despite significant advances in our understanding of severe thunderstorms, accurate forecasting of hail size remains challenging. Most operational methods designed for this purpose are radar-based. Edwards and Thompson (1998) found that radar-derived algorithms currently used to forecast hail show limited skill. This may, in part, be

related to the fact that hail forecasting research has been neglected recently, while other severe storm phenomena such as tornadoes and squall lines receive the bulk of research attention (Edwards and Thompson, 1998).

Issuing warnings for hail essentially involves three steps. Firstly, determine the potential for severe thunderstorms up to 24 hours in advance. Secondly, identify when and where the thunderstorms are expected to develop (i.e., determine the threat areas for different times). Thirdly, forecast the maximum hail size (up to 12 hours in advance) capable of being produced by the thunderstorms.

This study will focus on addressing the problem of predicting maximum hail size. Our approach is based on a modified version of Poolman's (1992) numerical model (hereafter referred to as HAILCAST). HAILCAST consists of a one-dimensional cloud model coupled with a time dependent hail growth model. Specifically, we extended and improved upon the FORTRAN code used by Poolman. We will show that HAILCAST displays significant skill when forecasting hail size, while avoiding some of the major short-comings of current and past hail forecasting techniques.

Before outlining the goals of this study in detail, the characteristics and formation of hailstorms in Alberta will be discussed, followed by the theory of hail growth and a review of hail forecasting techniques.

1.2 Alberta Hailstorms

Chisholm and Renick (1972) note that Alberta hailstorms span a broad range of size, type and duration. Severe hail in central Alberta, however, is usually produced by multi-cell or supercell thunderstorms. 90% of most hail swaths in central Alberta are less than 30 km in length and cover less than 200

km^2 (Kochtubajda and Gibson, 1992). Some intense and long-lived hailstorms, however, can produce hail swaths up to 300 km long and 2500 km^2 in area.

Thunderstorms develop in moist and convectively unstable air masses, and can produce heavy rain, lightning and hail (Rogers and Yau, 1996). An unstable atmosphere is characterised by cold air aloft and warm moist air in the planetary boundary layer (PBL). Reuter and Aktary (1995) found that in central Alberta, 97% of soundings from June-August were conditionally unstable for moist convection.

Strong updrafts are a necessary ingredient for the formation of hail, since they place an upper limit on the maximum hail size that can remain suspended within a thunderstorm (Johns and Doswell, 1992). The strength of the maximum updraft velocity is primarily determined by the CAPE (Convective Available Potential Energy), which represents the buoyant energy per unit mass. Ignoring water loading, entrainment and pressure-gradient effects, the maximum possible updraft velocity is given by $W_{max}= \sqrt{2CAPE}$.

While the amount of instability determines the strength of convection, the vertical wind shear determines the type of thunderstorm that will develop once the instability is released (Weisman and Klemp, 1986). Depending on the interaction of the updraft and vertical wind shear, convection will take on the form of an air-mass, multi-cell or supercell thunderstorm (Chisholm and Renick, 1972; Weisman and Klemp, 1986). Thus, high instability coupled with strong vertical wind shear, creates an ideal environment for severe thunderstorms capable of producing large hail (Weisman and Klemp, 1986).

Short-lived air-mass thunderstorms develop in a weakly sheared ($< 2x10^{-3}$ s^{-1}) and moderately unstable environment. They typically have a lifetime of 30-45 min, with weak to moderate updrafts (<20 ms^{-1}) lasting less than 20 min (Browning, 1977). The modest updrafts and short-duration thereof, are not

conducive to the formation of large hail, and air-mass thunderstorms rarely produce severe hail at the ground.

A moderate to highly unstable atmosphere (updrafts 20-40 ms^{-1}) with unidirectional wind shear ($2\text{-}5x10^{-3}$ s^{-1}) is required for the formation of multi-cell thunderstorms. These conditions are frequently observed in Alberta during the summer months (Chisholm and Renick, 1972). Multi-cell thunderstorms consist of an organised group of individual cells in different stages of development, with new cells continually developing on the right-flank of the storm complex (Browning, 1977). Individual cells are identifiable on radar for about 30 min, while the storm as a whole can persist for several hours (Chisholm and Renick, 1972).

The supercell storm environment is characterized by strong instability (updrafts >30 ms^{-1}) and strong veering of the environmental winds in the lowest 2-3 km AGL (Browning, 1977; Johns and Doswell, 1992). Supercell thunderstorms have a single steady-state and rotating updraft, that coexists with a downdraft for periods up to 60 min and occasionally several hours (Chisholm and Renick, 1972). This highly organised storm structure is ideally suited for the formation of severe hail (Kubesh et al., 1988; Miller et al., 1988), and despite their rare occurrence in Alberta, supercells cause immense hail damage over a large area (Chisholm and Renick, 1972).

Smith and Yau (1993) identified the criteria necessary for the formation of severe convective weather outbreaks in Alberta: 1) High latent energy (moisture) in the PBL, i.e. high precipitable water, 2) Strong thermodynamic instability, i.e. large CAPE, 3) Strong vertical wind shear and veering of the wind in the lowest 3 km AGL and 4) A trigger mechanism to lift a parcel within the PBL to its level of free convection. Trigger mechanisms can be present in the form of surface heating, moisture convergence, frontal boundaries, thunderstorm outflow boundaries, orographic uplift or low-level jets (McGinley, 1986). Strong (1986)

noted that on days with severe convection in Alberta, the morning sounding often has an inversion or capping lid near 800 hPa. This inversion forms in response to orographic subsidence east of the Continental Divide and allows the build-up of latent and sensible energy in the PBL through an increase of moisture and heat, while preventing the premature formation of deep convection. Knowing the timing and location of the removal of the lid, is crucial in forecasting the initiation of deep convection over the foothills.

Following the work of Strong (1986), Smith and Yau (1993) proposed a conceptual model for forecasting severe thunderstorm outbreaks in Alberta. Their model describes how the above criteria for severe convection are satisfied when the approach of a synoptic scale upper-air trough (cooling aloft) coincides with strong surface heating over the foothills of the Rocky Mountains. Differential heating between the plains and the eastward facing foothills, forces an easterly upslope flow from the plains (mountain-plain circulation). The interaction between the synoptic and mesoscale environments enhances the mountain-plain circulation and the transport of low-level moisture towards the foothills. The combination of the above factors leads to maximum instability over the foothills and the removal of the capping lid, triggering the formation of severe thunderstorms. The thunderstorms are then steered onto the plains by the mid and upper-level westerly winds.

1.3 Theory of Hail Growth

The objective of this section is to highlight the main physical and dynamical processes involved in hail growth and the reader is referred to the work of Macklin (1977) and List (1985) for a detailed discussion of hail growth.

1.3.1 Microphysics

Hailstones form when hail embryos accrete supercooled water droplets and ice crystals in clouds with vigorous updrafts (Garcia-Garcia and List, 1992). Hail embryos are an important component of hail growth, and thin sections of large hailstones reveal that each hailstone contains a distinct central growth unit (hail embryo), varying from 1 mm to 1cm in diameter (Macklin, 1977). Analysis of hailstones collected at the ground reveals that there are two types of hail embryos, frozen drops and graupel particles (e.g., Knight and Knight, 1978; Federer and Waldvogel, 1978; Knight, 1981), with embryos from a particular storm very rarely all graupel or all frozen drops. Figure 1.2 outlines the growth cycle from a cloud droplet to a hailstone. Note that this figure does not represent all the mechanisms involved, but only those considered most critical for hail growth.

The presence of supercooled cloud water (liquid water content or LWC) is critical for the growth of hail. Most of the hail growth occurs in the supercooled region of the cloud that extends between 0 °C and -40°C. Above the -40°C level, the cloud is usually completely glaciated due to the homogeneous freezing of cloud water, and hail can only grow slowly by accreting ice crystals. At temperatures above 0 °C melting of the hailstone occurs.

The rate of hail growth depends on the latent heat of fusion released by the accreted supercooled water and the transfer of this heat from the hailstone's surface. The surface temperature of a growing hailstone is typically a few degrees warmer than the in-cloud temperature and the amount of heating is primarily determined by evaporation and the conduction (and convection) of heat away from the hailstone.

Depending on the rate of heat transfer to and from the hailstone, one of two primary growth mechanisms results. If the growing hailstone accretes

supercooled water faster than the heat can be removed from its surface, the hailstone's temperature rises rapidly to 0 °C and it enters the so-called wet growth regime. During wet growth, the hailstone's surface is wet and all the accreted ice is collected, since the ice crystals readily "stick" to the surface (English, 1973). If the mass of the water on the hailstone's surface exceeds a critical limit, some of the water is shed in the form of droplets (Rasmussen et al., 1984b). This shedding process could be an important source of rain and new hail embryos in thunderstorms (Rasmussen and Heymsfield, 1987c; Kubesh et al., 1988). Laboratory studies indicate that melting hailstones (larger than 9 mm in diameter) shed droplets ranging from 300 μm to 3 mm in diameter, with a modal diameter of approximately 1 mm (Rasmussen et al., 1984b). The shedding of millimeter sized droplets can also occur during wet growth (Lesins and List, 1986; Garcia–Garcia and List, 1992).

If the rate of heat transfer away from the stone's surface is sufficiently large, the hailstone remains in the dry growth regime. Since the surface temperature of the hailstone is now below 0 °C, all the accreted water is frozen. However, only a small fraction of the intercepted ice crystals are accreted, since they do not readily "stick" to the dry surface of the hailstone (English, 1973).

Another mode of hail growth is spongy growth, in which unfrozen water is incorporated into a low density ice matrix (Lesins and List, 1986). Spongy growth is more likely at warmer temperatures and high liquid water contents. For example, a liquid water content of 4 gm^{-3} or more at -10 °C should produce this kind of growth (Lesins and List, 1986). Large natural hailstones very rarely exhibit spongy growth, since they tend to shed the excess water due to the centrifugal forces resulting from the tumbling motions of hail (Lesins and List, 1986; Garcia-Garcia and List, 1992).

Thin sections of hailstones collected at the ground typically display a number of concentric layers, alternating between opaque and transparent layers of

ice (Macklin, 1977). These layers result from the hailstone undergoing wet or dry growth as it passes through regions of varying temperature and liquid water content (Rogers and Yau, 1996). Dry growth layers are characterized by a white and opaque deposit, consisting of a high concentration of small air bubbles trapped as the cloud droplets rapidly freeze upon contact with the hailstone (Macklin, 1977). Conversely, wet growth layers are mostly transparent, with a lower concentration of larger air bubbles present in the frozen water deposit.

The rate of growth due to the accretion of supercooled water is proportional to the terminal velocity of the hailstone (related to diameter) and the liquid water content (LWC) of the cloud,

$$\frac{dD}{dt} = \frac{V_t E_w LWC}{2\rho_i}, \qquad (1.1)$$

where D is the diameter of the hailstone, V_t is the terminal velocity, ρ_i is the density of the hailstone, E_w is the collection efficiency (assumed to be unity for a hailstone collecting cloud droplets) and LWC the adiabatic liquid water content.

From Figure 1.1 it follows that the growth rate in hail diameter is proportional to the LWC. For example, the time required for hail to grow from 0.5 cm to 3 cm is about 10 minutes for a LWC of 5 gm^{-3}, or 20 minutes for 2.5 gm^{-3} (Knight and Knight, 1998). Using a conservative LWC of 2 gm^{-3}, Knight et al. (1982) estimated the growth time from a cloud droplet to a 3 cm hailstone to be 45-50 minutes, and this lies within the range of updraft lifetimes typically observed in severe Alberta hailstorms (Chisholm and Renick, 1972).

1.3.2 The Hail Growth Zone

Numerous modelling studies and isotope analyses of hailstones have shown there is a preferential region within hailstorms where maximum hail

growth occurs (English, 1973; Browning, 1977; Nelson, 1983; Foote, 1984; Miller et al., 1988). This so-called hail growth zone (HGZ) occurs at in-cloud temperatures between –20 °C and –40 °C.

The reason for this is threefold. Firstly, the maximum LWC is often located within this zone. Secondly, due to the low ambient temperatures, the heat transfer from the hailstone is sufficient to ensure that all or most of the accreted water is frozen. Carras and Macklin (1973) showed that at temperatures warmer than –12 °C, excess water is shed from large (>1cm) hail in the wet-growth regime. Thirdly, above the –20 °C level, the cloud is composed of a mixture of supercooled cloud droplets and ice crystals (Vali and Stansbury, 1965). A hailstone undergoing wet growth within this mixed-phased zone, in addition to accreting supercooled water, readily accretes ice crystals without adding heat to the hailstone. This allows more supercooled water to be accumulated before the onset of shedding, and accelerates the growth of the hailstone over what it would have been if all the available accreted mass were liquid (Nelson, 1983).

1.3.3 Storm Scale Features

We have identified two major microphysical criteria required for hail growth in thunderstorms, namely the presence of hail embryos and high liquid water contents. There are also several storm scale features that are important for hail growth. For maximum growth, it is essential that the growing hailstone resides in the HGZ long enough to reach an appreciable size. This can only be achieved if the terminal velocity of the hailstone is closely matched by the updraft as it grows within the storm (Browning, 1977). If the updraft is too strong, the hailstone will be rapidly carried upward through the storm and ejected into the anvil. On the other hand, if the updraft is too weak, the hailstone will fall prematurely from the storm. For the formation of severe hail, maximum updraft velocities in excess of 25 ms^{-1} are usually required in the HGZ (approximately the terminal velocity of a 2 cm hailstone). The maximum hail size is also limited by

the residence time of growing hail in the HGZ and this is determined by the width of the updraft and strength of the horizontal storm relative winds (Nelson, 1983; Miller et al., 1988). A broad band of strong updrafts and light horizontal storm relative winds maximize the residence time in the HGZ and increase the likelihood of severe hail reaching the ground. This was illustrated by two prolific hail producing storms observed during CCOPE (Cooperative Convective Precipitation Experiment). Both hailstorms had broad adiabatic updrafts with maximum updraft velocities >40 ms^{-1} (Musil et al., 1986; Kubesh et al., 1988).

Although growing hailstones can follow a myriad of trajectories during the lifetime of a thunderstorm, only a small percentage of hail trajectories produce large hail. By conducting detailed case studies of severe hailstorms using particle growth models coupled with storm airflow measurements from Doppler radar networks, researchers have identified those trajectories that are most likely to produce severe hail (e.g. Nelson, 1983; Foote, 1984; Rasmussen and Heymsfield, 1987c; Miller et al., 1988 and Brandes et al., 1995). These trajectories usually consist of a single ascent and descent through or around the main updraft. The model results show that large hailstones do not undergo recirculation. Graupel particles, which later form hail embryos, have been found to undergo recirculation on the periphery of the main updraft (Holler et al., 1994) in a manner similar to that proposed by Browning and Foote (1976).

The above trajectories are similar to those described in a conceptual model proposed by Browning and Foote (1976) for the growth of severe hail in a steady-state supercell. In this model, the hail growth consists of 3 stages (see Figure 1.3):

(1) Hail embryos form in a broad region of weak to moderate updrafts upwind of the main updraft, where they have sufficient time to reach millimeter sized particles as they are advected towards the updraft core.
(2) When the particles enter the HGZ, they are several millimeters in diameter and have significant terminal velocities (>15 ms^{-1}) preventing them from

being prematurely ejected into the anvil. Also, the low precipitation efficiency and entrainment commonly observed in the updraft core, ensure liquid water contents close to their adiabatic values within and on the periphery of the main updraft (Bluestein et al., 1988). As a result, the hailstones experience rapid growth as they are advected across the updraft core by the storm relative inflow.

(3) When the terminal velocity of the hailstones exceeds that of the updraft, they begin descending and continue to grow until the onset of melting below the freezing level.

The above process is only truly applicable to steady-state supercell storms and all hailstorms, even supercells, do not necessarily conform to the Browning and Foote (1976) model (e.g. Miller et al., 1990). In multi-cell storms, stages 2 and 3 occur within a mature cell, with the hail embryos being introduced into the main updraft by developing feeder or daughter cells upwind of the mature cell (Heymsfield et al., 1980; Krauss and Marwitz, 1984; Cheng and Rogers, 1988).

Another important factor that influences the final hail size, is the amount of melting the hailstone undergoes before reaching the ground. Rasmussen and Heymsfield (1987b) determined that the amount of melting depends on the initial size and density of the hailstone at the freezing level. Since these parameters determine the hailstone's terminal velocity and residence time below the freezing level. Foote (1984) showed that larger hailstones lose less of their initial mass due to melting than smaller hailstones. This can be attributed to the their reduced residence time in the melting layer. Furthermore, for a given hail size, the amount of melting increases as the height of the freezing level and the mean temperature of the downdraft air increase. The amount of melting is also sensitive to the relative humidity within the melting layer, with a high ambient relative humidity increasing the amount of melting (Rasmussen and Heymsfield, 1987b).

1.4 Review of Hail Forecasting Techniques

In this section we will review some past and current techniques used to monitor the presence of hail in thunderstorms and estimate the hail diameter at the ground.

1.4.1 Hail Forecasting Techniques Based on Radar Observations

Weather radar is ideal for monitoring the structure and development of thunderstorms, and since the implementation of the WSR-88D network in the United States, several algorithms have been developed to nowcast (0-6 hour forecast) hail based on radar-derived parameters. Edwards and Thompson (1998) review some of the more successful hail forecasting algorithms currently in use.

Until recently, the focus was on detecting the presence of hail, rather than determining the hail diameter or likelihood of severe hail. For example, Mather et al. (1976) found the presence of hail of any diameter to be closely related to the height of the 45 dBZ echo above the environmental freezing level. Waldvogel et al. (1979) developed a nomogram indicating the probability of hail at the ground based on these two parameters. In Alberta, Kochtubajda and Gibson (1992) suggest the presence of a 43 dBZ echo at 7 km AMSL, as a threshold for indicating the presence of severe hail at the ground. Dual polarization techniques have also been used extensively to identify the presence of hail in thunderstorms (Al-Jumily et al., 1991).

Another radar-derived parameter popular for nowcasting hail is VIL (Vertically Integrated Liquid). Large VIL values indirectly indicate the presence of hail, since they are associated with greater water mass in the cloud (Edwards and Thompson, 1998). VIL has been used successfully for predicting the existence of hail, but has not proven useful in distinguishing between severe and non-severe hail events (Wagenmaker, 1992). In an attempt to improve hail

forecasts using VIL, a number of researchers have attempted to adjust VIL data using several thermodynamic sounding parameters and storm characteristics, such as the height of the freezing level and storm top. However, Roeseler and Wood (1997) noted similar VIL density values (ratio of VIL to radar-estimated storm top) for non-severe days and those at the severe threshold. Further, in a study of 426 severe hail events across the contiguous United States, Edwards and Thompson (1998) found that most of the VIL based parameters currently used to predict the hail severity are practically useless, and VIL should not be used alone to estimate hail diameter.

Only recently has research been undertaken regarding the forecasting of the probability of severe hail and the maximum expected hail diameter at the ground using radar. Witt et al. (1998) note that the prediction of maximum hail diameter is the most difficult and challenging aspect of their Hail Detection Algorithm (HDA). Although the latest algorithms developed by Witt et al. (1998) display greater skill than previous techniques, indications are that there is a strong regional and seasonal dependence regarding the skill of the indices, due to variations of environmental factors impacting the melting of hail for example. Further, although the latest algorithms indicate increasing magnitude with increasing hail diameter, a wide range of hail sizes is often observed for a given value and caution should be exercised when applying threshold values for issuing warnings or estimates of hail diameter (Witt et al., 1998).

Regardless of the above caveats, perhaps the biggest set-back of radar-derived hail algorithms is that they are real-time, rather than predictive. This has serious implications regarding the lead time of warnings issued using the above techniques, since hail is already falling before a warning can be issued.

1.4.2 Hail Size Forecasting Based on Sounding Data

Fawbush and Miller (1953) made one of the earliest attempts to forecast hail diameter. Their method is based on a nomogram that relates CAPE (below the –5 °C level) to the observed hail diameter at the ground. Foster and Bates (1956) adopted a similar approach. They used the vertical velocity at –10 °C, since they proposed that the updraft velocity in this zone, is that required to sustain a fully grown hailstone.

Maxwell (1974) developed a nomogram relating the observed hail diameter at the ground, to the maximum updraft velocity and the temperature at the updraft maximum (Figure 1.4). The nomogram was developed by determining which combination of model output parameters (calculated using the steady-state one-dimensional cloud model of Chisholm (1973)), were highly correlated to the maximum observed hail size within the Alberta Hail Project (AHP) area. Diagnostic model runs were conducted for 210 hail days from 1969-1973. The nomogram was tested operationally for 19 hail days during the 1974 field season and correctly forecast the hail size on 63% of the hail days. This approach requires virtually no calculations and avoids the complication of estimating the residence time in the cloud and melting of the hailstone. The output from the 1D model is, however, sensitive to temperature and moisture values used to determine the maximum updraft velocity. Renick and Maxwell (1977) found the nomogram did not predict the maximum hail size effectively when the in-cloud freezing level was greater than 4.4 km AMSL and on such occasions, the model nearly always forecast hail considerably larger than was actually observed.

Moore and Pino (1990) used the Foster and Bates (1956) approach, but calculated the vertical velocity using a one-dimensional time independent cloud model developed by Anthes (1977). The vertical velocity (based on a modified sounding) at –10 °C is used to estimate the maximum hail diameter and allowance is made for the melting of the hailstone before reaching the ground. A forecast

afternoon sounding is prepared by modifying the PBL using a surface heating algorithm, while above the PBL, a subjective method is used to estimate the temperature changes by taking a small fraction of the geostrophic thermal advection (calculated using the morning wind profile).

Most of the above techniques have been found to be inaccurate when used operationally to forecast hail diameter. Leftwich (1984) evaluated the Fawbush and Miller technique and calculated a root mean square error in hail diameter greater than 2.5cm. Further, Doswell et al. (1982) found the Foster and Bates technique failed to discriminate between large and small hail events, and rarely forecast large hail. Moore and Pino (1990) found the skill of their model to be significantly better than that of Fawbush and Miller for 58 severe hail events in the southern plains of the United States. However, this model has not been evaluated for no hail and non-severe hail days.

1.4.3 Numerical Hail Models

To model hail growth, one ideally requires a three-dimensional time dependent cloud model with detailed microphysics (e.g., Xu, 1983). Multi-dimensional time dependent hailstorm models have been used for diagnostic studies of hailstorms and have helped improve our understanding of hail growth mechanisms and refine conceptual models for hail growth (e.g., Orville and Kopp, 1977; Clarke, 1982; Xu, 1983; Farley 1987; Kubesh et al., 1988). However, these models are not suited for operational forecasting at the present time, due to constraints on computing power and memory, as well as problems related to the accurate initialization of these models.

Brooks et al. (1992) discuss the formidable challenges involving input data and constraints of 3D models that must be overcome before they can be used operationally to forecast convective weather. In light of these problems, it is expected that many years will pass before forecasters can use 3D cloud model

output operationally to forecast hail size. Further, preliminary field experiments using a 3D cloud model, such as STORMTIPE (Storm Type Operational Research Model Tests Including Predictability Evaluation), are limited to a 240 km by 240 km domain in the American mid-west and access to the model output will most likely only be available for a select group of clients (Brooks and Doswell, 1993).

Until such time as 3D cloud model output data are freely available, 1D cloud models present the best alternative for forecasting hail size. One-dimensional cloud models are based on the assumption that atmospheric variables are only a function of height, and they have been used extensively to model hailstone growth (Musil, 1970; Dennis et al., 1972; Wisner et al., 1972; Dennis and Musil, 1973; Chisholm, 1973).

Poolman (1992) developed a 1D cloud model coupled with a time dependent hail growth model (with microphysics) to estimate maximum hail size. In this approach, the hailstone growth is modeled using microphysics, rather than directly relating the hail diameter to the vertical velocity as used in the nomogram techniques. The model calculates the maximum expected hail diameter at the ground and it includes the effects of melting. Poolman's model has been used operationally by the South African Weather Bureau to forecast maximum hail size, but it has not undergone a detailed evaluation, due to a lack of systematic hail size observations in South Africa.

1.5 Statement of Research Problems

1.5.1 Objectives

Our research has two major objectives. Firstly, we determine the sensitivity of the modelled hail growth to changes in input sounding data and key microphysical parameters. Secondly, we determine the skill of HAILCAST in forecasting hail diameter, with particular emphasis on forecasting large hail.

The first part of this thesis will focus on addressing the following questions:

- Is HAILCAST capable of realistically modelling thunderstorm updrafts and the growth of hail?
- How sensitive are the cloud model output parameters to changes in the input sounding data?
- How do these changes ultimately impact the forecast hail diameter?
- How sensitive is the forecast hail diameter to changes in various microphysical parameters and parameterisation schemes used to model the growth of hail?

Case studies of a severe and non-severe hail day will be undertaken to describe the model derived updraft profiles and simulated hail growth. Extensive sensitivity experiments will then be conducted to investigate the hail growth mechanisms and quantify how sounding data and microphysical parameters affect the growth of hail.

The second part of the thesis will address the following questions:

- How well do HAILCAST forecasts of maximum expected hail diameter evaluate against observations from a comprehensive hail observation network?
- Is the model capable of distinguishing between no hail, non-severe hail and severe hail days?
- Do the improved microphysics used in HAILCAST, enhance the model's forecast skill over Poolman's original SkyWatch hail model and a traditional nomogram approach of RAM (Renick and Maxwell, 1977)?
- What are the shortcomings and limitations of HAILCAST?

Previous evaluations of hail forecasting techniques have focused on severe days only (Moore and Pino, 1990; Edwards and Thompson, 1998). If the model is to be used operationally, however, it is important to determine its skill for all

days. The HAILCAST model will be evaluated for no hail, non-severe hail and severe hail days during three summers (1983-1985), using high quality and high density observations of maximum hail size during the Alberta Hail Project (AHP).

1.5.2 Outline of Thesis

Chapter 2 provides the background on HAILCAST and presents the model equations. In Chapter 3, two case studies are discussed in detail. These case studies illustrate the output of HAILCAST and determine its ability to realistically model hail growth in a severe and non-severe thunderstorm environment. Chapter 4 focuses on the results from sensitivity tests and determines the role of certain thermodynamic and microphysical parameters for the growth of large hail. This will be followed by a description of the data set used to run the model and verify the hail size forecasts in Chapter 5. HAILCAST is evaluated in Chapter 6 and these results are compared with the forecast skill of Poolman's model and the nomogram technique of Renick and Maxwell (1977). Finally, in Chapter 7, the major findings of our research are summarized and recommendations for future research presented.

2. THE HAILCAST MODEL

The HAILCAST model consists of two components, namely a steady-state one-dimensional cloud model and a one-dimensional (1D) time dependent hail model with microphysics. This chapter will focus on the calculation of the relevant thermodynamic, kinematic and microphysical parameters used in HAILCAST. Before discussing the cloud and hail models in greater detail, some of the advantages and disadvantages of this approach will be discussed.

Crum and Cahir (1983) noted that a 1D time independent cloud model showed skill when used to forecast thunderstorm top height. Further, 1D models are ideally suited for use operationally, since many model runs can be completed in a very short time, thereby allowing the forecaster to anticipate various scenarios by slightly modifying the surface boundary conditions. Moreover, due to their computational efficiency, 1D models are useful for the analysis of microphysical processes within clouds (Rogers and Yau, 1996).

The simplicity of the 1D steady-state approach, nevertheless, has some major shortcomings. Firstly, the model variables are only allowed to vary in the vertical. Neglecting horizontal motion precludes the direct modelling of wind shear, its impact on cloud entrainment and growth of the cloud (Reuter, 1985). Secondly, the cloud is modelled as being steady-state, whereas in reality thunderstorms are highly time dependant. Nevertheless, researchers have used the steady-state approach for periods up to 20 min when incorporating Doppler wind data into hail growth models with satisfactory results (e.g., Miller et al., 1988). The approach used in this thesis, is to assume the hailstone remains within a steady-state updraft for a finite time, after which it is assumed the updraft collapses or the hailstone is removed from the updraft and falls to the ground. Thirdly, by ignoring the three-dimensionality of the cloud, we are in effect modelling the adiabatic updraft core and hailstones do not spend their entire

lifetime in this region. In fact, large hail is nearly always found on the periphery of the main updraft (Musil et al., 1986). There is, however, observational evidence of low concentrations of large hail in the updraft core (Rasmussen and Heymsfield, 1987c; Miller et al., 1990).

A detailed discussion of the cloud and hail models is beyond the scope of this thesis and the reader is referred Musil (1970), Dennis and Musil (1973) and Poolman (1992), for a comprehensive discussion of the relevant models.

2.1 The Cloud Model

The first component of HAILCAST is a modified version of Poolman's (1992) steady-state one-dimensional cumulus cloud model. The cloud model provides vertical profiles of updraft velocity, in-cloud temperature and saturation mixing ratio for use in the hail growth model. The major components of the cloud model will now be discussed.

2.1.1 Calculation of Updraft Velocity

The vertical acceleration of an air parcel due to buoyancy is given by

$$\frac{d^2z}{dt^2} = g\left[\frac{T^* - T}{T} - \chi\right], \tag{2.1}$$

where z is the height, g the gravitational acceleration, T^* and T the virtual in-cloud and ambient temperatures respectively. The water-loading term, χ, represents the mixing ratio of condensed water substance present at each level within the cloud and is calculated as follows

$$\chi = w_{s0} - w_s, \tag{2.2}$$

where w_{s0} represents the saturation mixing ratio at cloud base and w_s the saturation mixing ratio at level z.

Defining the vertical velocity (W) as W=dz/dt and substituting this expression into 2.1 yields

$$W\frac{dW}{dz} = g\left[\frac{T^{*} - T}{T} - \chi\right]. \qquad (2.3)$$

Integrating 2.3 over height from the level of free convection (z_{lfc}) to the equilibrium level (z_{el}) yields

$$W^2 = W_o^2 + 2g\int_{lfc}^{el}[\frac{T^{*} - T}{T} - \chi]dz\,, \qquad (2.4)$$

where W_0 is the updraft velocity at cloud base. Chisholm (1973) measured cloud base updraft velocities of 4-6 ms^{-1} for Alberta hailstorms and in this study we assume W_0= 4 ms^{-1}. The impact of entrainment on T^{*} and χ is taken into account and discussed further in section 2.1.2.

In the above updraft calculations, the condensed water is assumed to remain with the parcel and the impact of non-hydrostatic pressure perturbation gradients is not taken into account. Schlesinger (1978) found that non-hydrostatic pressure gradients within thunderstorms could significantly decrease the updraft velocity. Conversely, strong veering of the wind in the low-levels, creates dynamically induced vertical pressure gradients which act to increase the vertical velocity (Rotunno and Klemp, 1982). Reuter (1985) found that in modelled clouds, non-hydrostatic pressure gradients are important for initiating penetrative downdrafts in the upper regions of the cloud.

2.1.2 Entrainment Mechanism

As a cumulus tower grows vertically, drier environmental air is entrained through the top (cloud top entrainment) and sides (lateral entrainment) of the cloud. Mixing of the relatively cool and dry environmental air with the updraft, lowers the saturation mixing ratio and temperature of the updraft air and decreases its buoyancy. The relative importance of cloud top versus lateral entrainment has been debated for many years (e.g., Cotton and Anthes, 1989).

Although a 1D time independent cloud model cannot realistically simulate entrainment, it is important to account for its presence if one wishes to realistically model vertical velocity and LWC profiles in clouds.

Poolman's cloud model parameterises both cloud top and lateral entrainment using the entrainment scheme of Betts (1982a,b). Betts' saturation-point analysis scheme, conserves certain thermodynamic variables during cloud entrainment. This method is flexible and allows the modeller to vary the percentage of environmental air that mixes with the cloud air. The reader is referred to Betts (1982a,b) for a detailed explanation of the entrainment approach adopted in Poolman's cloud model.

After conducting sensitivity tests, Poolman selected the type and amount of entrainment that minimised the impact on updraft velocity for different types of storms (e.g., multi-cell or supercell storms). In his study, the storm type was based on ranges of CAPE and vertical wind shear. In this thesis, we relate the entrainment to the interaction of CAPE and vertical wind shear using the so-called Energy Shear Index (ESI). The precise definition of the ESI and how it is related to storm type and entrainment in central Alberta is provided in Appendix A. Table 2.1 summarises the relation between the ESI and the type and amount of entrainment used in this thesis.

For supercell storms, Poolman only used 5% cloud top entrainment, i.e., the updraft core is assumed to be almost adiabatic. Observational evidence of near adiabatic updraft cores in convective clouds exists (Heymsfield, 1978; Paluch, 1979; Bluestein, 1988). Clouds with weaker updrafts on the other hand, tend to experience more entrainment. Boatman and Auer (1983), Reuter (1985) and Blyth et al. (1988) showed that cloud top entrainment dominates in large cumulus clouds. In contrast, smaller cumulus clouds are diluted mainly by lateral entrainment (Blyth et al., 1988).

The in-cloud temperature and saturation mixing ratio are initially calculated assuming the parcel rises along the pseudo-adiabat as determined by the temperature and pressure at cloud base. The new parcel temperature and saturation mixing ratio at each level, are calculated after allowing the mixing of environmental air with the parcel.

2.2 The Hail Model

A modified version of Poolman's one-dimensional (1D) time dependent hail model forms the second part of HAILCAST. The hail model is based on the work of Musil (1970) and Dennis and Musil (1973) and simulates the time growth history of individual hailstones.

Before outlining the components of the hail model, three major assumptions will be discussed. Firstly, the modelled hailstones are assumed to be spherical. Barge and Isaac (1970), Macklin (1977) and Matson and Huggins (1980) analysed hailstones collected at the surface and found that most hailstones were oblate spheroids. In numerical simulations of hail growth, English (1973) found that oblate hail tended to grow larger than spherical hail. Secondly, the accreted water and ice is initially assumed to form a high density (0.9 gcm^{-3}) deposit. However, allowance is made for spongy growth due to partial freezing of the excess water

on the surface of the hailstone should it enter a sufficiently cold region of the cloud. During wet growth and melting, densities may be higher than 0.9 gcm^{-3}, due to the presence of meltwater on the surface of the hailstone. In this model, recycling of the larger hailstones is not observed and hailstones in the wet growth regime are unlikely to re-enter the dry growth regime when descending, precluding the occurrence of spongy growth. Thirdly, the temperature is assumed to be uniform throughout the hailstone.

2.2.1 Environmental Conditions

In order to model hail growth, the environmental conditions in which the hailstone finds itself after each time step must be specified. Vertical profiles of pressure, in-cloud temperature, saturation mixing ratio, and vertical velocity calculated by the cloud model are used for this purpose. The total cloud water at any level is calculated by subtracting the saturation mixing ratio at that level from the saturation mixing ratio at cloud base. The adiabatic LWC is then calculated by multiplying this difference by the density of the updraft air at that level. The amount of cloud ice is determined using the relation of Vali and Stansbury (1965), which depletes the cloud water exponentially from near adiabatic values at –20 °C to zero at –40 °C.

2.2.2 Growth Equations

For spherical hail, the rate of change of mass (M) due to the accretion of supercooled water droplets and ice crystals is given by

$$\frac{dM}{dt} = \frac{dM_i}{dt} + \frac{dM_w}{dt} = \frac{V_t \pi D^2}{4} [\chi_w E_w + \chi_i E_i], \qquad (2.5)$$

where M_i and M_w represent the mass of accreted ice and liquid water per unit time interval, respectively. V_t is the terminal velocity of the hailstone (cms^{-1}), D the

diameter of the hailstone (cm), χ_w and χ_i are the concentrations of cloud water and cloud ice (gcm^{-3}) respectively, E_w and E_i represent the collection efficiencies of the accreted water droplets and ice crystals respectively. The relation $V_t\pi D^2/4$, represents the volume of a cylinder swept out per unit time interval by the hailstone.

The increase in mass due to deposition is ignored, since for particles >100 μm the increase in mass due to the accretion of supercooled water and ice crystals is much greater than that due to deposition (Dennis and Musil, 1973). The collection efficiency of accreted water during wet and dry growth is assumed to be $E_w = 1.0$, while the collection efficiency of ice crystals is set to $E_i = 1.0$ during wet growth and $E_i = 0.21$ during dry growth. The above mentioned collection efficiency for ice crystals during dry growth is near the upper limit of 0.25 used in modelling studies (see Orville, 1977). Also, Geresdi (1998) used 0.2 for the collection efficiency between hail and rimed ice particles.

2.2.3 Heat Balance Equations

The heat balance equations used to calculate the hailstone's temperature and fractional water content (F_w) are the same used by Dennis and Musil (1973). The growth phase and amount of accreted water that can be frozen by a growing hailstone, are controlled by the transfer of heat to and from its surface. The heat budget of a hailstone is governed by four heat transfer terms, namely: (1) Convection and conduction (Q_k), (2) Sublimation/evaporation (Q_s), (3) Latent heat of freezing due to the accretion of supercooled water (Q_a), (4) Accretion of ice crystals (Q_c). The temperature of a hailstone undergoing dry growth, is determined by the amount of heat lost and gained by the hailstone as it moves through the cloud and accretes supercooled water and/or ice crystals. Conversely, the temperature of a hailstone undergoing wet growth is assumed to remain at 0 °C.

The total heat exchange (Q_T) per unit time interval between the hailstone and the environment is given by

$$\frac{dQ_T}{dt} = \frac{dQ_k}{dt} + \frac{dQ_s}{dt} + \frac{dQ_a}{dt} + \frac{dQ_c}{dt} \qquad (2.6)$$

The convection and conduction of heat is determined using

$$\frac{dQ_k}{dt} = 2\pi DaK(T_a - T_s), \qquad (2.7)$$

where D is the diameter of the hailstone, a is the ventilation coefficient, K the thermal conductivity, T_a and T_s represent the ambient temperature and the hailstone's surface temperature respectively. Convection and conduction cool the hailstone (negative contribution) if it is warmer than the environment. Conversely, if the hailstone's surface temperature is cooler than the environment (during melting), convection and conduction increase its surface temperature (positive contribution).

The ventilation coefficient, a, plays a critical role in regulating the rate of heat transfer to and from the hailstone. Bailey and Macklin (1968) found that the ventilation coefficient for rough spheres increases rapidly for increasing Reynolds number. We model the ventilation coefficient using the same approach as Rasmussen and Heymsfield (1987a), which accounts for the increase in ventilation coefficient for increasing Reynolds number.

The heat exchange due to sublimation or evaporation is modelled using

$$\frac{dQ_s}{dt} = \begin{cases} -2\pi D_i a L_v D\Delta\rho & \text{for } T_s \geq 0\ ^\circ\text{C} \\ -2\pi D_i a L_s D\Delta\rho & \text{for } T_s < 0\ ^\circ\text{C} \end{cases}, \qquad (2.8)$$

where L_v is the latent heat of vaporisation and L_s is the latent heat of sublimation, D_i the diffusivity (cm^2s^{-1}), $\Delta\rho$ the difference in vapour density between the hailstone surface (ρ_s) and the environmental air (ρ_e) ($\Delta\rho = \rho_e - \rho_s$). Dennis and Musil (1973) assumed the vapour density varies between saturation with respect to water and saturation with respect to ice, depending on the ambient temperature. The vapour density at the hailstone's surface is taken as saturation with respect to water during wet growth and saturation with respect to ice during dry growth. Despite making a very small contribution to the mass increase of the hailstone, the deposition/sublimation term makes an important negative/positive contribution to the hailstone's heat budget when the hailstone is small (Dennis and Musil, 1973).

The heat exchange due to the freezing of accreted water is given by

$$\frac{dQ_a}{dt} = \frac{dM_w}{dt}(L_f - C_w(T_s - T_c)), \qquad (2.9)$$

where L_f is the latent heat of freezing at 0 °C, C_w the specific heat of water and T_c the in-cloud temperature. This term is of particular importance in high LWC regions of the cloud.

The heat loss due to the accretion of cloud ice is given by

$$\frac{dQ_c}{dt} = \frac{dM_i}{dt} C_i (T_c - T_s), \qquad (2.10)$$

where C_i is the specific heat of ice. The accretion of ice crystals only involves the transfer of sensible heat and always makes a negative contribution to the hailstone's heat balance.

During wet growth, the surface temperature of the hailstone is assumed to remain at 0 °C . The rate of change of F_w is then given by

$$\frac{dF_w}{dt} = -\frac{F_w}{M}\frac{dM}{dt} + \frac{1}{ML_f}\left[\frac{dQ_T}{dt}\right]. \qquad (2.11)$$

During dry growth F_w remains zero, while the change in surface temperature with time is given by

$$\frac{dT_s}{dt} = -\frac{T_s}{M}\left[\frac{dM}{dt}\right] + \frac{1}{MC_i}\left[\frac{dQ_T}{dt}\right]. \qquad (2.12)$$

The surface temperature and F_w of the hailstone are re-evaluated at each model time step using the above equations. Depending on the heat transfer, the hailstone undergoes wet or dry growth, as it is advected through regions in the cloud having different temperature and LWC values.

2.2.4 Shedding Scheme

Rasmussen and Heymsfield (1987a) used an empirically derived linear relationship to determine the maximum amount of surface water (in g) that can be retained for a given ice core mass before shedding, namely

$$M_{crit} = 0.268 + 0.1389M_i, \qquad (2.13)$$

where M_{crit} is the critical surface water mass and M_i the mass of the ice core of the hailstone.

If the amount of water on the surface of the hailstone (determined from F_w), exceeds M_{crit}, the excess water is shed. Lesins and List (1986) found that at high rotation rates, artificial hailstones in the wet growth regime shed all the excess water and Equation 2.13, therefore, is not necessarily valid for tumbling or gyrating hail.

2.2.5 Terminal velocity

The terminal velocity is calculated in three steps, using the scheme of Rasmussen and Heymsfield (1987a):

1) Calculate the Best number (X),

$$X = \frac{8Mg\rho_a}{\pi\eta_a^2}, \tag{2.14}$$

where M is the total mass of the hydrometeor, ρ_a the air density, η_a the dynamic viscosity of air, g the gravitational acceleration.

2) Determine the particle's Reynolds number from empirical Best number-Reynolds number relations. Hailstones larger than 2 cm in diameter (Re ~ 2.4 x10^4) are assumed to have a drag coefficient of 0.6.
3) Calculate the terminal velocity using the following relationship,

$$V_t = \frac{\eta_a \mathrm{Re}}{D\rho_a} \tag{2.15}$$

After each time step the hydrometeor is advected to its new height, depending on the difference between its terminal fall speed and the model-derived updraft velocity.

2.2.6 Duration of Hailstone Growth

The hailstone's residence in the supercooled region of the cloud is critical in determining its final size (section 1.3). In HAILCAST this residence time is governed by the duration of the updraft and the maximum updraft velocity. When using a steady-state 1D model, we are required to estimate (as realistically as possible) the maximum hail growth duration. Since the ESI is a good indicator of

storm type and updraft duration (Appendix A), the upper limit on the maximum hail growth duration was determined using the ESI for each sounding as described below.

The mature phase of an air-mass thunderstorm typically lasts 20 min, while in supercell storms, the updraft can last from 1 to 3 hours. Calculations of hail growth times using a modest LWC of 2 gm^{-3}, have shown 3 cm diameter hail can be grown from a cloud droplet in 45-50 min. Based on the above-mentioned updraft durations and hail growth times, a parabolic curve was used to relate the maximum hail growth duration to the ESI.

$$\text{Maximum Hail Growth Duration (min)} = \begin{cases} 20 & ESI \le 1.0 \\ -2.5*ESI^2 + 25*ESI - 2.5 & 1.0 < ESI \le 5.0 \\ 60 & ESI > 5.0 \end{cases} \quad (2.16)$$

The parabolic curve (Figure 2.1), shows a rapid increase in updraft duration for ESI values between 1 and 3, after which the rate of increase decreases.

2.3 Hail Growth Cycle

Following Poolman (1992), the growth cycle of a hailstone in the hail model can be described as follows:

1) A drizzle sized drop (300 μm in diameter) is introduced into the updraft at cloud base. This particle acts as a hail embryo and is assumed to originate from the shedding of water by melting hail already present in the cloud (Rasmussen et al., 1984b). The hail embryo initially consists entirely of water (F_w=1) and has the same temperature as the updraft air.

2) The hail embryo grows by coalescence at it rises through the lower parts of the cloud. When the embryo passes through the –8 °C level, it is assumed to freeze spontaneously (F_w=0) and enters the dry growth regime.

4) Above –20 °C the hail embryo enters the mixed-phase zone of the cloud and grows by accreting both supercooled water and ice crystals.

5) As the hail embryo intercepts supercooled water droplets, its temperature increases due to the latent heat of freezing associated with the accreted water. If the hailstone is unable to remove the heat added through accretion of water droplets fast enough, it enters the wet-growth regime (T_s= 0°C and F_w<1). If the heat transport is sufficiently large, the hailstone remains in the dry growth regime (T_s< 0°C and F_w=0).

6) After each time step (0.1s) the hailstone's increase in mass and new diameter are calculated. Depending on the heat transfer and growth regime, the changes in T_s or F_w are calculated using equations (2.11) and (2.12) respectively. If the hailstone is in the wet growth regime, the mass of surface water is tested using equation 2.13 and excess water is shed if it exceeds the critical limit. The hailstone's new diameter is then adjusted accordingly.

7) The hailstone continues to grow and rise vertically until its fall speed exceeds that of the updraft or the updraft collapses after a finite time using equation (2.16).

8) The greatest increase in diameter occurs as the hailstone descends through the supercooled region of the cloud, since it now has a large cross-sectional area.

9) During its descent, the calculations outlined in step 6 are repeated after each time step.

10) No more growth occurs after the hailstone descends below the 0 °C level, due to the shedding of meltwater on the hailstone's surface. Some hailstones melt completely before reaching the ground, and since no drop break-up mechanism is included in the model, drops as large as 9 mm in diameter are sometimes produced.

2.4 Comments on Numerical Methods

In this thesis, the cloud model was initialized with an upper-air sounding (25 hPa vertical resolution), the maximum surface temperature and corresponding dew-point. The FORTRAN code can be amended to read various input data formats. All model runs were conducted using a 40 MHz Silicon Graphics machine and typically took less than 10 s using a time step of 0.1s.

3. MODEL CASE STUDIES OF HAIL GROWTH

In this chapter, we describe the model-derived updraft profiles and hail growth time histories, for a severe and non-severe thunderstorm environment. The two days selected for this purpose are both characterised by relatively high CAPE, suggesting the presence of strong updrafts and thus the potential for severe hail. However, the cases differ in the amount of vertical wind shear. We show this determines the ESI, which impacts the modelled convective updraft strength and duration, as well as the hail growth.

3.1 Observed Synoptic Situation and Weather Conditions

3.1.1 11 July 1985

This day occurred during LIMEX-85 (Limestone Mountain Experiment-85), and it has been studied extensively by Smith and Yau (1993). We now briefly review the synoptic and observed weather conditions on this day.

After 1600 LDT (Local Daylight Time), several multi-cell storms developed in the foothills north of Rocky Mountain House and moved eastwards onto the plains. The maximum reflectivities of the most intense storms were observed to exceed 60 dBZ for several hours. A total of 228 hail reports were received within the northern-half of the Alberta Hail Project (AHP) area, of which 33 were severe (Deibert, 1985). The largest reported hail size was classified as golfball (3.3 to 5.3 cm in diameter) and the longest observed hailswath was estimated to be over 200 km long.

A short-wave trough upstream of central Alberta at 1800 LDT (Figure 3.1) dominated the upper-air circulation on this day. A mid-level jet (winds >25ms^{-1})

extended from southern British Columbia through central Alberta. At the surface, a closed low in southern Alberta resulted in a moist north-easterly upslope flow in the low levels (not shown). By 1800 LDT, a tongue of moist air (dew-points >10 °C) was orientated east-west over central Alberta, with the highest dew-points (greater than 12 °C) extending from north of Rocky Mountain House in the west, to Llyodminster in the east.

The most prominent features of the 1800 LDT upper-air sounding released from Penhold, are the strongly sheared wind profile and relatively high buoyant energy (Figure 3.2). The CAPE calculated from this sounding is 756 Jkg^{-1}. Easterly to north-easterly winds of 5 ms^{-1} in the boundary layer, veer to a west-south-westerly jet of 40 ms^{-1} near the tropopause (200 hPa).

The above synoptic setting satisfies all the criteria outlined in section 1.2 for severe thunderstorm outbreaks in central Alberta, namely: The presence of high latent and sensible energy in the PBL, high CAPE and veering of the wind profile in the lowest 3 km AGL. Moreover, the uplift and cooling aloft associated with the approaching trough, coincided with the maximum latent and sensible energy in the PBL. The combination of the above factors removed the capping lid present earlier in the day and provided a trigger mechanism to initiate and sustain vigorous convection.

3.1.2 24 August 1983

Numerous moderate intensity and disorganized storms developed in the mid-afternoon along the foothills west of Penhold and dissipated as they moved eastwards (Renick, 1983). Only 10 hail reports were received in the AHP area, with the largest observed hail being pea size (0.4-1.3 cm in diameter).

No significant upper-air trough was evident over or upwind of central Alberta on this day (Figure 3.3), with light north-westerly winds aloft. The

surface circulation was also dominated by light north-westerly winds. The PBL over central Alberta was moist with surface dew-points near 10 °C.

Figure 3.4 shows the 1800 LDT sounding released from Penhold. The atmosphere is conditionally unstable, with a CAPE of 1063 Jkg^{-1}. The wind profile is characterised by light north-westerly winds in the lower half of the troposphere, backing to south-westerly winds of 13 ms^{-1} near the tropopause (250 hPa).

Despite the abundance of CAPE, the above mentioned circulation pattern does not satisfy all the criteria required for severe thunderstorm outbreaks outlined by Smith and Yau (1993). This can mainly be attributed to the absence of an upper-air trough upwind of central Alberta and in turn the lack of vertical wind shear. Moreover, Smith and Yau noted that 50% of no-hail days in central Alberta are characterized by north-westerly surface winds and 45% by north-westerly winds at 500 hPa. Therefore, the disorganised and short-lived convection observed on this day, is consistent with the observed atmospheric conditions.

A number of thermodynamic and wind-derived parameters describing the thunderstorm environment on the above days are listed in Table 3.1.

3.2 Modelled Cloud Profiles and Hail Growth

3.2.1 11 July 1985

The relatively high CAPE of 756 Jkg^{-1} and strong vertical wind shear (6.5 $x10^{-3}$ s^{-1}) shown in Table 3.1, indicate the potential for strong and sustained deep convection. Moreover, the above CAPE implies a maximum buoyancy-derived

updraft velocity of 38.8 ms^{-1} capable of supporting large hail (approximately 5 cm in diameter) aloft.

Table 3.2 shows some of the environmental and model parameters utilized in the HAILCAST run for this day. The Energy Shear Index (ESI) of 4.9 m^2s^{-3}, implies the potential for strong multi-cell thunderstorms as described in Appendix A. The expected convection is classified by HAILCAST as a strong multi-cell thunderstorm and the updraft is modelled using 7.5% cloud top entrainment (see Table 3.2). The updraft duration is almost 60 min, consistent with CAPPI (Constant Altitude Plan Position Indicator) radar reflectivity data, which indicated that some of the convective cells lasted about one hour (Smith and Yau, 1993).

Figures 3.5 (a,b) show the model-derived profiles of updraft velocity and LWC. The vertical velocity increases from 4.0 ms^{-1} at cloud base to a maximum of 26.9 ms^{-1}. This is 69.3% of the maximum buoyancy derived value (determined using $W_{max}= [2*CAPE]^{0.5}$). The maximum updraft occurs in the mixed phase zone of the cloud near –23.0 °C (approximately 6750 m AGL). Above this maximum, the updraft velocity decreases rapidly to 0 ms^{-1} at the forecast cloud top near –49.6 °C (9700 m AGL). Figure 3.5b shows that the LWC increases from 0 gm^{-3} at cloud base to a maximum of 3.5 gm^{-3} at -26.4 °C (approximately 7200 m AGL). This closely corresponds to the height of the forecast maximum updraft velocity. Above this maximum, the water and ice content decreases to 3.0 gm^{-3} at the cloud top, where the cloud consists entirely of ice crystals.

Figure 3.6 (a-e) shows the growth time history of a hailstone simulated by the hail model. Depicted are the height (Z); in-cloud (TC) and hailstone temperature (TS); ground relative (VR) and updraft velocity (VU); growth rate (dD/dt); diameter (D) and finally the fractional liquid water content (F_w).

We will now discuss the model results depicted in Figure 3.6. Note that the term hailstone is extended to ice particles with diameters less than 5 mm. A 300

μm drop is introduced into the updraft at cloud base. The drop is then carried rapidly upwards, since its terminal velocity (approximately 1.0 ms^{-1}) is much lower than the updraft speed (>4 ms^{-1}). Initially the droplet consists entirely of water, but freezes after passing through the –8 °C level and enters the dry growth regime. The hailstone continues to rise rapidly through the supercooled region of the cloud and is 2 mm in diameter when it reaches the –40 °C level after 9 min. During this time, the hailstone remains in the dry growth regime and grows by accreting supercooled water droplets and ice crystals (above –20 °C). Due to the small diameter of the hailstone and short residence time in the supercooled region of the cloud, the rate of growth is slow (< 0.05 cm/min). There is, however, a slight increase in the growth rate between 6 and 8 min coinciding with the passage through the region of maximum LWC.

Near the –40 °C level, the difference between the hailstone's terminal velocity and the updraft speed decreases. The hailstone's rate of ascent now slows and it reaches the apex of its trajectory near 9670 m AGL (after 12 min). Between 12 and 46 min, the updraft velocity slightly lags behind the hailstone's increasing terminal velocity and the hailstone begins to gradually descend, while slowly accreting ice crystals (growth rate < 0.05 cm/min).

After 46 min the hailstone descends below the –40 °C level and once again enters the mixed-phase region of the cloud. This initiates a period of rapid growth between 46 and 57 min, since the hailstone is now 1.3 cm in diameter and located in a region of high LWC. The growth rate reaches a maximum of 0.41 cm/min at 57min (near the –20 °C level). During its descent, the hailstone encounters strong updrafts and is prevented from falling prematurely from the cloud. This maximises the hailstone's residence time in the Hail Growth Zone (HGZ) and allows the hailstone to grow substantially from 1.3 cm to 5 cm in diameter during its 14 min passage though the supercooled region of the cloud.

As the hailstone accretes water in the supercooled region of the cloud, the latent heat of freezing causes the hailstone's surface temperature to rise steadily and it enters the wet growth regime after 58 min at an in-cloud temperature of –12.6 °C. After 58 min, the shedding of excess water on the hailstone's surface slows the rate of growth. The maximum diameter of almost 5.0 cm is attained after 60 min and decreases thereafter due to melting below the freezing level. When the hailstone is near 3590 m AGL (-1.2 °C), the updraft collapses and the hailstone spends less than 3 min below the freezing level, despite a marked decrease in its terminal velocity due to melting. The hailstone reaches the ground after 62 min, with a final diameter of 4.1 cm (terminal velocity 28.5 ms^{-1}) and F_w of 0.13. Given the hailstone's low F_w (indicative of hard hail) and high impact velocity, it is expected that the modeled hailstone would be capable of causing serious damage.

3.2.2 24 August 1983

Table 3.1 lists the various thermodynamic and wind derived parameters for this day. Despite the high CAPE (1076 Jkg^{-1}), the lack of vertical wind shear yields an ESI of only 0.5 m^2s^{-3}. HAILCAST classifies the expected convection as a weak air-mass thunderstorm and the updraft is modelled using 10% lateral entrainment (Table 3.2). As shown below, this has a major impact on the maximum updraft velocity and size of hailstone capable of being supported by the updraft. The hail is modelled using an updraft duration of 20 min, consistent with the air-mass thunderstorms expected on this day.

Profiles of model-derived updraft velocity and LWC calculated by the cloud model are represented by the dashed lines in Figure 3.5(a, b). The vertical velocity increases from 4 ms^{-1} at cloud base to a maximum of 13.7 ms^{-1} at –2.8 °C (approximately 3250 m AGL). The maximum forecast updraft velocity is only 29.7% of the maximum buoyancy derived velocity of 46.1 ms^{-1}. Above this maximum, the updraft velocity decreases rapidly to 0 ms^{-1} at the forecast cloud

top near –29.0 °C (6660 m AGL). Figure 3.5b shows that the LWC increases from 0 gm^{-3} at cloud base to a maximum of 4.3 gm^{-3} at –24.9 °C (approximately 5800 m AGL). Above this maximum, the LWC decreases slightly to 4.2 gm^{-3} at the cloud top, where the cloud is composed of supercooled cloud droplets and ice crystals.

The time history of a modelled hailstone is shown in Figure 3.7 (a-e). The growth cycle and trajectory of the modeled hailstone on 24 August 1983 differs from that on 11 July 1985. A 300 μm drop introduced into the updraft at cloud base enters the dry-growth regime after rapidly rising above the –8 °C level. The hailstone is 5 mm in diameter when it reaches the top of its trajectory (5520 m AGL or -18 °C) after 12 min. As with the first case study, the rapid upward movement through the cloud is due to the particle's terminal velocity initially being much lower than the updraft speed. However, on this day, the maximum updraft velocity and height thereof are both much lower. As a result, the particle follows a lower trajectory through the cloud and never enters the mixed-phase zone or reaches the level of maximum LWC.

Due to the latent heat released by the freezing of supercooled water, the hailstone's surface temperature starts to deviate from the in-cloud temperature and it enters the wet growth regime after 15 min. Between 12 and 19 min the growth rate and diameter increase almost linearly and the hailstone continues to descend steadily through the cloud, despite encountering higher updraft velocities. The maximum growth rate of 0.24 cm/min occurs at 18 min near –8.0 °C and the hailstone reaches a maximum diameter of 1.9 cm after 19 min. The hailstone starts shedding excess unfrozen water near the –12.0 °C level.

The updraft collapses after 20 min when the hailstone is 3176 m AGL (-2.0 °C). As a result, the hailstone rapidly descends below the freezing level, but its rate of descent is slowed due to the shedding of excess meltwater. The hailstone spends less than 3 min below the freezing level and reaches the ground with a

final diameter of 1.2 cm (terminal velocity 13.6 ms^{-1}) and F_w=0.3. The small diameter and high fractional water content, suggest that hail produced by the model, would not be capable of causing serious damage.

3.3 Summary

The model-derived cloud profiles and hail growth time histories have been discussed for a severe and non-severe hail day. The thunderstorm environment observed on both days and how the respective updraft characteristics impacted the modelled hail growth are summarised below.

The thunderstorm environment on 11 July 1985 was characterised by relatively high instability and strong veering of the winds in the lowest 6 km AGL. As a result, long-lived multi-cell storms developed and produced golfball size hail at the ground. Based on an ESI of 4.9 m^2s^{-3} (calculated from a proximity sounding), HAILCAST classified the expected convection as a strong multi-cell thunderstorm, with an updraft duration of almost 60 min. The model-derived maximum updraft velocity on this day was 69.3% of the maximum buoyancy derived value.

Despite being rapidly carried aloft by the strong updrafts, the hailstone re-entered the mixed-phase zone of the cloud with a diameter of 1.3 cm and was prevented from prematurely falling from the cloud by strong updrafts. The presence of strong updrafts also maximized the hailstone's residence time in the HGZ (approximately 12 min) and the model forecast a maximum hail size of 4.1cm at the ground, which agrees well with the maximum observed hail size (i.e., golfball).

In contrast, on 24 August 1983 the atmosphere was also unstable, but lacked the vertical wind shear and this precluded the formation of organised and long-

lived thunderstorms. The ESI calculated from a proximity sounding was only 0.5 m^2s^{-3}. HAILCAST classified the expected convection as a weak air-mass thunderstorm, with an updraft duration of 20 min. The model-derived maximum updraft velocity was only 29.7% of the maximum buoyancy derived value and this significantly reduced the size of hail capable of being supported aloft. Further, the forecast trajectory within the cloud was very low and the hailstone never reached the level of maximum LWC or entered the mixed-phase region of the cloud. Due to low updraft velocities, short residence time in the HGZ and low trajectory within the cloud, the maximum forecast hail size at the ground was only 1.2 cm.

Had the convection on 24 August 1983 been modelled using 5% cloud top entrainment (used to model a supercell updraft) and updraft duration of 60 min, HAILCAST would have forecast a maximum updraft velocity of 28.4 ms^{-1} (near – 35.0 °C) and 4.1cm hail at the ground. Further, applying this maximum updraft velocity to the nomogram developed by Renick and Maxwell (see section 1.4.2), yields a maximum forecast hail size between 2.1 and 3.2 cm, which is considerably larger than the maximum observed hail size. This emphasises the importance of taking the combined effects of CAPE and vertical wind shear into consideration when modelling the strength and duration of convective updrafts. Moreover, it illustrates how entrainment reduces the maximum updraft velocity and height at which it occurs within the cloud. To date, most operational hail forecasting techniques have either neglected or only used a fixed rate of entrainment when calculating the maximum updraft velocity. This maximum updraft velocity is then used to infer the maximum hail size at the ground, using a nomogram or other empirical techniques. It is likely therefore, that these techniques would tend to overestimate hail size on days characterised by high CAPE and minimal vertical wind shear.

The above case studies also highlighted the importance of residence time in the HGZ for hail growth. This is consistent with observations and modelling

studies of hail growth (e.g., Foote, 1984; Miller et al., 1988). Of particular significance, is the hail model's ability to correctly reproduce some of the major hail growth characteristics observed by other researchers. For example, the greatest forecast hail growth (>0.3 cm/min) on 11 July 1985 occurred between –10 °C –30 °C, in close agreement with the location of the HGZ described in section 1.2. Further, shedding of excess meltwater was forecast to occur near –12.0 °C on both days, which closely agrees with the threshold for shedding determined in laboratory experiments by Carras and Macklin (1973).

In closing, for the above case studies, the modelled updraft profile and duration were consistent with the observed CAPE and vertical wind shear. Moreover, we have shown that the hail growth model reproduced the fundamental hail growth mechanisms and produced realistic hailstones at the ground in accordance with the modelled updraft characteristics.

4. MODEL SENSITIVITY EXPERIMENTS

The objective of this chapter is to determine the sensitivity of HAILCAST to small changes in input sounding data, entrainment and microphysical parameters. The control for the sensitivity experiments is based on a severe hailstorm sounding observed on 11 July 1985 (see section 3.1.1).

4.1 Sensitivity Experiments- Cloud Model

In this section, we investigate the sensitivity of the model derived updraft profiles and hail size to small changes in surface temperature, surface dew-point, magnitude of the vertical wind shear and amount of cloud entrainment.

4.1.1 Sensitivity to Surface Temperature and Dew-point

The location and timing of convection initiation depends crucially on the surface temperature and moisture content in the PBL. An air-mass is rarely homogeneous in space and time, and variations in static stability within an air mass are caused by changes in moisture and temperature resulting from mesoscale features such as outflow boundaries (Mueller et al., 1993).

When forecasting maximum hail size, the accurate modelling of the updraft profile and maximum updraft velocity are crucial. Further, changes in surface temperature and surface moisture affect the CAPE, and thus the strength of convection. For example, Bunkers (1996) found a significant difference in CAPE (1000 Jkg^{-1}) determined using the observed surface and mixed layer moisture (lowest 100 hPa). Similarly, Crook (1996) found small variations in surface temperature (1 °C) and moisture (1 gkg^{-1}) could differentiate between no convection and intense convection. Also the modelled maximum vertical velocity

was most sensitive to changes in the surface temperature at the convection/no convection boundary. However, once convection was established, the maximum vertical velocity was more sensitive to changes in the surface mixing ratio.

Table 4.1 lists the sensitivity experiments. Surface temperature and dew-point were varied between 2 °C below and 2 °C above the control values, using increments of 0.5 °C. The above ranges are based on variations in surface temperature and dew-point observed within mesonetworks (Mueller et al., 1993; Crook, 1996;). In Table 4.1, the strength of the simulated convection is quantified in terms of the model derived maximum updraft velocity (W_{max}) and temperature at which W_{max} is observed (T_{wmax}).

Figure 4.1 shows W_{max} increases monotonically for increasing temperature and dew-point, with the strongest updraft modelled for the highest temperature and lowest dew-point depression. Regarding T_{wmax}, higher temperatures and dew-points led to updraft maxima occurring at higher altitudes within the modelled cloud (Figure 4.2). These results are consistent with parcel theory: As the latent energy and sensible energy increase in the PBL, so does the buoyant energy and strength of the resulting cloud updraft.

W_{max} is clearly sensitive to small changes in surface temperature and dew-point. For example, a 1°C increase in temperature or dew-point increases W_{max} by 20% or more. This is equivalent to increasing the maximum hail size capable of being supported by the updraft from 2.2 cm to 3.5 cm (estimated using a drag coefficient of 0.55 at –20 °C) or approximately an increase in diameter of 50%. T_{wmax} is also sensitive to small changes in the temperature, and increasing the surface temperature or dew-point by 1 °C decreases T_{wmax} by about 30%. The changes in updraft strength and profile resulting from small variations in the surface thermodynamic variables have important implications for hail growth. Since the updraft strength affects the size of the hailstone capable of being

suspended in the storm, the height of the stone's trajectory and its residence time in the supercooled region of the cloud.

The impact of changing surface temperature and dew-point on the maximum hail size is shown in Figure 4.3. Figure 4.3 suggests large hail is modelled in the vicinity of the line joining the points (T= 27 °C; T_d = 11.5°C) and (T= 28.5 °C; T_d = 9 °C). This region represents an optimum range of W_{max} (23 ms^{-1} to 30 ms^{-1}) and T_{wmax} (-18 °C to –27 °C) associated with large hail forecast at the ground. To the left of this axis, increasing the temperature and/or dew-point is associated with larger hail. The largest hail (~4.6 cm) is predicted for a surface temperature and dew-point of ~27 °C and ~12 °C respectively (W_{max} ~30 ms^{-1} and T_{wmax} ~ –25 °C). For temperatures and dew-points greater than these "optimum" values, the maximum predicted hail size begins to decrease. This is contrary to the simple (but apparently faulty) notion that higher temperatures and dew-points lead to larger hail. To explain this discrepancy, hail growth time series for 3 trajectories determined using different surface temperature and dew-points (see points A-C on Figure 4.1) were constructed (Figure 4.4 a-c). Point B (hailstone B) represents the control. We recall that the maximum observed hail size on this day was golfball (3.3 cm to 5.2 cm).

Figure 4.4 compares the trajectories and hail size of the 3 cases. Due to the stronger updrafts experienced by hailstone C, it remains above –40 °C for 53 min versus 36 min for hailstone B. As a result, hailstone C is still in the glaciated portion of the cloud when the updraft collapses after 60 min and only spends 3 min (compared to 14 min for hailstone B) in the supercooled region of the cloud during its descent. This drastically reduces the mass of supercooled water (and ice) hailstone C accretes during its downward trajectory, resulting in a final diameter of only 2.1 cm versus 4.1 cm for hailstone B. Moreover, the W_{max} and T_{wmax} corresponding to point C on Figure 4.1, do not lie within the optimum range of values mentioned in the previous paragraph (Table 4.1).

In contrast, hailstone A never enters the glaciated portion of the cloud, because of its lower W_{max} and warmer T_{wmax}. As a result, hailstone A grows fast enough to reach the ground as a 2.5 cm hailstone before the updraft collapses. Due its favourable trajectory, it appears W_{max} is the primary limiting factor in determining the maximum hail size of hailstone A and not the updraft duration (maximum hail growth time). Once again, the W_{max} and T_{wmax} corresponding to point A, do not lie within the window for large hail growth.

Figure 4.3 also shows that no severe hail is forecast for $W_{max} < 18$ ms^{-1} and $T_{wmax} > -15$ °C. Hailstones growing in such an updraft profile would unlikely reach severe hail size, owing to the weak updrafts and relatively warm in-cloud temperatures encountered during their passage through the cloud.

The above findings suggest the following: On days with strong updrafts and $T_{wmax} < -27$ °C, the maximum predicted hail size is sensitive to the upper-limit of 60 min placed on the updraft duration. Under such conditions, the modelled hailstone does not always descend below –40 °C before the updraft collapses. Without updrafts to prolong its residence time in HGZ, the hailstone then falls rapidly through the mixed-phase zone of the cloud, thereby reducing its final diameter at the surface. The observation of an optimum level of T_{wmax} was also found in modelling studies conducted by Dennis and Musil (1973). They noted that although the final hailstone diameter increased for increasing W_{max}, the maximum diameter was strongly influenced by T_{wmax}, with the largest hail being favoured for T_{wmax} values near –30 °C. For values of T_{wmax} less than –30 °C, Dennis and Musil (1973) proposed that hail becomes trapped above the HGZ in the glaciated portion of the cloud and the maximum predicted hailstone diameter at the ground is limited by the finite lifetime of the cloud.

4.1.2 Sensitivity to Entrainment

The realistic modelling of cloud entrainment ideally requires a time dependant 3D cloud model (see discussion in section 2.1.2). Further, although we refer to two different entrainment mechanisms, what is modelled by HAILCAST as lateral entrainment, in reality could have occurred as cloud top entrainment earlier in the cloud's lifetime.

Sensitivity experiments were conducted for lateral and cloud top entrainment between 0-10% (Table 4.2). Using 5% lateral entrainment lowers W_{max} from 28.6 ms^{-1} to 21.9 ms^{-1} and significantly increases T_{wmax} from –30.2 °C to –14.1 °C. This in turn influences the hail growth, with slightly larger hail produced (2.5 cm versus 2.3 cm). This can be attributed to the higher T_{wmax}, which allows the modelled hailstone to spend most of its lifetime within the supercooled region of the cloud and reach the ground before the updraft collapses. When the lateral entrainment is increased to 10%, the lower W_{max} (18.1 ms^{-1}) and higher T_{wmax} (-12.4 °C), result in only 1.5 cm hail reaching the ground.

Table 4.3 shows that using 5% cloud top entrainment has very little impact on W_{max} (27.2 ms^{-1} versus 28.6 ms^{-1} for the control). The higher entrainment does, however, increase T_{wmax} form -30.2 °C to –26.3 °C, resulting in a shorter residence time of the hailstone above –40 °C and larger hail at the ground (3.9 cm versus 2.3 cm for no entrainment). This once again highlights the sensitivity of the modelled hail growth to the residence time above –40 °C and the location of the hailstone relative to the –40 °C level when the updraft collapses. Increasing the cloud top entrainment to 10% also has minimal impact on W_{max} (26.2 ms^{-1}), but increases T_{wmax} from –26.3 °C to –22.6 °C. The modelled hailstone size is now slightly smaller than the 5% entrainment case (3.7 cm versus 3.9 cm), but the hailstone reaches the ground sooner (58.3 min versus 62.8 min). This underscores the enhanced hail growth experienced by the hailstone along its lower trajectory within the storm.

The above sensitivity tests have shown that including entrainment in the updraft calculations lowers W_{max} and increases T_{wmax} from values obtained for adiabatic ascent. In HAILCAST, an increase in lateral entrainment has a more pronounced impact on W_{max}, T_{wmax} and the modelled hail size than for an equivalent increase in cloud top entrainment. There is an increase in forecast hail size when the entrainment is increased from 0% to 5% for both cloud top and lateral entrainment. This can be attributed to the longer residence time of the modelled hailstone in the supercooled portion of the cloud on such occasions.

4.1.4 Sensitivity to Vertical Wind shear

Changes in vertical wind shear also impact the modelled updraft profile and hail size. The type and amount of entrainment are determined by the Energy Shear Index (ESI), which depends on the wind shear (see Appendix A). To determine the impact of wind shear on the updraft profile and hail growth, the wind shear was varied over a range of 40% above and below the control case value.

Table 4.4 suggests W_{max} and T_{wmax} are not significantly influenced by changes as large as 20% in the vertical wind shear. This is because the resultant ESI values (2.9 m^2s^{-3} to 4.9 m^2s^{-3}) all fall within ESI ranges corresponding to cloud top entrainment and small changes in cloud top entrainment have little impact on W_{max} and T_{wmax} (see section 4.1.3)

The changes in ESI also impact the maximum hail growth time (see Chapter 2, section 2.2.5). Table 4.4 shows the modelled updraft duration decreases from 60 min (ESI of 4.9 m^2s^{-3}) to 49 min (ESI of 2.9 m^2s^{-3}) when the vertical wind shear is decreased by 40%. This results in a marked decrease in predicted hail size from 4.1cm to 2.3 cm. As mentioned previously, an upper threshold limit of 60 min is placed on the maximum hail growth time in HAILCAST, even for ESI values >5.0 m^2s^{-3}. Therefore, increasing the wind shear above the control value

has little impact on the forecast maximum hail size, since the maximum hail growth duration for the control is very close to 60 min (Table 4.4).

The sensitivity results indicate that a 20% change in wind shear usually has little effect on the modelled hail size. However, the same may not be true on days when the ESI approaches the threshold of 1.0 m^2s^{-3} that discriminates between cloud top entrainment and lateral entrainment. This is illustrated on 2 August 1984, a day with a high CAPE of 2518 Jkg^{-1}, but little vertical wind shear ($3.8x10^{-4}$ s^{-1}). These conditions yielded an ESI of only 0.9 m^2s^{-3} and the updraft was modelled using 10% lateral entrainment (Table 4.5). The resulting W_{max} and T_{wmax} were 29.6 ms^{-1} and –20.5 °C respectively, indicating a favourable updraft profile for the growth of large hail. However, due to the short updraft duration of 20 min, only small hail aloft was modelled and melted before reaching the ground (not shown). When the vertical wind shear was increased by 5%, the ESI increased to 1.1 m^2s^{-3} and the storm was modelled using 10% cloud top entrainment. As a result, W_{max} increased to 39.1 ms^{-1}, T_{wmax} decreased to –35.8 °C and the maximum hail growth duration increased marginally to 20.2 min. HAILCAST now predicted a maximum hail size of 1.6 cm at the ground, which agreed with the maximum observed hail size on this day. Further increases in the vertical wind shear (and ESI) resulted in progressively larger hail, due to the increase in the maximum predicted hail growth time (Table 4.5).

4.2 Sensitivity Experiments - Hail Model

In this section, the focus is on the model sensitivity to changes in selected microphysical parameters and parameterisation schemes. Hail growth is a complicated process and is influenced by many factors. However, we will only investigate the model sensitivity for those factors considered most important to the hail growth process.

4.2.1 Embryo Diameter

The diameter of the hail embryo introduced at the base of the updraft was increased from 100 μm to 1000 μm in increments of 100 μm. All the sensitivity experiments were run using the control updraft profile and in-cloud properties based on the sounding and observed surface conditions of 11 July 1985.

Table 4.6 indicates that the final predicted hail size is not sensitive to changes in embryo diameter for embryos larger than 300 μm. The time to ground, however, decreases from 61.9 minutes to 50.9 minutes for a 300 μm and 1000 μm embryo respectively. A 100 μm hail embryo introduced at the base of the updraft, is only predicted to reach the ground as a 1.5 cm hailstone after 66.5 min, compared to 4.1 cm for the control (300 μm).

Figure 4.5 (a-c) shows the time histories of 3 hailstones initialized using a 100 μm (A), 300 μm (B) and 1000 μm (C) hail embryo respectively. Due to its larger diameter, hailstone C takes longer to reach –40 °C and is slightly larger than the other hailstones at this level. Thus, hailstone C soon accumulates sufficient mass to descend below –40 °C and enters the supercooled region of the cloud before the updraft collapses. Hailstone C reaches the ground after 50.9 min as a 3.9 cm hailstone. Hailstone A, however, is smaller than the others when it reaches –40 °C and due to its lower terminal velocity, becomes trapped in the glaciated portion of the cloud. Moreover, because of its smaller diameter and growth rate, hailstone A only re-enters the supercooled region of the cloud shortly before the updraft collapses. Hailstone A then rapidly descends through the HGZ and is only 1.5 cm in diameter when it reaches the ground after 66.5 min.

The above sensitivity experiments indicate that on days with strong updrafts, the final predicted hail size is not sensitive to the initial embryo diameter provided the initial hail embryo exceeds 300 μm. The time to reach the ground however, is

significantly reduced for the larger embryos. This is due to their lower trajectory and larger cross-sectional area, which increase the residence time and growth rate in the HGZ during their descent. Conversely, if the hail embryo is smaller than 200 μm, it is rapidly advected above –40 °C and becomes trapped in the glaciated portion of the cloud. The final hail size is now strongly dependant on the hailstone's position with respect to the –40°C level when the updraft collapses. Should the updraft collapse before the hailstone re-enters the supercooled region of the cloud, the hailstone rapidly descends through the HGZ and is much smaller when its reaches the ground. These results are consistent with the findings of English (1973). She found that in modelled storms with weak updrafts, a wide range of embryo sizes (300-800 μm) could produce the same maximum hail size. However, for storms with strong updrafts (>25 ms^{-1}), the largest hail was only modelled using embryos >800 μm. The reason for the higher embryo diameter threshold in the English (1973) study, is because the hail embryos were introduced in a region of stronger updrafts higher in the modelled cloud.

4.2.2 Collection Efficiency of Ice

Model studies use a wide range of values for the collection efficiency of ice crystals (E_i) during dry growth, with E_i values varying between 0.1 and 0.25 (Orville, 1977). Table 4.7 lists sensitivity experiments for E_i values over this range.

Ice collection efficiencies less than 0.2, lead to smaller hail and longer hail growth times. For example, for E_i=0.1, 1 cm hail is predicted at the ground after 69 min, versus 4.1 cm after 61.9 min for E_i=0.21. Increasing E_i between 0.2 and 0.25 has a negligible impact on the final hail size, but the time for the hail to reach the ground decreases from 61.9 min to 56.1 min. A critical range of E_i values from 0.16 to 0.19 seems to impact the hail growth, with the modelled hail diameter doubling from 1.5 cm to 3.2 cm over this range.

Figure 4.6 (a-c) shows the growth of 3 hailstones using E_i values of 0.15 (hailstone A), 0.21 (hailstone B) and 0.25 (hailstone C) respectively. The three hailstones follow almost identical trajectories until they are carried above the –40 °C level. However, once in the glaciated portion of the cloud, hailstone A grows slower than B and C, and when the updraft collapses it is still located above –40 °C. Hailstone A then rapidly descends through the HGZ and reaches the ground as a 1.4 cm hailstone. Hailstone C on the other hand, accretes ice crystals much faster (due to the higher E_i) and descends below –40 °C after approximately 36 min. This is followed by a rapid increase in diameter as it descends through the HGZ and reaches the ground as a 3.9 cm hailstone after 56.1 min. The control (hailstone B) behaves in a similar fashion, but due to the lower E_i, only descends below –40 °C after approximately 45 min and is 4.1 cm in diameter when it reaches the ground after 61.9 min.

The above experiments indicate that the maximum modelled hail size at the ground, is only sensitive to the E_i when hailstones are advected above –40 °C. If the E_i is too small, hailstones become trapped above –40 °C and are unable to re-enter the supercooled region of the cloud before the updraft collapses. This in turn significantly reduces their residence time in the HGZ and results in smaller hail at the ground.

4.2.3 Liquid Water Content

The presence of supercooled water is a necessary condition for the growth of hail, with high LWC favouring rapid growth (see discussion in section 1.3). In HAILCAST, the updraft is assumed to be near adiabatic for supercell storm environments, with increasing entrainment (sub-adiabatic LWC values) for environments with less CAPE and vertical wind shear (see Appendix A).

In the sensitivity experiments we reduced the LWC between 100% and 75% of the control value (determined using 7.5% cloud top entrainment). Reducing the

LWC by 10% results in a marked decrease in the forecast hail size and increase hail growth time, with 2.5 cm hail predicted to reach the ground after 64.7 min. When the LWC is reduced by 25% only 0.9 cm hail is predicted to reach the ground after 67.7 min (not shown). Time histories of hailstones growing in clouds with sub-adiabatic LWC (not shown) indicate that hailstones tend to follow higher trajectories within the cloud, since they accrete less mass during their upward trajectory. As a result, in convective clouds with sub-adiabatic LWC, hailstones are more likely to become trapped in the glaciated portion of the cloud. The hailstones then either fail to descend below –40 °C before the updraft collapses, or accrete less supercooled water and cloud ice as they pass through the HGZ during their downward trajectory. This ultimately leads to smaller hail at the ground. These results are consistent with findings reported by Ziegler et al. (1983), Rasmussen and Heymsfield (1987c) and Miller et al. (1990).

4.2.4 Ventilation Coefficient

Rasmussen and Heymsfield (1987a) (hereafter referred to as RAH87) used the heat transfer coefficient determined experimentally by Bailey and Macklin (1968). When calculating the ventilation coefficient, this heat transfer coefficient takes into account the increased heat transfer from naturally rough hailstones for increasing diameter. To validate the importance of increased heat transfer for the growth of large hail, sensitivity experiments were conducted using the ventilation coefficient calculations of Pruppacher and Rasmussen (1979) (hereafter referred to as PAR79) and those of RAH87. Figure 4.7 shows the increase in the magnitude of the ventilation coefficient with higher Reynolds number using RAH87 and PAR79. An additional experiment was conducted using a heat transfer coefficient (χ) of 0.60, versus the control value of 0.76 used in HAILCAST.

Table 4.8 (a-c) indicates that the ventilation coefficient scheme is critical for the growth of large hail. The model run using PAR79 predicts a final hail

diameter at the ground of only 1.7 cm versus 4.1 cm for the control run. Figure 4.8 shows that during the upward pass through the cloud, the trajectories and characteristics of the two hailstones are identical. However, once they re-enter the supercooled region of the cloud, the temperature of the hailstone modelled using PAR79 starts to rise faster than the control, enters the wet growth regime sooner (52 min versus 56 min for the control) and starts shedding excess water after approximately 54 min. At this point, the hailstone is in a region of high LWC and relatively warm in-cloud temperatures (>-20 °C) and due to the reduced heat transfer, is unable to freeze any of the accreted water and ice. The hailstone subsequently starts to shed the excess water on the surface. This leads to a reduction of mass and the hailstone reaches the ground with a diameter of only 1.7 cm.

Changes in the heat transfer coefficient from 0.76 to 0.6 (for Reynolds numbers greater than 24000) had no impact on the final hail size on the day in question. Rasmussen and Heymsfield (1987b) found for melting hail, there was a slight increase (approximately 1mm) in the model predicted hail size when the heat transfer coefficient was reduced from 0.76 to 0.6. The scheme used by RAH87 is considered more appropriate than that of PAR79 when modelling the heat transfer from hailstones, since the ventilation coefficient used by PAR79 was determined for water droplets less than 2.5 mm in diameter. Thus, it is considered inappropriate to apply their equations to hailstones several cm in diameter. Moreover, the increased heat transfer from large artificial hailstones has been confirmed in recent wind tunnel experiments (Greenan and List, 1995).

4.2.5 Terminal Velocity Scheme

The hailstone's trajectory and residence time in the HGZ also depends on the terminal velocity of the growing hailstone. Thus, changes in the terminal velocity influence the hail growth process. Perhaps the most uncertainty associated with the calculation of terminal velocity for hailstones, is selecting the appropriate drag

coefficients and determining over which diameter ranges they apply. Macklin and Ludlam (1961) found that a drag coefficient (C_D) of approximately 0.6 is a reasonable mean for hailstones > 1 cm in diameter. Böhm (1992) calculated that the drag coefficient converges to 0.598 for increasing diameter of spheroidal hailstones. English (1973) on the other hand, used a constant drag coefficient of 0.55 when calculating the terminal velocity of rough spherical hailstones. Rasmussen and Heymsfield (1987a) used a drag coefficient of 0.6 for Reynolds numbers greater than $2x10^4$ (>2 cm diameter).

In light of the aforementioned variability in the drag coefficient, sensitivity experiments were conducted to determine the role of different drag coefficients on hail growth, when applied to various diameter ranges. The results are listed in Table 4.10, where RAH1 refers to the model run using $C_D = 0.55$ for hailstones 1cm or larger, RAH2 $C_D = 0.6$ for hailstones 1 cm or larger and RAH3 $C_D = 0.55$ for hailstones 2 cm or larger.

Table 4.10 shows that for the range of values used in these experiments, the final model derived hail size at the ground is insensitive to small changes in the drag coefficient or over which diameter range it is applied. For example, RAH2 results in slightly smaller hail at the ground (3.6 cm versus 4.1 cm) and shorter time to ground than the control (58.2 min versus 61.9 min). This is understandable, since a hailstone modelled using RAH2 (not shown) will, due to its higher terminal velocity, spend less time in the HGZ during its downward trajectory resulting in smaller hail at the ground.

4.2.6 Additional Sensitivity Experiments

The sensitivity of HAILCAST was also investigated for several other parameters that were thought to be important for hail growth in the model, but were found to have negligible impact on the modelled hail size.

The temperature at which the hail embryo freezes was varied between –8 °C (control), -15 °C and –20 °C. For the case studied here, there was no impact on the modelled hail size or hail growth time. This is most likely due to the hail embryo being rapidly advected through the cloud, and any possible changes in growth rate resulting from the above nucleation temperatures, would not have time to significantly impact the hailstone's final size.

Model studies of hail growth use various parameterisation schemes to convert cloud water into ice due to the freezing of cloud droplets at progressively colder temperatures. Three common schemes were compared in order to determine the sensitivity of hail growth to this process. The scheme used in HAILCAST depletes the cloud water from near adiabatic values at –20 °C to all ice at –40 °C using an exponential function developed by Vali and Stansbury (1965). Miller (1988) reduced the LWC from adiabatic values at –35 °C to zero at –40 °C using a linear function. Miller et al. (1990), however, chose to deplete the cloud water linearly from adiabatic values at –25 °C to zero at –40 °C. However, sensitivity tests (not shown) suggest that the model derived final hail size and hail growth times are almost the same, regardless which of the above schemes is used.

Little difference in the final hail size was found when using the shedding scheme developed by Chong and Chen (1974) and that of RAH87. For example, the final model derived hail size using the shedding scheme of Chong and Chen was 3.8 cm, versus 4.0 cm for RAH87. This observation is in agreement with sensitivity tests conducted by Rasmussen and Heymsfield (1987b), who found the two schemes produced very similar hail diameters at the ground (especially for hail > 2.0 cm). They propose the main difference between the two schemes is the distribution of shedding with height, rather than the absolute mass of water shed.

The hail growth was also found to be insensitive to the time step used in the growth calculations. Model runs were conducted using time steps of 0.01s,

0.1s and 1.0s. The resulting hail diameter at the ground and hail growth times were almost identical.

4.3 Summary and Conclusions

Sensitivity experiments using a severe hailstorm sounding have been conducted to determine the sensitivity of HAILCAST to changes in input sounding data, entrainment and key microphysical parameters. The cloud variables of interest are W_{max} (the maximum updraft velocity) and T_{wmax} (temperature at the altitude of the maximum updraft).

The W_{max} and T_{wmax} are sensitive to small changes in surface temperature and dew-point, with the stronger updrafts modelled using higher surface temperatures and lower dew-point depressions. On the case day of 11 July 1985, an increase of 1°C in surface temperature or dew-point increased W_{max} by about 20% and lowered T_{wmax} by approximately 30%. Hence, small changes in surface temperature and dew-point can have a significant impact on the modelled hail size, since they determine the amount of entrainment, maximum hail growth time, as well as W_{max} and T_{wmax}. Further, the sensitivity experiments suggest there is an optimum range of W_{max} (23 ms^{-1} to 30 ms^{-1}) and T_{wmax}(-18 °C to -27 °C) associated with large model derived hail at the ground. The upper limit of the above T_{wmax} range, corresponds well with the optimum T_{wmax} of -30 °C found by Dennis and Musil (1973) for the growth of large hail.

Including entrainment in the updraft calculations reduces W_{max} and increases T_{wmax}. Further, model runs conducted using entrainment tended to produce smaller hail at the ground. W_{max} and T_{wmax} are not significantly influenced by changes in the magnitude of the wind shear as large as 20%, unless the ESI lies close to the threshold value of 1 m^2s^{-3} used to discriminate between lateral and cloud top entrainment when modelling the updraft.

The hail growth was found to be most sensitive to the following microphysical parameters, when varied over the range of values used in other hail modelling studies:

(1) **Hail Embryo Diameter:** If the hail embryo was too small (<200 μm), only small hail was forecast at the surface on days with strong updrafts (>25 ms^{-1}). Increasing the embryo size led to larger hail and decreased the hail growth time.

(2) **Ventilation coefficient:** The increase in ventilation coefficient for increasing diameter is crucial for the growth of large hail, since the increased heat transfer form the stone delays the onset of wet growth and melting, and in turn the shedding of excess water. Excluding the heat transfer coefficient from the ventilation coefficient calculations, decreased the forecast hail diameter by as much as 60%.

(3) **LWC:** Reducing the LWC by only 10% reduced the final hail diameter by 40%. This highlights the significance of an adiabatic updraft core in creating a favourable environment for hail growth.

(4) **E_i:** When the modelled hailstone entered the glaciated portion of the cloud, the magnitude of E_i was also critical in determining the final hail diameter. If the collection efficiency was too small ($E_i < 0.2$), the model hailstone became trapped in the glaciated portion of the cloud resulting in smaller hail diameter at the ground.

The modelled hail growth was found to be insensitive to parameterisation schemes used to calculate the terminal velocity, cloud ice, embryo freezing temperature and shedding of excess water during wet growth and melting.

An important observation from the above sensitivity experiments, is the sensitivity of the hail model to the hailstone's residence time above –40 °C and location of the hailstone with respect to this level when the updraft collapses. Any changes in the input data or microphysics that reduces T_{wmax} below its

optimum value (T_{wmax} ~ -27 °C) or increases the hailstone's residence time above –40 °C, will result in smaller hail at the ground. On such occasions, the maximum predicted hail size is strongly limited by the finite updraft duration and not only W_{max}. This finding is in line with observations made in other modelling and case studies of hailstorms (see section 1.3).

In closing, this chapter has highlighted the sensitivity of modelled hail growth to changes in the input sounding data and key microphysical parameterisation schemes. Of all the parameters considered in the above sensitivity experiments, small variations in the surface temperature and dew-point appear to have the greatest impact on the maximum modelled hail size. Further, the impact of these changes overshadows some of the changes in modelled hail size found by varying other parameters in the hail model.

5. ALBERTA HAIL PROJECT DATA SET

Before evaluating the model forecasts in Chapter 6, problems associated with identifying proximity soundings and evaluating hail forecasts will be discussed. This is followed by a description of the upper-air and hail data set used for the evaluation, and a brief description of the 1983-1985 hail seasons.

5.1 Problems Intrinsic to Evaluating Model Forecast Hail Size

Doswell and Brooks (1993) note that there are two primary errors that can cause numerical model guidance to be incorrect, namely:

- An incorrect forecast of environmental conditions or invalid proximity sounding are used to initialise the model.
- Even if the environmental conditions are represented correctly, the numerical model may not be capable of generating a forecast in line with the observations.

The second error may be due to certain shortcomings of the model, assumptions made in the modelling process or an inadequate understanding (and modelling) of the mechanisms at work. For now, we will concentrate on addressing the problem of proximity soundings.

In order to objectively evaluate the skill of a cloud and hail model, it is imperative to use a sounding representative of the environmental conditions in which the thunderstorms developed. According to Golden et al. (1986): "A representative sounding that correctly describes the precedence or proximity near-environment of a tornadic or hail-producing thunderstorm may depend on the direction and distance of the sounding from the storm/tornado, time of year,

geography, terrain and especially the type of mesoscale storm-initiating mechanism".

Unfortunately, obtaining proximity soundings is complicated by the high spatial and temporal variability usually evident in a given thunderstorm environment (Brooks and Doswell, 1994). Because of these complications, proximity soundings are usually identified by applying spatial and temporal constraints between soundings and the actual storms. Soundings satisfying these constraints are then inspected subjectively to identify and remove problem soundings.

Darkow (1969) defined a proximity sounding using the following three criteria:

(1) Release of sounding occurred within 80 km of a tornado.

(2) Tornado occurred 45 min before or 60 min after the balloon was released.

(3) Sounding sampled the same air-mass in which the thunderstorm developed.

Brooks and Doswell (1994), on the other hand, selected all soundings within 160 km and one hour of tornado observations. These soundings were then subjectively inspected to remove any soundings deemed not representative of the thunderstorm environment. Moore and Pino (1990) used hail events that occurred within 3 hours of the sounding time and 100 km of the launch site to evaluate their hail forecasting technique.

Despite strictly applying the above spatial and temporal criteria, one is not guaranteed a sounding will be representative. This is especially the case for rapidly evolving atmospheric conditions or in the presence of sharp temperature and moisture gradients, such as is the case for storms triggered by the passage of fronts or drylines. Recent studies by Brooks et al. (1996) during VORTEX-95 (Verification of the Origins of Rotation in Tornadoes Experiment), indicate that soundings as little as 60 km apart displayed significantly different temperature

and moisture profiles in the boundary layer. Burgess (1988) presents an example in which a sounding only 40 km and 30 minutes removed from a supercell failed to properly represent the storm's environment. There is also the danger that the sounding is too close to a thunderstorm and represents the storm circulation itself, rather than the unmodified environment that created the storm (Weisman et al., 1998). In numerical experiments, Weisman et al. showed that a convective storm's impact on its environment increases significantly for increasing magnitudes of the environmental wind shear and CAPE. The wind shear in particular was strongly influenced, with shear through the lowest 6 km nearly doubling within 10 km of a supercell's updraft. Impacts on CAPE were less significant, with CAPE reduced by 10-15% in the inflow regions of the stronger storms. They conclude that proximity soundings should be taken 20-30 km from existing supercell storms to properly represent the relationship between the storm and its local environment.

When evaluating hail forecasts, another problem arises, namely the verification and observation of hail at the surface. Due to its high temporal and spatial variability, recording the hailfall at the surface is very difficult. Morgan and Towery (1975) presented results of a hailstorm that moved over a very high-density observation network (hailpads every 100-200 m). Maximum sizes ranged from 1-3 cm. The largest hail (3 cm) only covered 1% of the total area of the network, while 80% was covered by hail <2 cm in diameter. Therefore, the maximum hail size from this storm would have most likely been underestimated by a coarse observation network.

To summarise: Assuming the numerical model used to forecast the hail size is physically valid, when evaluating the forecasts, one ideally requires a sounding representative of the atmospheric conditions in which the storm develops, as well as high density and accurate observations of hail size at the surface. In an attempt to satisfy both these criteria, it was decided to use upper-air and hail size data

collected during the Alberta Hail Project. Some background and nature of these observations is discussed in section 5.2 and 5.3 below.

5.2 Alberta Hail Project Hail Data

The Alberta Hail Studies Project (formed in 1957) was the precursor to the Alberta Hail Project (AHP) which operated from 1974-1985. The initial motivation for these research projects was concern over increasing agriculture losses due to hail damage in the early fifties and a need to understand the nature and formation of hailstorms. The potential and viability of hail suppression was also investigated. For more information on the Alberta Hail Project and asscociated data sources, the reader is referred to the following web-site: http://datalib.library.ualberta.ca/AHParchive/.

The AHP target area covered approximately 48000 km^2 and was centred on the radar site located at Red Deer's Industrial Airport in Penhold, see Figure 5.1. Each spring, hail cards (Figure 5.2) were mailed to approximately 19464 farmers in the project area (Renick, 1983). On any given day, between 10% and 20% of the farmers would respond, yielding an average of one observer per 12-24 km^2 (Wojtiw, 1975). In addition, from 20 June to 31 August telephone surveys were conducted to verify radar observed storms and this resulted in observation densities as high as one report per 3 km^2 (Wojtiw, 1975). As a result, it is expected that on any given day, only a very small percentage of hail reaching the surface went undetected. Given the problems associated with observing hail mentioned in section 5.1, the AHP hail data set is considered to be both comprehensive and of high quality, making it ideally suited for evaluating the HAILCAST model.

5.3 AHP Upper-air and Surface Data

Although hail data was available for the each summer (May-August) during the AHP upper-air data from Penhold was only archived (in digital form) from 1983-1985. This reduced the number of years for validating HAILCAST. On the other hand, it allowed us to focus on carefully selecting a smaller, but high quality proximity sounding data set.

From 1983-1985, soundings were released from Penhold twice daily at 0615 and 1715 LDT between mid June until the end of August (Table 5.1). Since the maximum temperature (and convective instability) is observed in the late afternoon and most of the thunderstorm activity occurs between 1600-2000 LDT (Admirat et al., 1985), it was decided to only consider the 1715 LDT soundings.

In addition to the problems discussed in section 5.1, the presence of the foothills west of Penhold added another complication when selecting proximity soundings. Under weakly forced synoptic conditions, thunderstorms are more likely to develop over the foothills than over the plains. The reason for this is as follows. Soundings on days when thunderstorms develop in the foothills are usually characterised by a capping lid in the vicinity of the Lifting Condensation Level (LCL). On days with no synoptic forcing (absence of a short-wave trough aloft or upslope flow), surface heating can't erode the lid and deep convection is limited to the foothills where local orographic uplift is sufficient to initiate convection. Thus, the Penhold soundings on these days were not considered representative of the thunderstorm environment in the foothills.

Keeping the above mentioned factors related to identifying proximity soundings in mind, the following criteria were used to exclude hail events too far removed in space and time from the 1715 LDT Penhold sounding:

- Days when the hailstorms developed and produced hail more than 100 km from Penhold or when hailstorms were not observed within 3 hours (before or after) of the 1715 LDT sounding.
- Days when the exact location and timing of the maximum hail size was uncertain..
- Days when thunderstorm development was limited to the foothills.

Soundings satisfying the above criteria were then inspected individually to isolate soundings not considered representative of the observed convection (or lack thereof). Soundings were removed form the data set if any of the following conditions were met:

- Soundings with missing temperature, dew-point or wind data at any level.
- Soundings modified by the passage of a thunderstorm outflow boundary.
- Soundings taken in rain or during a thunderstorm (so called "raintemp").

The above criteria are similar to those used by Moore and Pino (1990), Leftwich (1984) and Brooks and Doswell (1994) for selecting proximity soundings.

Information contained within the AHP field reports from 1983-1985 proved an invaluable aid when identifying proximity soundings, for example:

- For selected days during the 1983 and 1984 season, the location and size of hail swaths within the project area were indicated. Discrimination was made between general hail swaths and areas with walnut or larger hail. The aforementioned information was not archived for 1985.
- For each day from 20 June - 31 August, information regarding the time of development and radar derived storm characteristics (e.g. cloud top height and max reflectivity of the most significant storms) were recorded. A 500 hPa or surface analysis of western Canada valid for 1800 LDT was also provided.

Although there is no way of unequivocally determining if the soundings adequately depicted the storm-scale setting on all days, we believe the above selection criteria yielded the most representative soundings given the temporal and spatial limitations of the Penhold sounding data set. A complete list of all days excluded from the data set and reasons why are given in the Appendix B.

Another factor critical for an accurate hail forecast, is to initialise the model using the surface temperature and dew-point representative of the air feeding or entering the updraft of the thunderstorms. As was shown in Chapter 4, the cloud updraft and in turn hail size are very sensitive to small changes in the surface temperature and dew point. The maximum surface temperature and dew-point judged to be most representative of the storm environment were used as input for HAILCAST. These data were available from the AHP field reports for selected days during the 1983 and 1984 seasons with either:

- 10 or more hail reports
- Grape–sized hail
- Cloud seeding activity
- Research flights

For the remaining days, including the entire 1985 season, these data were not available and certain assumptions had to be made regarding the maximum surface temperature and dew-point. On these days, the surface temperature and dew-point observed at Penhold at the time of the sounding (approximately 1715 LDT) were deemed to be representative of the storm inflow. There were also a number of days (all no-hail days or non-severe) when the moisture in the boundary layer was very shallow, with a rapid decrease in dew-point between the surface (905-915 hPa) and the first data level at 900 hPa, see Figure 5.3. The importance of the depth of surface moisture in initiating or inhibiting convection has been discussed by Mueller at al. (1993). If these surface values were used as input for HAILCAST, the model tended to over-forecast the strength of convection. In

order to determine more appropriate values for low-level moisture, the 900 hPa dew-point was used if the difference between this value and the surface dew-point was greater than 2 °C.

For the purpose of this thesis, AHP hail and sounding data from 20 June to August 31 were used to evaluate the model. The reasons for selecting this time frame were threefold. Firstly, during this period, telephone surveys of hail size were conducted in addition to the hail network observations. Secondly, the location, timing and characteristics of hailstorms were available from the AHP field reports. Thirdly, the maximum surface temperature and dew-point were provided for selected days in the AHP field reports. A total of 219 soundings were screened and 160 days (73% of the available soundings) were identified as adequate proximity soundings. Of these soundings, 98 days were made on no hail days, 42 on non-severe hail days and 20 on severe hail days (Table 5.2).

5.4 Hail Size Classification used During the AHP

In addition recording the time of observation and duration of the hail, observers within the AHP were requested to report the most common and the largest hail size. For this purpose the AHP used a six hail size categories associated with familiar objects (Table 5.4).

In an attempt to quantify the forecast hail size error (see Chapter 6, section 6.2.3.), a representative diameter was determined for each hail size category for comparison with the forecast values. This was achieved by calculating the median diameter for the corresponding diameter range in each category. For hail greater than golfball a representative diameter of 6.4 cm was selected and this corresponds to the diameter of a tennis ball (Charlton et al., 1998).

When evaluating the maximum hail size forecasts, it was also important to specify the criteria used to identify the maximum hail size observed on each day. For this thesis, the largest hail size category having one or more reports, was used to represent the maximum hail size observed in the network on a given day. However, one must keep in mind that despite the dense observer network, it is possible that the largest hail size went undetected on some days. Regarding the accuracy of the hail observations, comparisons with measurements using aluminium hail pads, suggest observers were reliable in measuring hail larger than 30 mm with an error margin of approximately 10% (Admirat et al., 1985).

Finally, a hail day was considered severe when the largest observed hail category was 'walnut' or larger, i.e. diameter ≥2.1 cm. This is very similar to the criteria of ≥2.0 cm used by Environment Canada to identify severe weather days.

5.5 Hailfall Activity During the 1983-1985 Summer Seasons

There is significant year to year variability in the number of hail reports within the AHP area, with a clear seasonal variation in the frequency of hail reports (Wojtiw, 1975). Hail is almost exclusively limited to the period from June to August, with 97% of the hail activity in central Alberta occurring during this time (Wojtiw, 1975). The frequency of hail in May and September is very low, with small hail predominating. The number of hail days and hail reports (days one or more hail reports) peaks in July, with an average of 19.1 days and 1304.3 hail reports respectively. These values represent 37.5% and 50.4% of the season totals for the period 1974-1985 (Deibert, 1985). Hail occurs on an average of 51 days between June and August, of which 20 are severe and 31 non-severe (Smith et al., 1998). Table 5.3 lists the hailfall statistics for the summers of 1983 to 1985 and shows that the number of hail days and hail reports were below average during these seasons.

6. EVALUATION OF HAILCAST AGAINST OTHER FORECASTING TECHNIQUES

In this chapter, maximum hail size forecasts (using HAILCAST) are evaluated for three summer seasons (1983-1985) against observations of maximum hail size within the Albert Hail Project (AHP) area. We also wish to determine if the improved microphysics used in HAILCAST improve the forecast skill over the original SkyWatch model and nomogram approach of RAM (Renick and Maxwell, 1977). To this end, the SkyWatch and RAM hail forecasts are also evaluated against the AHP hail data and compared with the skill of the HAILCAST forecasts. The chapter concludes with a discussion of the forecast skill of the models and possible explanations for the shortcomings and differences in forecast skill.

6.1 Forecast Skill Scores

Contingency tables were constructed for 160 HAILCAST hail forecasts between 1983 and 1985 (Appendix C). Table 6.1 shows the 2x2 contingency table used to calculate the skill scores.

Referring to Table 6.1 we introduce the following terminology:

- A Hit (H) constitutes correctly forecasting the occurrence of hail.
- A Miss (M) is recorded when hail is observed and not forecast.
- A False Alarm (FA) is recorded when hail is forecast and not observed.
- A Null (N) forecast is recorded when no hail is forecast and no hail is observed.

We computed the following skill scores based on the contingency tables: Probability of Detection (POD), False Alarm Rate (FAR), Heidke Skill Score (HSS) and BIAS (B). These skill scores are defined in Table 6.2.

The POD and FAR vary between 0 and 1, with higher POD and FAR scores indicating increased and decreased forecast skill respectively. The HSS is a popular skill score for forecast verification (e.g., Alford, 1998) and is considered a measure of the true skill of a forecast, since it takes all values in the contingency table into account. The POD and FAR on the other hand give no credit for correct null forecasts. HSS varies between -1 for absolutely no forecast skill and 1 for a perfect forecast. Generally, a HSS greater than 0.40 is considered good. A BIAS score of 1 indicates that a particular event is equally over-forecast and under-forecast. BIAS scores less than 1 and greater than 1, indicate a tendency to under-forecast and over-forecast an event respectively.

6.2 HAILCAST Model Evaluation

To determine the model's skill in correctly identifying hail days and more importantly severe hail days (hailstone diameter of at least 2.1 cm), the above forecast skill scores were calculated using contingency tables (Appendix C) differentiating between hail days and severe hail days respectively.

6.2.1 Forecast Skill Statistics

(a) Hail Forecasts

HAILCAST displayed significant skill in detecting the occurrence of hail and scored a mean POD of 0.85 for the 3 seasons evaluated here (Table 6.3). This equates to correctly forecasting 53 of the observed 62 hail days. The FAR was relatively low at 0.26 (19 false alarms). HAILCAST showed significant skill

overall, with a HSS of 0.64. The model, however, displayed a positive BIAS of 1.16, indicating a tendency to over-forecast hail days somewhat. A possible explanation for this positive bias will be discussed later in section 6.4.2.

There is some year-to-year variability in the skill scores. For example, the FAR in 1984 was 0.36 versus only 0.16 in 1983. Moreover, although the POD was highest in 1984, the overall model skill was the lowest of the three years, due to the relatively high number of false alarms that season.

(b) Severe Hail Forecasts

The lower portion of Table 6.3 lists the skill scores for the severe hail forecasts. HAILCAST displayed significant skill when forecasting the occurrence of severe hail, with a POD of 0.89 (identified 18 of the 20 severe hail days) and HSS of 0.67. The FAR for the severe hail day forecasts was higher than the hail forecasts at 0.40 (12 false alarms). The relatively high BIAS of 1.5, indicates the model's tendency to over-forecast severe hail events. Once again, HAILCAST displayed the lowest skill in 1984, due to the greater number of false alarms that season.

6.2.2 HAILCAST Forecast Hail Size Category Evaluation

To test the model's skill in accurately forecasting the hail size category, the modelled hail sizes were compared against the observed hail size categories. To do this, each forecast diameter was placed in the appropriate hail size category shown in Table 5.4 and compared with the maximum observed size category for the day. Here a hit constitutes correctly forecasting the maximum observed hail size category. The hail size category forecasts are listed in Appendix D. To determine if the model displayed any bias or weakness when forecasting severe

hail for example, the model forecasts were evaluated for no-hail days, all hail days, non-severe and severe hail days.

(a) No-Hail Days

HAILCAST correctly forecast the hail size category (i.e., no hail) for 81% the 98 no-hail days (Table 6.4). Including hits within one size category increased the percentage of hits to 83%. HAILCAST only forecast shot sized hail on one occasion, with the remainder of the incorrect forecasts (17%) calling for pea-size hail or larger.

(b) All Hail Days

HAILCAST forecast the correct hail size category for 38% of the 62 hail days (Table 6.4). The model tended to underestimate the hail category, with 40% of the forecasts one or more categories too small. Hail one or more categories too large was forecast for 22% of all hail days, 6% of which were two or more categories too large. Nevertheless, 81% of the forecasts were within one size category.

(c) Non-severe Hail Days

HAILCAST correctly forecast the size category on 37% of the non-severe hail days, with 74% of the forecasts within one size category (Table 6.4). Once again, the model tended to underestimate the hail size category, with 39% of the forecasts one or more categories too small, compared to 24% one or more categories too large. Only 9% of the forecasts were two or more categories too large.

(d) Severe Hail Days

HAILCAST correctly forecast the hail size category for 39% of the 20 severe hail days (Table 6.4). Further, the model correctly forecast 94% of the severe days within one size category. As was the case for the non-severe hail days, the model tended to underestimate the hail size category, with 43% of severe hail days one or more categories too small. However, only 6% of the forecasts were two or more categories too small. The model rarely overestimated the hail size category on severe hail days, with 18% of the forecasts one category too large. No hail forecasts were two or more categories too large.

Table 6.5 shows that HAILCAST correctly forecast the hail size category for 64.7% of the 160 days during the 1983-1985 summer seasons. Further, 82% of the forecasts were within one size category, with more than 92% of the forecasts within two categories of the maximum observed hail size.

6.2.3 Error Analysis

In an attempt to determine the magnitude of the forecast hail diameter error, absolute errors (in cm) were calculated for each of the 160 days using the Absolute Error (AERROR) given by

$$AERROR = | D_{obs} - D_{fcst} |, \qquad (6.1)$$

where D_{obs} is the representative diameter of the maximum observed hail size category (see section 5.5) and D_{fcst} the maximum forecast hail diameter at the ground. It must be emphasised that the median diameters (D_{obs}) do not necessarily represent the largest observed hail diameter at the ground. HAILCAST was evaluated for no-hail days, all hail days, non-severe and severe hail days respectively. The absolute errors for all 160 days are listed in Appendix E.

For all 160 days the mean absolute error was 0.63 cm, while for the non-hail days the mean error was only 0.26 cm (Table 6.9). The mean error of 1.27 cm on severe hail days was noticeably larger than for non-severe hail days (0.76 cm) and this is most likely due to the greater impact of outliers on the smaller data set for severe hail days. The above statistics suggest the model hail diameter forecasts are fairly accurate, with a mean absolute error of 1 cm for all hail days.

6.3 Comparison Between HAILCAST, SkyWatch and RAM Hail Forecasts

In this section the SkyWatch and RAM (Renick and Maxwell, 1977) hail forecasts are evaluated against the AHP hail data and compared with the skill of the HAILCAST forecasts. We are particularly interested in determining how critical the microphysics are for hail growth. Some of the microphysics used in the original SkyWatch model were considered inappropriate, and we decided to replace selected microphysical parameters based on findings from more recent studies of hail growth. The changes made to the SkyWatch cloud and hail model are discussed and motivated in Appendix F.

6.3.1 Forecast Skill Statistics

(a) Hail Forecasts

The models are evaluated using the same techniques as in section 6.2, except the absolute error analysis is not included, since the RAM nomogram only forecasts the hail size category and not hail size per se. The hail size category forecasts of SkyWatch and RAM are listed in Appendix D.

Table 6.7 shows that the forecast skill for all three models was similar, with each scoring a POD greater than 83%. HAILCAST scored the highest HSS of

0.64 and a marginally lower FAR than the other two techniques. Although RAM scored the highest POD of 0.90, it also scored the highest FAR of 0.33. All three techniques displayed a positive BIAS, indicating a tendency to over-forecast hail; this was especially true for RAM which scored a BIAS of 1.39.

(b) Severe Hail Forecasts

HAILCAST displayed the highest overall skill of the three techniques (Table 6.7). Its HSS of 0.67 was significantly higher than those of SkyWatch (0.40) and RAM (0.54) respectively. HAILCAST also scored the highest POD of 0.89, which was some three times greater than that of SkyWatch. The FAR for HAILCAST and SkyWatch were comparable; RAM scored the highest FAR of 0.45. HAILCAST tended to over-forecast severe hail events more often than RAM, while SkyWatch tended to under-forecast severe hail events.

6.3.2 Hail Size Category Evaluation

(a) No-Hail Days

Approximately 81% of the HAILCAST and SkyWatch hail category forecasts were correct (Table 6.8). This is almost 9% higher then RAM. More than 81% of the hail forecasts for all three techniques were within one hail size category, with SkyWatch performing best at 88%. RAM was more likely to overestimate the hail size category, with 29% of the forecasts one or more categories too large, compared to approximately 19% for HAILCAST and SkyWatch.

(e) All Hail Days

HAILCAST was noticeably more accurate than the other techniques when forecasting the hail size category, with 38% of the forecasts being correct (Table 6.9). This is double the percentage of correct forecasts achieved by SkyWatch.

Although HAILCAST tended to overestimate the hail size category, 81% of the forecasts were within one size category and this was markedly higher than the other techniques. All three techniques tended to underestimate the hail size category. This was especially the case for SkyWatch, with 71% of the forecasts one or more categories too small. HAILCAST and RAM were more likely to overestimate the hail size category, with approximately 20% of the forecasts one or more categories too large.

(c) Non-severe Hail Days

The results for HAILCAST and RAM were similar to those for all hail days, (Table 6.10). However, the percentage of correct forecasts within one size category was 7% lower for HAILCAST. There was a slight improvement in the SkyWatch forecasts, with the number of hits within one size category increasing from 61% to 72%.

(d) Severe Hail Days

Table 6.11 indicates HAILCAST's significant skill when forecasting the size category on severe hail days. 39% of the HAILCAST forecasts were correct and this was almost triple the number of correct SkyWatch forecasts. Further, 94% of the HAILCAST forecasts were within one size category, which was significantly higher than the other two techniques. This was due to HAILCAST only forecasting hail more than one category too small for 6% of the forecasts, compared to almost 30% for the other two techniques. As was the case for the non-severe hail days, all the techniques tended to underestimate the hail size category. This was especially true for SkyWatch, with 82% of all forecasts one or more categories too small. The techniques rarely significantly overestimated the hail size category on severe hail days, although HAILCAST was most likely to overestimate the hail size by one size category.

The frequency of correct hail size category forecasts for all days are summarised in Table 6.12. HAILCAST displayed the greatest overall skill in correctly forecasting the hail size category, with 64.7% of the 160 forecasts correct, versus 56.7% and 54% for SkyWatch and RAM respectively. Moreover, 82% of all HAILCAST forecasts were within one size category, compared to 74.7% for SkyWatch and 77.3% for RAM. Thus, HAILCAST was more accurate in forecasting the hail size category than the other two techniques.

6.4 Discussion and Conclusions

6.4.1 Summary of Findings

The major findings regarding the evaluation of HAILCAST maximum hail size forecasts for three summers season are as follows:

- HAILCAST showed significant skill in forecasting the occurrence of hail, with a POD of 85% for all hail days.
- HAILCAST showed significant skill in distinguishing between hail and no hail days, with a HSS of 64%.
- HAILCAST showed significant skill in forecasting severe hail days, with a POD 89% and HSS of 67%.
- HAILCAST showed a positive BIAS, especially for the severe hail days.
- HAILCAST correctly forecast the hail size category for 38% of the 62 hail days, with 81% the forecasts within one size category.
- HAILCAST correctly forecast the hail size category for 39% of the 20 severe hail days, with 94% of the forecasts within one size category.
- HAILCAST proved fairly accurate in forecasting the maximum hail size at the ground, with a mean absolute error <1 cm for all hail days, increasing to approximately 1.3 cm for severe hail days.

The performance of HAILCAST was also significantly better than that of the SkyWatch model and RAM, and we note the following:

- On hail days, HAILCAST scored the highest HSS and lowest FAR of all three techniques.
- On severe hail days, HAILCAST scored the highest HSS and POD. In particular, HAILCAST's HSS was 27% and 13% higher than the corresponding scores for SkyWatch and RAM respectively.
- All three models displayed a positive BIAS when forecasting hail. However, on the severe days SkyWatch displayed a distinct negative BIAS, while HAILCAST displayed a positive BIAS.
- HAILCAST was significantly more accurate than other techniques when forecasting the hail size category for all hail days. This was particularly true for the severe hail forecasts, when the percentage of correct forecasts were 25% and 10% higher than SkyWatch and RAM respectively.
- All three models consistently underestimated the hail size category. This was particularly true for SkyWatch on severe hail days, when 82% of the forecasts were one or more categories too small.
- HAILCAST and RAM were more likely to overestimate the hail size category than SkyWatch on hail days.
- HAILCAST achieved the highest percentage of correct forecasts and forecasts within one size category.

The above summary indicates that the improved microphysics used in HAILCAST significantly improved the model's ability to correctly and accurately forecast severe hail days compared to the original SkyWatch model. However, the same was not true when forecasting the occurrence or non-occurrence of hail, with HAILCAST performing only marginally better than SkyWatch. Regarding the performance of HAILCAST versus the RAM nomogram, incorporating the coupled cloud and hail model with microphysics did improve the overall skill and accuracy of the hail forecasts, especially for the severe days. Moreover, the

forecast skill of HAILCAST was more consistent than other techniques for all three summer seasons evaluated here.

6.4.2 Discussion

Regarding the weaker performance of SkyWatch and RAM, it must be kept in mind their forecast skill was negatively biased by their poor performance when forecasting severe hail in 1985. This could be attributed to the low surface temperatures (< 20 °C) and dew-points (< 10 °C) observed on four of the eight severe days in 1985. These values were lower than the means observed for the 20 severe hail days used in this study (Table 6.13).

The thunderstorms that produced hail on the above days developed following the passage of a cold front, but ahead of an approaching upper-air trough. This implies that synoptic scale forcing was responsible for initiating the thunderstorms rather than surface heating. Strong (1986) referred to these as post-cold-frontal thunderstorms and proposed they develop when the front and associated cloud pass over the capping lid, leaving low-level moisture trapped under an inversion. Cold air advection at 850 hPa behind the front is then sufficient to remove the capping lid and release the instability.

Due to the cooler and drier conditions mentioned above, the maximum updraft velocity forecast on all four days by HAILCAST was less than 20 ms^{-1} and at in-cloud temperatures warmer than –20 °C. As a result, the RAM nomogram forecast pea or smaller hail. Given the dynamic nature of these hail events, it is not surprising that the RAM technique failed to correctly forecast the severe hail. The above examples illustrate the advantage of using a hail model with microphysics versus the nomogram approach and that the RAM nomogram may not be not suitable for forecasting severe hail during post-cold-frontal thunderstorm events.

The tendency of the SkyWatch model to significantly underforecast severe hail events could probably be related to the parameterisation schemes and microphysics used in the model. An embryo size of 100 μm was used in the SkyWatch hail model. In Chapter 4, we showed that for a day with strong updrafts, the predicted hail at the ground using this diameter was much smaller than for a 300 μm embryo (used in HAILCAST) on days with strong updrafts. Further, ventilation coefficients for large hail (>2 cm) calculated using the equations of Poolman (1992), were significantly smaller than values determined using the scheme of Rasmussen and Heymsfield (1987a). Rasmussen and Heymsfield (1987b) note the importance of the increased the ventilation coefficient for the growth of large hail. Therefore, it is conceivable the combination of these factors could result in SkyWatch consistently underestimating the hail size on days with strong updrafts.

A point of concern was the positive BIAS of RAM and HAILCAST when forecasting the occurrence of non-severe and severe hail days respectively. Renick and Maxwell (1977) found their nomogram ineffective for forecasting hail size on days when the in-cloud freezing level was above 4.4 km MSL. On these days, the observed hail sizes were often considerably smaller than those forecast by the nomogram. This short-coming was not considered when determining the RAM forecast hail categories and may account for the nomogram's tendency to over-forecast hail days (i.e., relatively high BIAS and FAR).

To determine if there was any plausible explanation for the tendency of HAILCAST to over-forecast hail events, a total of 19 days were identified when hail was forecast but not observed. Severe hail was forecast on four of these days (Table 6.14). Despite sufficient moisture and convective instability, convection is sometimes prevented or inhibited due to lack of a trigger mechanism (Mueller et al., 1993). The Smith and Yau (1993) conceptual model for severe weather outbreaks in Alberta (Chapter 1) stresses the need for the interaction of the synoptic and mesoscale environments to initiate severe convection. Smith and

Yau found that 94% of all severe hail days were associated with an upper-air trough upwind of Alberta. In contrast, 71% of no-hail days had an upper-ridge. The minimal wind shear and subsidence aloft observed on such occasions result in short-lived air mass thunderstorms developing that rarely produce large hail.

Table 6.14 shows that on 17 of the 19 days when HAILCAST forecast hail, the upper-air over the project area at 1800 LDT was dominated by an upper-air ridge, with only towering cumulus (TCU) or cumulus clouds (CU) being reported in the AHP area (Renick, 1983; Renick 1984; Deibert, 1985). Weak thunderstorms were observed on only one of these days (9 July 1984), in association with a trough that moved through the project area earlier in the day. On the two days when a trough was located upwind of Alberta, thunderstorm development was limited to the foothills, with no hail reported within the project area.

An example of the importance of a trigger mechanism in initiating deep convection is shown in Figures 6.1 and 6.2. On 1 August 1985 the upper-air was dominated by a cut-off low over Oregon, with a weak upper-ridge and light winds over Alberta (not shown). Surface conditions were relatively moist with a maximum temperature and dew-point of 27 °C and 15 °C being observed at Penhold. Using the parcel method for these conditions yielded a CAPE of 2634 Jkg^{-1}. However, only TCU were observed in the foothills west of Sundre.

On the following day, the cut-off low weakened and was situated over southern Montana, while the upper flow over Alberta was once again dominated by a weak ridge and light winds. Surface conditions were similar to the previous day, with a maximum temperature and dew-point of 29 °C and 13 °C. The CAPE calculated using these surface conditions was 2518 Jkg^{-1}. However, on this day, thunderstorms producing grape size hail developed over the south-western quadrant of the project area. Apart from some cooling near the 700 hPa level, the

tephigrams for both days were very similar (Figure 6.1 and Figure 6.2) and this is reflected in the close agreement in the CAPE values.

Why then did thunderstorms develop on one day and not the other? The answer lies in the synoptic chart shown in Figure 6.2. On 2 August, a weak front extended from northern to south-western Alberta. The passage of the front created sufficient uplift to lift a surface parcel to its LFC and release the CAPE. The surface convergence associated with this front is reflected by the cooling near the 700 hPa level, which is indicative of vertical motion in the boundary layer (Johns and Doswell, 1992). On 1 August, however, no such trigger mechanism was present and deep convection was limited to the foothills.

Neglecting days when a ridge dominated the upper-air over the AHP area, reduces the number of false alarms of hail to 2 (from 19). Applying the upper-ridge criteria for days when severe hail was forecast and not observed, reduces the number of false alarms to 1 (from 4). Therefore, excluding days associated with an upper-ridge would significantly reduce the FAR and positive BIAS of HAILCAST.

It is important to remember that HAILCAST calculates the maximum hail size according to the expected convective instability and is not capable of determining if factors will be present to inhibit or prevent this instability being released. To overcome this shortcoming, it is recommended HAILCAST should be used conjunction with a decision tree method used for forecasting thunderstorms and severe thunderstorms (e.g., Colquhoun and Mills, 1998).

Despite the limitations of using a one-dimensional hail model, if equipped with a representative sounding and knowledge of the expected circulation pattern, the above evaluation suggests a forecaster can use HAILCAST confidently when forecasting hail. Moreover, HAILCAST provides excellent guidance when estimating the maximum expected hail size category for that day.

7. CONCLUSIONS AND SUGGESTIONS FOR FUTURE WORK

In light of the destructive capability of hailstorms, it is important to issue timely warnings for the occurrence of severe hail. However, despite continuous advances in our understanding of severe thunderstorms, the accurate forecasting of hail size remains challenging. Hence, this thesis addresses the problem of predicting maximum hail size at the ground. Our approach uses a one-dimensional cloud model coupled with a time-dependent hail growth model known as HAILCAST. Specifically, we adopted the numerical code developed by Poolman (1992) and modified the microphysics based on findings from recent studies of hail growth.

The major objectives of our research are twofold. Firstly, we wish to determine the sensitivity of the modelled hail growth to changes in key thermodynamic and microphysical parameters. Secondly, we wish to determine the skill of HAILCAST in forecasting maximum hail diameter, with particular emphasis on forecasting large hail. We now summarise the major findings pertinent to the above mentioned objectives and the specific questions listed in section 1.5.1.

7.1 Conclusions

The first part of the thesis focuses on determining the sensitivity of HAILCAST to changes in input sounding data and entrainment, using a severe hailstorm sounding observed on 11 July 1985. The major findings regarding the sensitivity of the modelled updraft were:

- The maximum updraft velocity (W_{max}) increased with warmer temperatures and lower surface dew-point depressions.
- The temperature at the level of the maximum updraft (T_{wmax}) decreased with warmer surface temperatures and lower surface dew-point depressions.
- W_{max} and T_{wmax} were sensitive to small changes in surface temperature and dew-point: A 1 °C increase in temperature or dew-point increased W_{max} by ~20% and lowered T_{wmax} by ~ 30%.
- Including entrainment in the updraft calculations reduced W_{max} and increased T_{wmax}.
- W_{max} and T_{wmax} were not significantly influenced by changes in the vertical wind shear as large as 20%, unless the ESI was close to the threshold value of 1 m^2s^{-3} used to discriminate between lateral and cloud top entrainment.

Small changes in surface thermodynamic parameters had a significant impact on the modelled hail diameter, since they determined the amount of entrainment, maximum hail growth time, W_{max} and T_{wmax}. In particular we note the following:

- Small variations (~1°C) in surface temperature and dew-point significantly changed the maximum forecast hail diameter at the ground by up to 50%.
- For the severe hailstorm sounding used in this study, there appeared to be an optimum range of W_{max} (23 ms^{-1} to 30 ms^{-1}) and T_{wmax} (-18 °C to –27 °C) associated with large model derived hail at the ground.
- On days with strong updrafts (W_{max} >25 ms^{-1} and T_{wmax} < -27 °C), the final hail diameter was sensitive to the upper-limit of 60 min placed on the updraft duration/maximum hail growth time.

The sensitivity of hail growth to various microphysical parameters and parameterisation schemes was also investigated. In particular, the sensitivity tests showed that the final hail diameter was most sensitive to the following microphysical parameters:

- **Hail Embryo Diameter:** If the hail embryo was too small (<200 μm), only small hail was forecast at the ground on days with strong updrafts (~25 ms^{-1}). Increasing the embryo diameter led to larger hail and decreased the hail growth time.
- **Ventilation Coefficient:** The increase in ventilation coefficient for increasing diameter is crucial for the growth of large hail, since the increased heat transfer form the hailstone delays the onset of wet growth and melting, and in turn the shedding of excess water. Excluding the heat transfer coefficient from the ventilation coefficient calculations, decreased the final forecast hail diameter by as much as 60%.
- **LWC:** Reducing the LWC by only 10% reduced the final hail diameter by 40%. This highlights the significance of an adiabatic updraft core in creating a favourable environment for hail growth.
- **Collection Efficiency (E_i):** When the modelled hailstone entered the glaciated portion of the cloud, the magnitude of E_i was also critical in determining the final hail diameter. If the E_i was too small ($E_i < 0.2$), the model hailstone became trapped in the glaciated portion of the cloud, resulting in smaller hail diameter at the ground.

The modelled hail growth was found insensitive to schemes used to calculate the terminal velocity, cloud ice, embryo freezing temperature, and shedding of excess water during wet growth and melting.

To summarise: Small variations in the surface temperature and dew-point greatly impacted the maximum predicted hail diameter at the ground. Hail growth was also very sensitive to the hailstone's residence time above –40 °C and location of the hailstone with respect to this level when the updraft collapsed. Any changes in the input sounding data or microphysics that increased the height of the hailstone's trajectory or residence time above –40 °C, resulted in smaller hail at the ground. In other words, the maximum hail diameter is not solely determined by W_{max}, but is also dependent on T_{wmax} and the updraft duration. The

importance of taking the combined effects of CAPE and wind shear into consideration when modelling the updraft strength and duration, and in turn the hail growth, was also emphasised in case studies of a severe and non-severe hail day (Chapter 3).

In the second part of the thesis, we evaluated HAILCAST for no, non-severe and severe hail days during three summers (1983-1985), using observations of maximum hail size collected within the Alberta Hail Project (AHP) area. This is probably one of the world's most comprehensive data sets for observations of maximum hail size over a large area. The major results from the HAILCAST evaluation are summarised below:

- HAILCAST showed significant skill in forecasting the occurrence of hail, with a POD of 85% for all hail days.
- HAILCAST showed significant skill in distinguishing between hail and no hail days, with a HSS of 64%.
- HAILCAST showed significant skill in forecasting severe hail days, with a POD 89% and HSS of 67%.
- HAILCAST showed a positive BIAS, especially for the severe hail days.
- HAILCAST correctly forecast the hail size category for 38% of the 62 hail days, with 81% the forecasts within one size category.
- HAILCAST correctly forecast the hail size category for 39% of the 20 severe hail days, with 94% of the forecasts within one size category.
- HAILCAST proved fairly accurate when forecasting the maximum hail diameter at the ground, with a mean absolute error of 1.0 cm for all hail days, increasing to approximately 1.3 cm for severe hail days.

We also wished to determine if the improved microphysics used in HAILCAST increased the forecast skill over the nomogram approach of RAM (Renick and Maxwell, 1977) and the original SkyWatch model. The SkyWatch and RAM hail forecasts were, therefore, also evaluated against the AHP hail data

and compared with the skill of the HAILCAST forecasts. The major findings were:

- On hail days, HAILCAST scored the highest HSS and lowest FAR of all three techniques.
- On severe hail days, HAILCAST scored the highest HSS and POD. The HSS of HAILCAST was 27% and 13% higher than the corresponding scores for SkyWatch and RAM respectively.
- On severe hail days, SkyWatch showed a distinct negative BIAS.
- HAILCAST was significantly more accurate than other techniques when forecasting the hail size category on days with hail. On severe hail days, the percentage of correct HAILCAST forecasts was some 25% and 10% higher than those for SkyWatch and RAM respectively.
- All three models consistently underestimated the hail size category. This was particularly true for SkyWatch on severe hail days, with 82% of the forecasts one or more categories too small.
- On hail days, HAILCAST and RAM were more likely to overestimate the hail size category than SkyWatch.
- HAILCAST scored the highest percentage of correct forecasts and forecasts within one size category for all days.

The improved microphysics incorporated in HAILCAST significantly improved the model's forecast skill for severe hail days compared to SkyWatch. However, the same was not true when forecasting the occurrence or non-occurrence of hail days, with HAILCAST performing only marginally better than SkyWatch. Regarding the performance of HAILCAST versus the RAM nomogram, incorporating the coupled cloud and hail model with microphysics, did improve the overall skill and accuracy of the hail forecasts, especially for the severe days.

We noticed that HAILCAST displayed a positive BIAS when forecasting hail events. A possible explanation for this is that HAILCAST calculates the maximum hail diameter based on the expected convective instability. The model is not capable of determining if factors will be present that will prevent this instability from being released. This can result in a high FAR and positive BIAS. Thus, HAILCAST should be used in conjunction with the thunderstorm forecasting decision tree method of Colquhoun (1987) and conceptual model for severe thunderstorm outbreaks in Alberta (Smith and Yau, 1993). Such an approach would rule out hail on days when, although the atmosphere is conditionally unstable, there is either no trigger mechanism present or certain circulation patterns (such as an upper-air ridge) are expected to inhibit convection.

This thesis shows that HAILCAST provides a skilful aid for forecasting non-severe and severe hail. Moreover, HAILCAST provides excellent guidance of the maximum expected hail size category while avoiding some of the short-comings of current and past hail forecasting techniques. This is despite the limitations of a 1D cloud model and the expected uncertainty of the input sounding data.

7.2 Suggestions for Future Work

As mentioned previously, the 1D steady-state approach used in the HAILCAST cloud model is not ideally suited for modelling processes such as entrainment. Furthermore, the sensitivity experiments indicate that the maximum modelled hail diameter is strongly dependent on the residence time within the strong updraft. A natural improvement, therefore, would be to incorporate a time dependent cloud model in HAILCAST (rather than a steady-state cloud model). This would allow for a more realistic modelling of the cloud parameters (such as LWC and W_{max}) with time, and address the problem of determining the updraft duration. A time dependent three-dimensional cloud model combined with the hailstone growth model might also be useful for making individual case studies.

Of some concern is the excessive melting experienced by modelled hailstones below the freezing level (see Chapter 3). The most likely explanation for the excessive melting, is that below cloud base, the modelled hailstones fall through the ambient temperature and humidity profiles observed at the time of the sounding and not the storm's downdraft. Rasmussen and Heymsfield (1987b) found that the amount of melting is strongly dependent on the temperature and humidity profiles through which hailstone falls below the freezing level. We recommend, therefore, that future versions of HAILCAST should estimate the temperature and relative humidity of the downdraft below the freezing level using a process similar to that of Foster (1958).

Crook (1996) found that given numerical model sensitivity to small variations in surface temperature and moisture, convection initiation has limited predictability, at least for models initialized with data from the present observing systems. One means of improving the predictability of the atmosphere, is to perform a number of simulations (ensembles) each starting with slightly different initial conditions. As long as the different initial conditions span the domain of expected error in the initial fields, the ensemble mean should provide a better forecast than most individual forecasts (Brooks and Doswell, 1993). Brooks et al. (1992) and Brooks and Doswell (1993) suggest the use of a quasi-Monte Carlo or probabilistic approach, rather than a deterministic approach used in previous studies to forecast the type of convection. The probabilistic approach requires the forecaster to vary the input data over a range of values expected in the area where the convection is anticipated. Further, if the forecast value of a particular input variable (such as surface moisture) is uncertain, the forecaster can conduct numerous model runs for a range of moisture values expected on the day in question.

The quasi-Monte Carlo approach also considers scenarios that may have been considered unlikely, thereby reducing the number of surprises. Moreover, each

event can be allocated a probability and the forecaster can use this information to decide which scenario is most likely for the expected conditions.

The HAILCAST model is ideally suited to this approach, since a large number of model runs can be carried out within a very short period of time. As was shown in Chapter 4, the modelled hail diameter is most sensitive to small changes in the surface temperature and dew-point. We suggest that future users of HAILCAST first determine the expected maximum temperature and corresponding dew-point expected in the target area, and then run the model over a range of surface conditions.

Issuing timely warnings of severe hail is critically dependent on the availability of a sounding representative of the expected thunderstorm environment. Further, a forecaster is often required to determine the likelihood of severe thunderstorms over a large area and this would require many soundings. This is particularly true for rapidly evolving weather systems or if the air mass is non-homogenous in space and time. Unfortunately, current sounding networks are very coarse and soundings are only conducted twice daily. One means of addressing the problem of obtaining representative soundings in advance, would be to use a regional numerical prediction model (NWP) to provide prognostic soundings at each grid-point within the model domain. A technique suggested by Colquhoun and Mills (1998) would then be applied at each grid-point, to determine whether conditions are favourable for the formation of thunderstorms. HAILCAST would then be initialized using the prognostic sounding and surface data at grid points where thunderstorms are expected. This approach would also allow forecasters to identify areas most at threat for hail, as well as providing an estimate of the maximum hail diameter. Mills and Colquhoun (1998) noted that a similar approach has considerable potential for providing guidance when forecasting areas of thunderstorms and severe thunderstorms. In light of HAILCAST's sensitivity to small changes in the input sounding data, it is proposed the NWP model should be run using a quasi-Monte Carlo or similar

ensemble approach. Future research should focus on implementing and evaluating forecasts of maximum hail diameter using the above methodology through detailed case studies.

REFERENCES

Admirat , P., G.G. Goyer, L. Wojtiw, E.A. Carte, D. Roos, and E.P. Lozowski, 1985: A comparative study of hail in Switzerland, Canada and South Africa. *J. of Climatol.*, **5**, 35-51.

Aktary, N., 1993. Analysis of Conditional Symmetric Instability in central Alberta. Ph.D. Thesis, Dept. Earth and Atmospheric Sciences, University of Alberta, 146 pp.

Alford, P., 1998: An improved approach to severe thunderstorm advice and warning verification in Australia. 18th Conference on Severe Local Storms, San Francisco, Amer. Meteor. Soc., 703-707.

Al-Jumily, K.J., R.C. Charlton, and R.G. Humphries, 1991: Identification of rain and hail with circular polarization radar. *J. Appl. Meteor.*, **30**, 1075-1087.

Anthes, R.A., 1977: A cumulus parameterization scheme utilizing a one-dimensional cloud model. *Mon. Wea. Rev.*, **105**, 270-286.

Bailey, I.H., and W.C. Macklin, 1968: Heat transfer from artificial hailstones. *Quart. J. Roy. Meteor. Soc.*, **94**, 93-98.

Barge, B.L., and G.A. Isaac, 1970: The shape of Alberta hailstones. *J. Rech. Atmos.*, **7**, 11-20.

Betts, A.K., 1982: Saturation point analysis of moist convective overturning. *J. Atmos. Sci.*, **39**, 1484-1505.

Betts, A.K., 1982: Cloud thermodynamics models in saturation point coordinates.

J. Atmos. Sci., **39**, 2182-2191.

Bluestein, H.B., E.W. McCaul, Jr., G.P. Byrd, and G.R. Woodall, 1988: Mobile sounding observations of a tornadic storm near the dryline: The Canadian Texas storm of 7 May 1986. *Mon. Wea. Rev.*, **116**, 1790-1804.

Blyth, A.M., M. Alan, W.A. Cooper, and J.B. Jensen, 1988: A study of the source of entrained air in Montana cumuli. *J. Atmos. Sci.*, **45**, 3944-3964.

Boatman, J.F., and A.H. Auer, Jr., 1983: The role of cloud top entrainment in cumulus clouds. *J. Atmos. Sci.*, **45**, 1517-1534.

Böhm, J.P., 1992: A general hydrodynamic theory for mixed-phase microphysics. Part I: Drag and fall speed of hydrometeors. *Atm. Res.*, **27**, 253-274.

Brandes, E.A., J. Vivekanandan, J.D. Tuttle, and C.J. Kessinger, 1995: A study of thunderstorm microphysics with multiparameter radar and aircraft observations. *Mon. Wea. Rev.*, **118**, 1640-1664.

Brooks, H.E., C.A. Doswell III, and R.A. Maddox, 1992: On the use of mesoscale and cloud-scale models in operational forecasting. *Wea. Forecasting*, **7**, 120-132.

Brooks, H.E., C.A. Doswell III, 1993. STORMTIPE: A forecasting experiment using a three-dimensional cloud model. *Wea. Forecasting*, **8**, 352-363.

Brooks, H.E., C.A. Doswell III, and J. Cooper1994: On the environments of tornadic and nontornadic mesoscyclones. *Wea. Forecasting*, **9**, 606-618.

Brooks, H.E., M.T. Carr, and J.E. Ruthford, 1996: Preliminary analysis of soundings from VORTEX-95. Preprints, 18th Conference on Severe Local

Storms, San Francisco, Amer. Meteor. Soc., 133-136.

Browning, K.A., and G.B. Foote, 1976: Airflow and hail growth in supercell storms and some implications for hail suppression. *Quart. J. Roy. Met. Soc.*, **102**, 499-533.

Browning, K.A., 1977. The Structure and Mechanisms of Hailstorms. Meteor. Monogr., No. 38, 1-43.

Bunkers, M.J., 1996: Examination of the pre-convective environment associated with a severe nontornadic supercell: Variations in CAPE and SREH. Preprints, 18th Conference on Severe Local Storms, San Francisco, Amer. Meteor. Soc., 703-707.

Burgess, D.W., 1988: The environment of the Edmond, Oklahoma, tornadic storm. Preprints 15th Conference on Severe Local Storms, Baltimore, Amer. Meteor. Soc., 292-295.

Carras, J.N., and W.C. Macklin, 1973: The shedding of accreted water during hailstone growth. *Quart. J. Roy. Meteor. Soc.*, **99**, 639-648.

Charlton, R.B., B.M. Kachman, L. Wojtiw, 1995. Urban hailstorms: A view from Alberta. *Natural Hazards*, **12**, 29-75.

Charlton, R.B., B.M. Kachman, and L. Wojtiw, 1998. The Edmonton tornado and hailstorm: A decade of research. CMOS Bulletin, **26**, 56 pp.

Cheng, L., and D.C Rogers, 1988: Hailfalls and hailstorm feeder clouds-an Alberta case study. *J. Atmos. Sci.*, **45**, 3533-3545.

Chisholm, A.J., and J.H. Renick, 1972: The kinematics of multi-cell and

supercell Alberta hailstorms. Hail Studies Report 72-2, Alberta Research Council, 24-31.

Chisholm, A.J., 1973. Alberta Hailstorms. Part I: Radar case studies and airflow models. Meteor. Monogr., No. 36, Amer. Meteor. Soc., 1-36.

Chong, S., and C.S. Chen, 1974: Water shells on ice pellets and hailstones. *J. Atmos. Sci.*, **31**, 1384-1391.

Clarke, T.L., 1982: Cloud modeling in three spatial dimensions. Hailstorms of the High Plains, Vol. II: Case Studies of the National Hail Research Experiment, C.A. Knight and P. Squires, Eds., Colorado Assoc. Universities Press, Boulder, 225-247.

Colquhoun, J.R., and G.A. Mills, 1998: Thunderstorm and severe thunderstorm prediction using a decision tree and mesoscale NWP model. Preprints, 19th Conference on Severe Local Storms, Minneapolis, Amer. Meteor. Soc., 607-609.

Cotton W.R., and A.A. Anthes, 1989: Storm and Cloud Dynamics, Academic Press Inc., San Diego, 883 pp.

Crook, N.A., 1996: Sensitivity of moist convection forced by boundary layer processes to low-level thermodynamic fields. *Mon. Weather. Rev.*, **124**, 1767-1785

Crum, T.D., and J.J. Cahir, 1983: Experiments in shower top forecasting using an interactive one-dimensional cloud model. *Mon. Weather. Rev.*, **111**, 829-835.

Darkow, G.L., 1969: An analysis of over sixty tornado proximity soundings.

Preprints, 6th Conf. on Severe Local Storms, Chicago, Amer. Meteor. Soc., 218-221.

Deibert, R., 1985: Field program report. Alberta Research Council. Natural Resources Division, Atmospheric Sciences Department, Canada, 70 pp.

Dennis, A.S., and D.J. Musil, 1973: Calculations of hailstorm growth and trajectories in a simple cloud model. *J. Atmos. Sci.*, **30**, 278-288.

Doswell, C.A. III, J.T. Schaefer, D.W. McCann, T.W. Schlatter, and Wobus, H.B., 1982: Thermodynamic analysis procedures at the National Severe Storms Forecast Centre. Preprints, 9th Conf. Weather Forecasting and Analysis, Seattle, Amer. Meteor. Soc., 304-309.

Edwards, R., and R.L. Thompson, 1998: Nationwide comparisons of hail size with WSR-88D vertically integrated liquid water and derived thermodynamic sounding data. *Wea. Forecasting*, **13**, 277-285.

English, M., 1973. Alberta Hailstorms. Part II: Growth of large hail in the storm. Meteor. Monogr., No. 36, Amer. Meteor. Soc., 37-98.

Farley, R.D., 1987: Numerical modelling and hailstone growth. Part III: Simulation of an Alberta hailstorm- natural and seeded cases. *J. of Clim. and Appl. Meteor.*, **26**, 789-812.

Fawbush, E.J., and R.C. Miller, 1953: A method of forecasting hailstone size at the earth's surface. *Bull. Amer. Meteor. Soc.*, **34**, 235-244.

Federer, B., J. Jouzel, and A. Waldvogel, 1978: Hailstone trajectories determined from crystallography, deutrium content and radar backscattering. *Pageoph.*, **116**, 112-129.

Foote, G.B., 1984: A study of hail growth utilizing observed storm conditions. J. *Climate and Appl. Meteor.*, **23**, 84-101..

Foster, D.S., and F.C. Bates, 1956: A hail size forecasting technique. *Bull. Amer. Meteor. Soc.*, **35**, 135-140.

Foster, D.S., 1958: Thunderstorm gusts compared with computed downdraft speed. *Mon. Wea. Rev.*, **86**, 91-94.

Garcia-Garcia, F., and R. List, 1992: Laboratory measurements and parameterizations of supercooled water skin temperatures and bulk properties of gyrating hailstones. *J. Atmos. Sci.*, **49**, 2058-2073.

Geresdi, I., 1998: Idealised simulation of the Colorado hailstorm: Comparison of bulk and detailed microphysics., *Atmos. Res.*, **45**, 237-252.

Golden, J.H., R. Serafin, V. Lally, and J. Facundo, 1986: Atmospheric sounding systems. *Mesoscale Meteorology and Forecasting*, P.S. Ray, Ed., Amer. Meteor. Soc., 50-70.

Greenan, B.J., and R. List, 1995: Experimental closure of the heat and mass transfer theory of spheroidal hailstones. *J. Atmos. Sci.*, **52**, 3797-3815.

Heymsfield , A.J., 1978: The characteristics of graupel particles in northeastern Colorado cumulus congestus clouds. *J. Atmos. Sci.*, **35**, 284-295.

Heymsfield, A.J., A.R. Jameson, and H.W. Frank, 1980: Hail growth mechanisms in a Colorado storm. Part II: Hail formation processes. *J. Atmos. Sci.*, **37**, 1789-1807.

Holler, H., V.N. Bringi, J. Hubbert, M. Hagen, and P.F. Meischner, 1994: Life

cycle and precipitation formation in a hybrid-type hailstorm revealed by polarimetric and Doppler radar measurements. *J. Atmos. Sci.*, **51**, 2500-2522.

Johns, R.H. and C.A., Doswell III, 1992: Severe local storm forecasting. *Symposium on weather forecasting.* Amer. Meteor. Soc., 1992, 225-236.

Knight, C.A., J.L. Miller, N.C. Knight, and D. Breed, 1982: The 22 June 1976 Case study: Precipitation formation. Hailstorms of the High Plains, Vol. II: Case Studies of the National Hail Research Experiment, C.A. Knight and P. Squires, Eds., Colorado Assoc. Universities Press, Boulder, 61-89.

Knight, C.A., and N.C. Knight, 1978: Cyndrical ice accretions as simulations of hail growth: II. The structure of fresh and annealed accretions. *J. Atmos. Sci.*, **35**, 1997-2009.

Knight, N.C., 1981: Climatology of hailstone embryos. *J. Appl. Meteor.*, **20**, 750-755.

Knight, C.A., and N.C. Knight, 1998: Hailstorms. Unpublished manuscript.

Kochtubajda, B., and C. Gibson, 1992: A study to evaluate existing hail detection algorithms for the Alberta region. Atmospheric Environment Service, Downsview, Ontario, Canada.

Krauss T.W., and J.D. Marwitz, 1984: Precipitation processes within an Alberta supercell hailstorm. *J. Atmos. Sci.*, **41**, 1025-1034.

Kubesh, R.J., D.J. Musil, R.D. Farley, and H.D. Orville, 1988: The 1 August CCOPE Storm: Observations and modeling results. *J. Appl. Meteor.*, **27**, 216-243.

Leftwich, P.W., 1984: Operational experiments in prediction of maximum expected hailstone diameter. Preprints, 10th Conf. on Weather Forecasting and Analysis, Amer. Meteor. Soc., Clearwater Beach, 525-528.

Lesins, G.B., and R. List, 1986: Sponginess and drop shedding of gyrating hailstones in a pressure-controlled icing wind tunnel. *J. Atmos. Sci.*, **43**, 2813-2825.

List, R., 1985. Properties and Growth of Hailstones. Thunderstorm Morphology and Dynamics, Norman, OK, Univ. of Oklahoma Press, 411 pp.

Macklin, W.C., 1977, and F.H. Ludlam, 1961: The fallspeed of hailstones. *Quart. J. Roy. Meteor. Soc.*, **87**, 72-81.

Macklin, W.C., 1977. The characteristics of natural hailstones and their interpretation. Meteor. Monogr., No. 38, 65-88.

Mather, G.K., D. Treddenick, and R. Parsons, 1976: An observed relationship between the height of the 45 dBZ contours in storm profiles and surface hail reports. *J. Appl. Meteor.*, **15**, 1336-1340.

Matson, R.J., and A.W. Huggins, 1980: The direct measurement of the sizes, shapes, and kinematics of falling hailstones. *J. Atmos. Sci.*, **37**, 1107-1125.

Maxwell, J.B., 1974: Unpublished LMA diagnostic results. Atmospheric Environment Service, Toronto, Ontario.

McGinley, J., 1986. Nowcasting Mesoscale Phenomena. *Mesoscale meteorology and forecasting*, P.S. Ray, Ed., Amer. Meteor. Soc., 657-688.

Miller, L.J., J.D. Tuttle, and C.A. Knight, 1988: Airflow and hail growth in a

severe Northern High Plains supercell. *J. Atmos. Sci.*, **45**, 736-762.

Miller, L.J., J.D. Tuttle, and G.B. Foote, 1990: Precipitation production in a large Montana hailstorm: Airflow and particle growth. *J. Atmos. Sci.*, **57**, 1619-1646.

Mills, G.A., and J.R. Colquhoun, 1998: Objective prediction of severe thunderstorm environments: Preliminary results linking a decision tree with an operational regional NWP model. Wea. Forecasting in print.

Modahl, A.C., 1979: Low-level wind and moisture variations preceding and following hailstorms in Northeast Colorado. *Mon. Wea. Rev.*, **107**, 442-449.

Moore, J.T., and J.P. Pino, 1990: An interactive method for estimating maximum hailstone size from forecast soundings. *Wea. Forecasting*, **5**, 508-526.

Morgan, G.M., and N.G. Towery, 1975: Small-scale variability of hail and its significance for hail prevention experiments. *J. Appl. Meteor.*, **14**, 763-770.

Mueller, C.K., J.W. Wilson, and N.A. Crook, 1993: The utility of sounding and mesonet data to nowcast thunderstorm initiation. *Wea. Forecasting*, **8**, 132-146.

Musil, D.J., 1970: Computer modeling of hailstone growth in feeder clouds. *J. Atmos. Sci.*, **26**, 474-482.

Musil, D.J., A.J. Heymsfield, and P.L. Smith, 1986: Microphysical characteristics of a well-developed weak echo region in a High Plains supercell thunderstorm. *J. Climate and Appl. Meteor.*, **25**, 1037-1051.

Nelson, S.P., 1983: The influence of storm flow structure on hail growth. *J. Atmos. Sci.*, **40**, 1965-1983.

Orville, H.D., 1977: A review of hailstone-hailstorm numerical simulations. Meteor. Monogr., No. 38, 49-61.

Orville, H.D., and F.J. Kopp, 1977: Numerical simulation of the life history of a hailstorm. *J. Atmos. Sci.*, **34**, 1596-1618.

Paluch, I.R., 1978: Size sorting of hail in a three-dimensional updraft and implications for hail suppression. *J. Appl. Meteorology*, **17**, 763-777.

Paluch, I.R., 1979: The entrainment mechanism in Colorado cumuli. *J. Atmos. Sci.*, **36**, 2467-2478.

Poolman, E.R., 1992: Die voorspelling van haelkorrelgroei in Suid-Afrika. M.Sc. Thesis, Faculty of Engineering, University of Pretoria, 113 pp.

Pruppacher, H.R., and R. Rasmussen, 1979: A wind tunnel investigation of the rate of evaporation of large water drops falling at terminal velocity in air. *J. Atmos. Sci.*, **36**, 1255-1260.

Rasmussen, R.M., and A.J. Heymsfield, 1987a: Melting and shedding of graupel and hail. Part I: Model physics. *J. Atmos. Sci.*, **44**, 2754-2763.

Rasmussen, R.M., and A.J. Heymsfield, 1987b: Melting and shedding of graupel and hail. Part II: Sensitivity study. *J. Atmos. Sci.*, **44**, 2764-2782.

Rasmussen, R.M., and A.J. Heymsfield, 1987c: Melting and shedding of graupel and hail. Part III: Investigation into the role of shed drops as hail embryos in the 1 August CCOPE severe storm. *J. Atmos. Sci.*, **44**, 2783-

2803.

Rasmussen, R.M., and V. Levizzani and H.R. Pruppacher, 1984b: A wind tunnel and theoretical study on the melting behaviour of atmospheric ice particles. III: Experiment and theory for spherical ice particles of radius >500 μm. *J. Atmos. Sci.*, **41**, 381-388.

Renick, J.H. and J.B. Maxwell, 1977. Forecasting hailfall in Alberta. Meteor. Monogr., No. 38, Amer. Meteor. Soc., 145-151.

Renick, J.H., 1983: Field program report. Alberta Research Council. Natural Resources Division, Atmospheric Sciences Department, Canada, 64 pp.

Renick, J.H., 1984: Field program report. Alberta Research Council. Natural Resources Division, Atmospheric Sciences Department, Canada, 60 pp.

Reuter, GW., 1985: Observations and numerical simulations of mixing mechanisms in South African cumulus congestus clouds. Sci. Rept. MW-95, Stormy Weather Group, McGill University, 286 pp.

Reuter, G.W. and L. Aktary, 1995: Convective and symmetric instabilities and their effects on precipitation: Seasonal variations in central Alberta during 1990 and 1991. *Mon. Wea. Rev.*, **123**, 153-162.

Roeseler, C.A., and L. Wood, 1997: VIL density and associated hail size along the northwest Gulf coast. Preprints, 28th Conf. on Radar Meteorology, Austin, Amer. Meteor. Soc., 434-435.

Rogers, R.R., and M.K. Yau, 1996. A short course in Cloud Physics. Butterworth- Heinemann, 290 pp.

Rottuno, R., and J.B. Klemp 1982: The influence of the shear-induced pressure gradient on thunderstorm motion. *Mon. Wea. Rev.*, **110**, 136-151.

Sanders, F., 1986: Temperatures of air parcels lifted from background, application and nomograms. *Wea. Forecasting*, **1**, 190-205.

Schaefer, J.T., and R.P. McNulty, 1996: Using mean humidity as an aid for forecasting thunderstorms and their characteristics. Preprints, 18th Conference on Severe Local storms, San Francisco, Amer. Meteor. Soc., 650-653.

Schlesinger, R.E., 1978: A three-dimensional numerical model of an isolated thunderstorm: Part 1: Comparative experiments for variable wind shear. *J. Atmos. Sci.*, **35**, 690-713.

Smith, S.B., and M.K. Yau, 1993: The causes of severe convective outbreaks in Alberta. Part I. A comparsion of a severe outbreak with two nonsevere events. *Mon. Wea. Rev.*, **109**, 1099-1125.

Smith, S.B., and M.K. Yau, 1993: The causes of severe convective outbreaks in Alberta. Part II: Conceptual model and statistical analysis. *Mon. Wea. Rev.*, **109**, 1126-1134.

Smith, S.B, G.W. Reuter, and M.K. Yau, 1998: The episodic occurrence of hail in central Alberta and the Highveld of South Africa. *Atm. Ocean.*, **36**, 169-178.

Strong, G.S., 1986. Synoptic to mesoscale dynamics of severe thunderstorm environments: A diagnostic study with forecasting applications. Ph.D. Thesis, Dept. Geography, University of Alberta, 345 pp.

Vali, G., and E.J. Stansbury, 1965: Time-dependant characteristics of the heterogeneous nucleation of ice. Sci. Rept., MW-41, Montreal, McGill University, 31 pp.

Wagenmaker, R.B., 1992: Operational detection of hail by radar using heights of VIP-5 reflectivity echoes. *Natl. Wea. Dig.*, **17**, 2-5.

Waldvogel, A., B. Federer, W. Schmid, and P.Grimm, 1979: Criteria for the detection of hail cells. *J. Appl. Meteor.*, **18**, 1521-1525.

Weisman, M.L., and J.B. Klemp, 1982: The dependence of numerically simulated convective storms on vertical wind shear and buoyancy. *Mon. Wea. Rev.*, **110**, 504-520.

Weisman, M.L., M.S. Gilmore, and L.J. Wicker, 1998: The impact of convective storms on their local environment: What is an appropriate ambient sounding? Preprints, 19th Conf. on Severe Local Storms, Minneapolis, Amer. Meteor. Soc., 238-241.

Weisman, M.L., and J.B. Klemp, 1986. Characteristics of isolated storms. *Mesoscale Meteorology and Forecasting*, P.S. Ray, Ed., Amer. Meteor. Soc., 331-357.

Wisner, C., H.D. Orville, and C. Meyers, 1972: A numerical model of a hail-bearing cloud. *J. Atmos. Sci.*, **29**, 1160-1181.

Witt, A., M.D. Eilts, G.J. Stumpf, J.T. Johnson, E. DeWayne Mitchell, and K.W. Thomas, 1998: An enhanced hail detection algorithm for the WSR-88D. *Wea. Forecasting*, **13**, 286-303.

Wojtiw, L., 1975. Climatic summaries of hailfall in central Alberta (1957-1973).

Alberta Research Council, 102 pp.

Xu, J.L., 1983: Hail growth in a three-dimensional cloud model. *J. Atmos. Sci.*, **40,** 185-203.

Young, K.C., 1977: A numerical examination of some hail suppression concepts. Meteor. Monogr., No. 38, 195-214.

Ziegler, C.L., P.S. Ray, and N.C. Knight, 1983: Hail growth in an Oklahoma multicell storm. *J. Atmos. Sci.*, **40,** 1768-1792.

Appendix A: ESI and Storm Type

The calculation of CAPE and vertical wind shear used to determine the Energy Shear Index (ESI) will be described before proceeding with a detailed description of the ESI.

Calculation of CAPE and Vertical Wind Shear

CAPE is calculated by integrating the difference in virtual temperature between the environment and a parcel rising along the pseudo-adiabat, between the Level of Free Convection (LFC) and the Equilibrium Level (EL), and is defined by

$$CAPE = R_d \int_{p_{lfc}}^{p_{el}} [T^*(p) - T(p)] d\ln p, \qquad \text{(A-1)}$$

where R_d is the gas constant, T^* and T are the virtual temperatures of the parcel the environmental air respectively, p_{el} the pressure of the EL and p_{lfc} the pressure at the LFC.

In numerical simulations of convective storms in various vertical wind shear regimes, Weisman and Klemp (1986) determined that the type of thunderstorm was strongly dependent on the magnitude of the vertical wind shear in the lowest 5-6 km AGL. In this thesis, the vertical wind shear (S) is calculated by the magnitude of the shear vector between 850 hPa and the 6 km (approximately 475 hPa) winds.

Calculation of the Energy Shear Index (ESI)

In studies of Alberta hailstorms, Chisholm and Renick (1972) found that the magnitude of the vertical wind shear in the lowest 6 km AGL increased as the convection intensified from air-mass to supercell thunderstorms. The role of CAPE in determining the strength of convection and its interaction with the vertical wind shear in determining storm type, has already been discusses in section 1.2. To combine the effect of buoyancy and vertical wind shear in the cloud model, the Energy Shear Index (ESI) in units of m^2s^{-3} is defined by

$$ESI = CAPE*S. \qquad \text{(A-2)}$$

The rationale behind the ESI, is to combine the effects of buoyancy and the vertical wind shear in the lowest half of the troposphere, with larger products indicating an increased potential for severe thunderstorms. It is proposed therefore, that the ESI is ideally suited for determining the type and severity of convection.

To determine threshold values for classifying storm type in central Alberta, ESI values were calculated for 160 proximity soundings at Penhold from June 21- August 31 (1983-1985) and grouped into no-hail, non-severe and severe hail days. The results are summarised in Table A1.

Table A1 shows that there is a distinct increase in the mean and maximum ESI values from no-hail to severe hail days, associated with the increased CAPE and wind shear typically observed on severe hail days. Chisholm and Renick (1972) noted that most severe hailstorms in central Alberta are strong multi-cell or supercell thunderstorms. Keeping this in mind and using the ESI statistics from Table A1, four storm types were determined for utilisation in the cloud model (Table A2).

Table A1: ESI (m^2s^{-3}) statistics for 98 no hail days, 42 non-severe hail days and 20 severe hail days observed during the summers 1983-1985.

Day	Statistics	1983	1984	1985
	Mean ESI	4.6	4.8	3.2
Severe Hail	**Std. Deviation**	1.4	1.9	2.1
	Maximum ESI	6.8	7.1	5.7
	Minimum ESI	3.0	2.3	1.2
	Mean ESI	1.3	2.6	1.9
Non-Severe Hail	**Std. Deviation**	1.9	1.4	1.0
	Maximum ESI	8.4	4.7	3.5
	Minimum ESI	0.4	0.0	0.0
	Mean ESI	0.7	0.8	0.9
No Hail	**Std. Deviation**	0.8	0.7	0.7
	Maximum ESI	2.8	2.3	3.3
	Minimum ESI	0.0	0.0	0.0

Table A2: Storm type classification scheme based on the ESI.

Storm Type	ESI Range (m^2s^{-3})	Description
0	[0;1]	Towering cumulus or Weak Air-mass Thunderstorms
I	(1;3]	Air-Mass or Weak Multi-cell Thunderstorms
II	(3;5]	Strong Multi-cell Thunderstorms
III	>5	Supercell Thunderstorms

Applying the above classification system to the ESI values in Table A1 implies that most severe hailstorms in central Alberta during the summers of 1983-1985 were strong multi-cell storms, with supercell storms being infrequent. This is in agreement with the findings of Chisholm and Renick (1972).

Appendix B: Days Excluded from the Data Set

Key

A = Soundings with missing temperature, dew-point or wind data at any level

B = Soundings modified by the passage of outflow boundary

C = Soundings taken in rain or during a thunderstorm (so called "raintemp")

D = Days when the hailstorms developed and produced hail more than 100 km from Penhold or when hailstorms were not observed within 3 hours of the 1715 LDT sounding

E = Days when the exact location and timing of the maximum hail was uncertain

F = Days when thunderstorm development was limited to the foothills.

Table B1: Days excluded from the model evaluation data set for 1983.

Date	Reason for Exclusion
830620	C
830625	D/E
830627	C
830630	C
830701	C
830705	D
830708	E/D
830711	A
830712	C
830714	A
830715	C
830719	A
830720	D
830725	D
830801	D/F
830805	A
830808	F/D
830814	F/D
830816	D
830818	A
830826	E
830828	E

Table B2: Days excluded from the model evaluation data set for 1984.

Date	Reason for Exclusion
840624	D
840629	E
840717	F
840718	F
840719	F
840720	B
840801	F/D
840805	D/E
840810	D
840811	F
840813	E
840818	D
840819	D
840823	F
840825	A
840831	F

Table B3: Days excluded from the model evaluation data set for 1985.

Date	Reason for Exclusion
850620	E
850622	D/F
850624	C
850628	D/F
850705	D/E
850706	A
850707	A
850713	D/E
850714	A
850716	C
850719	B
850722	D/E
850807	B
850808	B
850811	C
850812	C
850814	C
850815	C/B
850821	C
850825	C/B
850831	C

Appendix C: Contingency Tables

Table C1: HAILCAST contingency table for 62 hail days from 1983-1985.

		Forecast	
		Hail	**No Hail**
Observed	**Hail**	53	9
	No Hail	19	79

Table C2: HAILCAST contingency table for 20 severe hail days from 1983-1985.

		Forecast	
		Severe Hail	**No Severe Hail**
Observed	**Severe Hail**	18	2
	No SevereHail	12	128

Table C3: SkyWatch contingency table for 62 hail days from 1983-1985.

		Forecast	
		Hail	**No Hail**
Observed	**Hail**	52	10
	No Hail	20	78

Table C4: SkyWatch contingency table for 20 severe hail days from 1983-

1985.

		Forecast	
		Severe Hail	**No Severe Hail**
Observed	**Severe Hail**	7	13
	No SevereHail	4	136

Table C5: RAM contingency table for 62 hail days from 1983-1985.

		Forecast	
		Hail	**No Hail**
Observed	**Hail**	56	6
	No Hail	30	68

Table C6: RAM contingency table for 20 severe hail days from 1983-1985.

		Forecast	
		Severe Hail	**No Severe Hail**
Observed	**Severe Hail**	13	7
	No SevereHail	10	130

Appendix D: Hail Size Category Forecasts

Table D1: Forecast hail size categories versus observed for HAILCAST, SkyWatch and RAM for the summer of 1983.

Date	Observed	HAILCAST	SkyWatch	RAM
83621	PEA	PEA	SHOT	SHOT
83622	WALNUT	WALNUT	WALNUT	WALNUT
83623	NONE	NONE	NONE	NONE
83624	WALNUT	GOLF	GOLF	>GOLF
83626	NONE	NONE	NONE	NONE
83628	NONE	NONE	NONE	NONE
83629	PEA	NONE	NONE	NONE
83702	GRAPE	NONE	NONE	NONE
83703	GRAPE	PEA	SHOT	SHOT
83704	NONE	GRAPE	PEA	PEA
83706	GOLF	GOLF	GRAPE	GOLF
83707	GRAPE	GRAPE	NONE	PEA
83709	NONE	NONE	NONE	NONE
83710	NONE	NONE	NONE	NONE
83713	WALNUT	GOLF	PEA	GRAPE
83716	PEA	PEA	SHOT	SHOT
83717	GRAPE	GRAPE	WALNUT	WALNUT
83718	NONE	PEA	GRAPE	GRAPE
83721	WALNUT	WALNUT	WALNUT	GOLF
83722	NONE	NONE	NONE	NONE
83723	NONE	GRAPE	PEA	PEA
83724	GOLF	>GOLF	WALNUT	WALNUT
83726	GRAPE	WALNUT	PEA	PEA
83727	NONE	NONE	NONE	NONE
83728	GRAPE	PEA	NONE	SHOT
83729	PEA	WALNUT	SHOT	PEA
83730	NONE	NONE	NONE	NONE
83731	NONE	NONE	NONE	NONE
83802	NONE	NONE	NONE	NONE
83803	GOLF	GOLF	WALNUT	WALNUT
83804	NONE	NONE	NONE	NONE
83806	NONE	NONE	NONE	NONE
83807	NONE	NONE	NONE	NONE
83809	NONE	GRAPE	NONE	SHOT
83810	NONE	NONE	NONE	NONE
83811	NONE	NONE	NONE	NONE
83812	NONE	NONE	NONE	NONE
83813	NONE	NONE	NONE	NONE
83815	GOLF	WALNUT	GRAPE	GOLF
83817	GRAPE	WALNUT	PEA	GRAPE
83819	NONE	NONE	NONE	NONE
83820	PEA	PEA	SHOT	PEA
83821	NONE	NONE	NONE	NONE
83822	NONE	NONE	NONE	NONE
83823	GRAPE	NONE	PEA	GRAPE
83824	PEA	PEA	SHOT	PEA
83825	PEA	PEA	PEA	PEA
83827	GRAPE	PEA	GRAPE	GRAPE
83829	NONE	NONE	NONE	NONE
83830	NONE	NONE	NONE	NONE
83831	NONE	NONE	NONE	NONE

Table D2: Forecast hail size categories versus observed for HAILCAST, SkyWatch and RAM for the summer of 1984.

Date	Observed	HAILCAST	SkyWatch	RAM
84620	SHOT	PEA	PEA	PEA
84621	SHOT	NONE	NONE	NONE
84622	GRAPE	PEA	SHOT	PEA
84623	NONE	SHOT	NONE	PEA
84625	WALNUT	WALNUT	PEA	GRAPE
84626	NONE	NONE	NONE	NONE
84627	NONE	WALNUT	SHOT	PEA
84628	NONE	NONE	SHOT	PEA
84630	NONE	NONE	NONE	PEA
84701	NONE	NONE	SHOT	NONE
84702	NONE	PEA	PEA	PEA
84703	NONE	NONE	NONE	NONE
84704	PEA	WALNUT	PEA	PEA
84705	GRAPE	PEA	SHOT	PEA
84706	GOLF	WALNUT	PEA	PEA
84707	NONE	PEA	SHOT	SHOT
84708	NONE	PEA	SHOT	SHOT
84709	NONE	PEA	PEA	PEA
84710	NONE	WALNUT	NONE	PEA
84711	GRAPE	GRAPE	GRAPE	GRAPE
84712	WALNUT	GOLF	WALNUT	WALNUT
84713	NONE	NONE	NONE	NONE
84714	NONE	NONE	NONE	NONE
84715	NONE	PEA	NONE	SHOT
84716	NONE	NONE	NONE	NONE
84721	GRAPE	GOLF	GRAPE	PEA
84722	NONE	NONE	NONE	NONE
84723	NONE	NONE	NONE	NONE
84724	NONE	NONE	NONE	NONE
84725	NONE	NONE	NONE	NONE
84726	GRAPE	GRAPE	GRAPE	GOLF
84727	NONE	NONE	NONE	NONE
84728	>GOLF	GOLF	GRAPE	>GOLF
84729	NONE	NONE	NONE	SHOT
84730	GRAPE	GOLF	GRAPE	WALNUT
84731	NONE	NONE	NONE	NONE
84802	GRAPE	GRAPE	PEA	GRAPE
84803	GRAPE	GOLF	GRAPE	WALNUT
84804	PEA	PEA	NONE	PEA
84806	GOLF	WALNUT	WALNUT	WALNUT
84807	NONE	GRAPE	NONE	PEA
84808	NONE	NONE	NONE	NONE
84809	NONE	PEA	PEA	GRAPE
84812	GRAPE	NONE	NONE	NONE
84814	NONE	NONE	NONE	SHOT
84815	NONE	NONE	NONE	NONE
84816	NONE	NONE	NONE	NONE
84817	GRAPE	GRAPE	GRAPE	WALNUT
84820	NONE	NONE	NONE	NONE
84821	NONE	NONE	NONE	NONE
84822	NONE	NONE	NONE	NONE
84824	WALNUT	GRAPE	GRAPE	WALNUT
84826	NONE	NONE	NONE	NONE
84827	NONE	NONE	NONE	SHOT
84828	NONE	NONE	PEA	PEA
84829	NONE	NONE	NONE	NONE
84830	NONE	NONE	NONE	NONE

Table D3: Forecast hail size categories versus observed for HAILCAST, SkyWatch and RAM for the summer of 1985.

Date	Observed	HAILCAST	SkyWatch	RAM
85621	GRAPE	GRAPE	PEA	PEA
85623	GOLF	WALNUT	PEA	PEA
85625	NONE	SHOT	SHOT	SHOT
85626	NONE	NONE	NONE	NONE
85627	NONE	NONE	PEA	WALNUT
85629	NONE	NONE	NONE	NONE
85630	NONE	NONE	PEA	GRAPE
85701	NONE	WALNUT	GRAPE	PEA
85702	NONE	NONE	NONE	NONE
85703	NONE	NONE	NONE	NONE
85704	NONE	NONE	NONE	NONE
85708	NONE	NONE	NONE	NONE
85709	NONE	NONE	NONE	PEA
85710	PEA	NONE	SHOT	GRAPE
85711	GOLF	GOLF	GRAPE	WALNUT
85712	WALNUT	GRAPE	SHOT	PEA
85715	NONE	NONE	NONE	NONE
85717	GRAPE	GRAPE	PEA	SHOT
85718	PEA	NONE	NONE	NONE
85720	NONE	NONE	NONE	NONE
85721	NONE	NONE	NONE	NONE
85723	WALNUT	WALNUT	PEA	PEA
85724	GRAPE	GRAPE	SHOT	EA
85725	NONE	NONE	NONE	NONE
85726	NONE	NONE	NONE	NONE
85727	NONE	NONE	NONE	NONE
85728	GRAPE	PEA	PEA	PEA
85729	NONE	PEA	SHOT	PEA
85730	PEA	GRAPE	GRAPE	GRAPE
85731	NONE	NONE	NONE	NONE
85801	NONE	WALNUT	WALNUT	WALNUT
85802	GRAPE	NONE	WALNUT	WALNUT
85803	GRAPE	WALNUT	WALNUT	WALNUT
85804	>GOLF	WALNUT	GRAPE	GOLF
85805	GRAPE	PEA	NONE	SHOT
85806	NONE	NONE	NONE	SHOT
85809	GRAPE	GRAPE	PEA	SHOT
85810	NONE	GRAPE	PEA	PEA
85813	SHOT	NONE	NONE	NONE
85816	NONE	NONE	NONE	NONE
85817	NONE	NONE	NONE	NONE
85818	NONE	NONE	NONE	NONE
85819	NONE	NONE	NONE	NONE
85820	NONE	NONE	NONE	NONE
85822	NONE	NONE	NONE	NONE
85823	NONE	NONE	NONE	NONE
85824	NONE	NONE	NONE	NONE
85826	NONE	NONE	NONE	NONE
85827	NONE	NONE	NONE	NONE
85828	NONE	NONE	SHOT	SHOT
85829	NONE	NONE	NONE	NONE
85830	WALNUT	WALNUT	PEA	PEA

Appendix E: Absolute Diameter Errors

Table E1: Absolute errors for HAILCAST forecasts from June-August 1983.

Date	Observed Category	Representative Diameter (cm)	Forecast Diameter (cm)	AERROR (cm) (cm)
83621	PEA	0.8	1.1	0.3
83622	WALNUT	2.7	2.3	0.4
83623	NONE	0	0	0
83624	WALNUT	2.7	4.8	2.1
83626	NONE	0	0	0
83628	NONE	0	0	0
83629	PEA	0.8	0	0.8
83702	GRAPE	1.7	0	1.7
83703	GRAPE	1.7	1	0.7
83704	NONE	0	2	2
83706	GOLF	4.3	3.8	0.5
83707	GRAPE	1.7	1.7	0
83709	NONE	0	0	0
83710	NONE	0	0	0
83713	WALNUT	2.7	3.8	1.1
83716	PEA	0.8	0.7	0.1
83717	GRAPE	1.7	1.4	0.3
83718	NONE	0	0.8	0.8
83721	WALNUT	2.7	2.2	0.5
83722	NONE	0	0	0
83723	NONE	0	1.5	1.5
83724	GOLF	4.3	5.4	1.1
83726	GRAPE	1.7	3.1	1.4
83727	NONE	0	0	0
83728	GRAPE	1.7	1.1	0.6
83729	PEA	0.8	2.4	1.6
83730	NONE	0	0	0
83731	NONE	0	0	0
83802	NONE	0	0	0
83803	GOLF	4.3	3.3	1
83804	NONE	0	0	0
83806	NONE	0	0	0
83807	NONE	0	0	0
83809	NONE	0	1.3	1.3
83810	NONE	0	0	0
83811	NONE	0	0	0
83812	NONE	0	0	0
83813	NONE	0	0	0
83815	GOLF	4.3	2.2	2.1
83817	GRAPE	1.7	2.8	1.1
83819	NONE	0	0	0
83820	PEA	0.8	1.1	0.3
83821	NONE	0	0	0
83822	NONE	0	0	0
83823	GRAPE	1.7	0	1.7
83824	PEA	0.8	1.2	0.4
83825	PEA	0.8	1	0.2
83827	GRAPE	1.7	1	0.7
83829	NONE	0	0	0
83830	NONE	0	0	0
83831	NONE	0	0	0

Table E2: Absolute errors for HAILCAST forecasts from June-August 1984.

Date	Observed Category	Representative Diameter (cm)	Forecast Diameter (cm)	AERROR (cm)
84620	SHOT	0.2	1.3	1.1
84621	SHOT	0.2	0	0.2
84622	GRAPE	1.7	0.9	0.8
84623	NONE	0	0.4	0.4
84625	WALNUT	2.7	2.7	0
84626	NONE	0	0	0
84627	NONE	0	2.1	2.1
84628	NONE	0	0	0
84630	NONE	0	0	0
84701	NONE	0	0	0
84702	NONE	0	0.9	0.9
84703	NONE	0	0	0
84704	PEA	0.8	2.2	1.4
84705	GRAPE	1.7	1.2	0.5
84706	GOLF	4.3	2.4	1.9
84707	NONE	0	0.4	0.4
84708	NONE	0	0.9	0.9
84709	NONE	0	1.2	1.2
84710	NONE	0	2.6	2.6
84711	GRAPE	1.7	1.3	0.4
84712	WALNUT	2.7	5	2.3
84713	NONE	0	0	0
84714	NONE	0	0	0
84715	NONE	0	1.2	1.2
84716	NONE	0	0	0
84721	GRAPE	1.7	3.8	2.1
84722	NONE	0	0	0
84723	NONE	0	0	0
84724	NONE	0	0	0
84725	NONE	0	0	0
84726	GRAPE	1.7	1.7	0
84727	NONE	0	0	0
84728	>GOLF	6.4	4.8	1.6
84729	NONE	0	0	0
84730	GRAPE	1.7	4.7	3
84731	NONE	0	0	0
84802	GRAPE	1.7	1.7	0
84803	GRAPE	1.7	3.9	2.2
84804	PEA	0.8	1	0.2
84806	GOLF	4.3	2.6	1.7
84807	NONE	0	1.3	1.3
84808	NONE	0	0	0
84809	NONE	0	0.4	0.4
84812	GRAPE	1.7	0	1.7
84814	NONE	0	0	0
84815	NONE	0	0	0
84816	NONE	0	0	0
84817	GRAPE	1.7	1.6	0.1
84820	NONE	0	0	0
84821	NONE	0	0	0
84822	NONE	0	0	0
84824	WALNUT	2.7	2	0.7
84826	NONE	0	0	0
84827	NONE	0	0	0
84828	NONE	0	0	0
84829	NONE	0	0	0
84830	NONE	0	0	0

Table E3: Absolute errors for HAILCAST forecasts from June-August 1985.

Date	Observed Category	Representative Diameter (cm)	Forecast Diameter (cm)	AERROR (cm)
85621	GRAPE	1.7	1.5	0.2
85623	GOLF	4.3	2.6	1.7
85625	NONE	0	0.3	0.3
85626	NONE	0	0.0	0
85627	NONE	0	0.0	0
85629	NONE	0	0.0	0
85630	NONE	0	0.0	0
85701	NONE	0	2.1	2.1
85702	NONE	0	0	0
85703	NONE	0	0	0
85704	NONE	0	0	0
85708	NONE	0	0	0
85709	NONE	0	0	0
85710	PEA	0.8	0	0.8
85711	GOLF	4.3	4.1	0.2
85712	WALNUT	2.7	1.8	0.9
85715	NONE	0	0	0
85717	GRAPE	1.7	1.3	0.4
85718	PEA	0.8	0	0.8
85720	NONE	0	0	0
85721	NONE	0	0	0
85723	WALNUT	2.7	2.2	0.5
85724	GRAPE	1.7	1.8	0.1
85725	NONE	0	0	0
85726	NONE	0	0	0
85727	NONE	0	0	0
85728	GRAPE	1.7	1	0.7
85729	NONE	0	1.3	1.3
85730	PEA	0.8	1.6	0.8
85731	NONE	0	0	0
85801	NONE	0	3.1	3.1
85802	GRAPE	1.7	0	1.7
85803	GRAPE	1.7	2.4	0.7
85804	>GOLF	6.4	2.2	4.2
85805	GRAPE	1.7	0.5	1.2
85806	NONE	0	0	0
85809	GRAPE	1.7	1.8	0.1
85810	NONE	0	1.6	1.6
85813	SHOT	0.3	0	0.3
85816	NONE	0	0	0
85817	NONE	0	0	0
85818	NONE	0	0	0
85819	NONE	0	0	0
85820	NONE	0	0	0
85822	NONE	0	0	0
85823	NONE	0	0	0
85824	NONE	0	0	0
85826	NONE	0	0	0
85827	NONE	0	0	0
85828	NONE	0	0	0
85829	NONE	0	0	0
85830	WALNUT	2.7	2.1	0.6

Appendix F: Improvements to the SkyWatch Model

Improvements to Cloud Model

Only one change was made to the cloud model. Poolman (1992) used different ranges of CAPE and vertical wind shear (representative of the South African thunderstorm environment) to determine the storm type and amount of entrainment used in the updraft calculations. However, as was shown in Appendix A, the ESI is an appropriate means of classifying storm type in Alberta and the ranges of ESI shown in Table A2 were deemed more representative for classifying storm type in central Alberta.

Improvements to Hail Growth Model

The HAILCAST hail growth model differs from SkyWatch in the following ways:

(1) Updraft Duration: Poolman (1992) assumed a steady-state updraft for the first 40 min of the model run. After 40 min, a sinusoidal function was used to reduce the updraft velocity at each level to 0 ms^{-1} after 60 min. The same updraft duration was used regardless of the expected storm type. Considering the importance of hail growth on the residence time in the supercooled region of the cloud discussed in section 1.3, we formulated a second order polynomial relating the maximum hail growth duration to the ESI (see Equation 2.16). This is considered a major improvement over the previous scheme, particularly for thunderstorms developing in a low shear environment.

(2) Embryo Diameter: Poolman (1992) used an initial embryo diameter of only 100 μm. Sensitivity experiments in Chapter 4 showed that on days with strong

updrafts, the maximum modelled hail size was dependant on the size of the initial hailstone embryo, with small embryos (<200 μm in diameter) resulting in much smaller hail at the ground. Since the primary purpose of HAILCAST is to forecast severe hail events, we selected a hailstone embryo diameter of 300 μm.

(3) Ventilation coefficient: Equations determined experimentally by (Kinzer and Gunn, 1951) were used to calculate the ventilation coefficient in the SkyWatch hail model. However, for large hailstones these values were found to be orders smaller than those calculated using the equations of Rasmussen and Heymsfield (1987a). To better model the increased heat transfer (larger ventilation coefficients) from large hailstones, we used the method recommended by Rasmussen and Heymsfield (1987a).

(4) Terminal Velocity scheme: Poolman (1992), used a drag coefficient of 0.6 to compute the terminal velocity for all particles >1 mm in diameter. Generally, this low drag coefficient is only valid for particles greater than 1 cm in diameter. In light of this discrepancy, we implemented the improved terminal velocity calculation of Rasmussen and Heymsfield (1987a).

(5) Shedding Scheme: Poolman (1992) implemented the shedding scheme of Chong and Chen (1974) to model the shedding of excess water on the surface of a growing hailstone. Rasmussen and Heymsfield (1987a) used an empirically derived linear relationship to determine the maximum amount of surface water that can be retained for a given ice core mass before shedding. This scheme is used in HAILCAST.

FIGURES

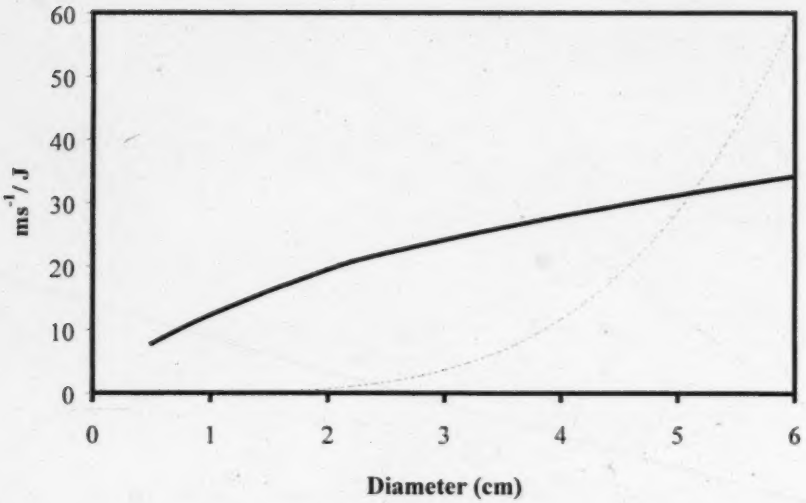

Figure 1.1: Kinetic energy (dashed line) and terminal velocity (solid line) versus hailstone diameter.

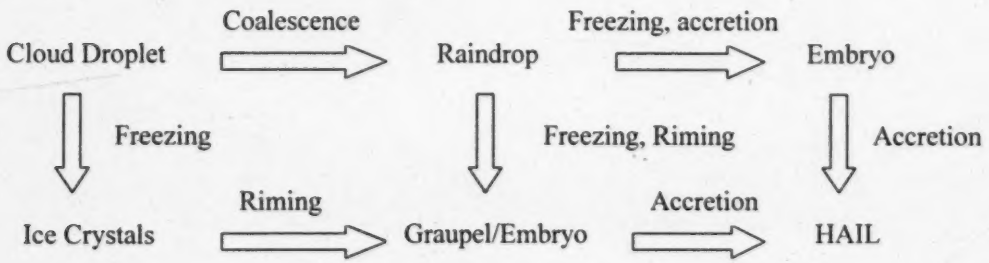

Figure 1.2: Schematic indicating the primary growth mechanisms from cloud droplet to hail. Coalescence refers to the collision and merging of two water droplets, accretion refers to an ice particle collecting supercooled water droplets or small ice crystals, and riming refers to the accretion of supercooled droplets in the form of a low density ice deposit. Adapted from Knight and Knight, (1998).

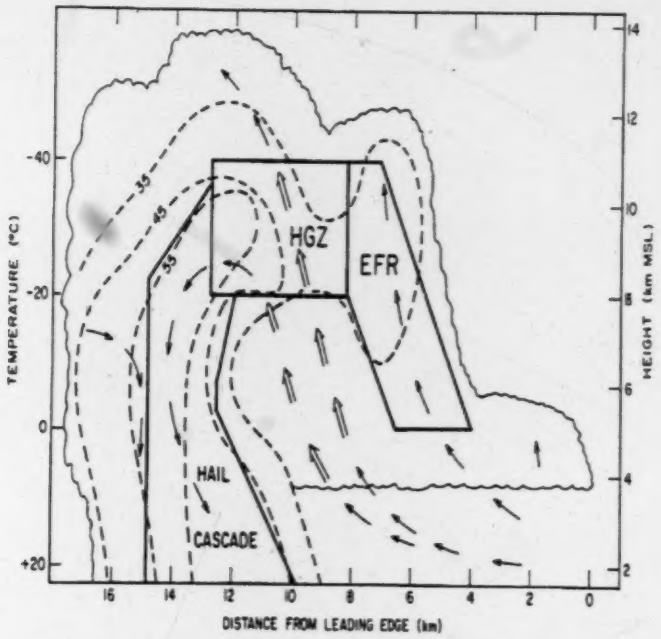

Figure 1.3: Cross-section of a multi-cell hailstorm showing the embryo formation region (EFR), hail growth zone (HGZ) and hail cascade. The radar reflectivity factors are indicated by dashed lines (in dBZ) and airflow by arrows (Adapted from K.C. Young, 1977).

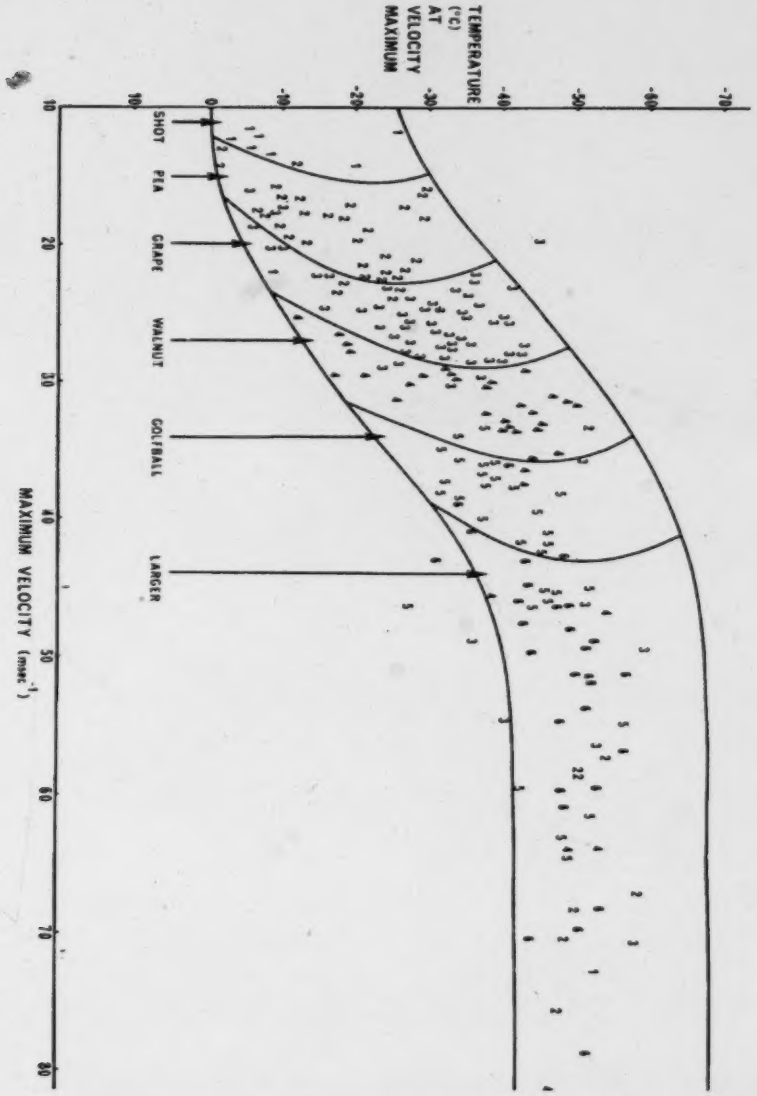

Figure 1.4: Nomogram developed for forecasting maximum hail size in Alberta. Numbers 1 to 6 (shot through greater than golfball) correspond to the maximum observed hail size at the surface, versus the forecast maximum updraft velocity and temperature at the updraft maximum. Adapted from Renick and Maxwell (1977).

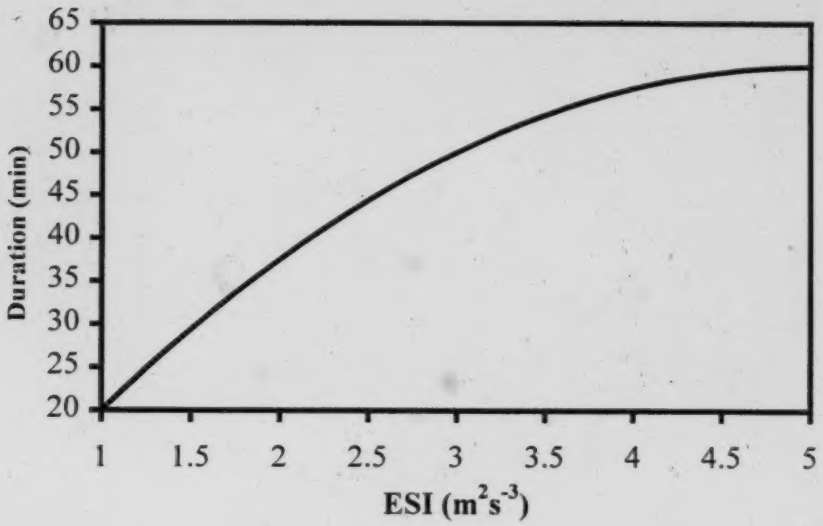

Figure 2.1: Maximum hail growth duration as a function of the Energy Shear Index (ESI).

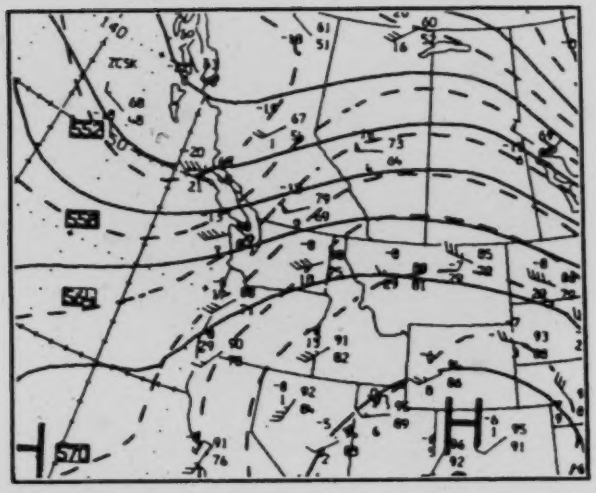

Figure 3.1: 500 hPa analysis for 1800 LDT on 11 July 1985. Solid contours represent the 500 hPa height (in gpm), and dashed isopleths the 1000-500 hPa thickness. Wind speeds are in knots with a full barb equivalent to 10 knots and a flag 50 knots.

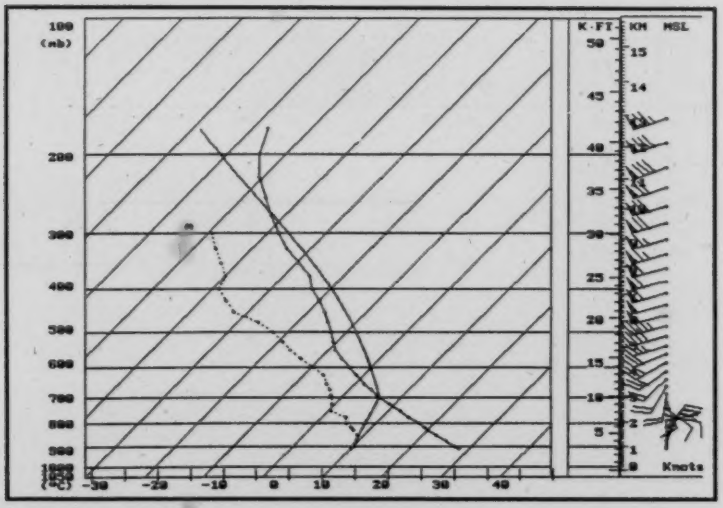

Figure 3.2: Upper-air sounding released from Penhold at 1715 LDT on 11 July 1985 plotted on a skew T-log P diagram. The dashed line represents the dew-point profile, the solid line the environmental temperature and the curved solid line the pseudoadiabat. The boundary layer has been mixed out based on the maximum temperature of 28 °C.

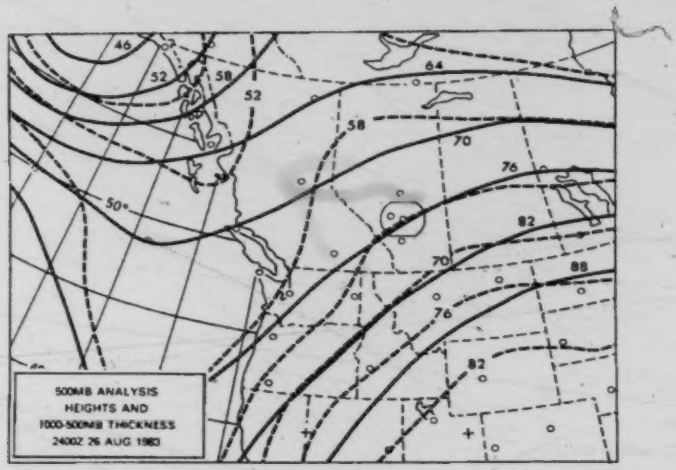

Figure 3.3: Same as Figure 3.1 except for 24 August 1983.

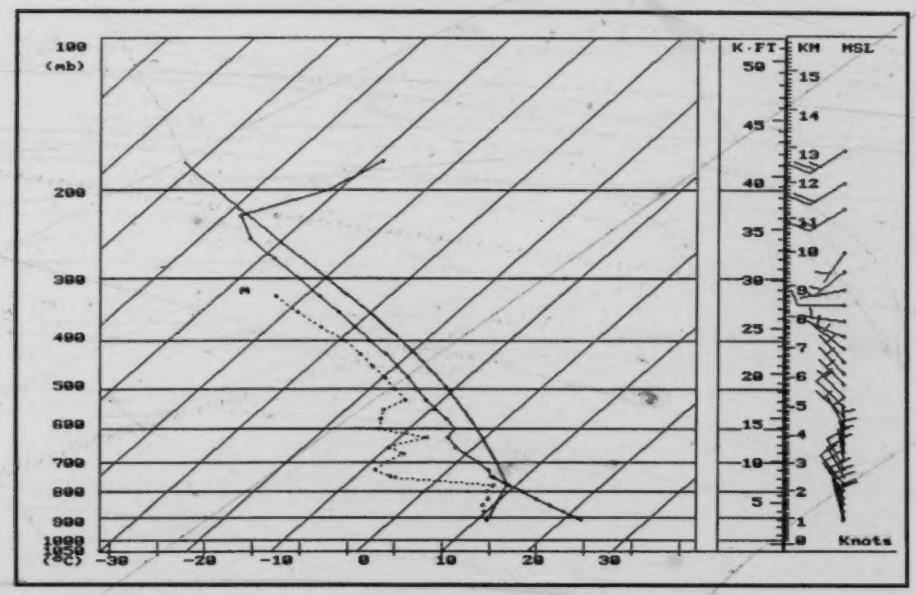

Figure 3.4: Same as Figure 3.2, except for 24 August 1983. The boundary layer has been mixed out based on the maximum temperature of 22 °C.

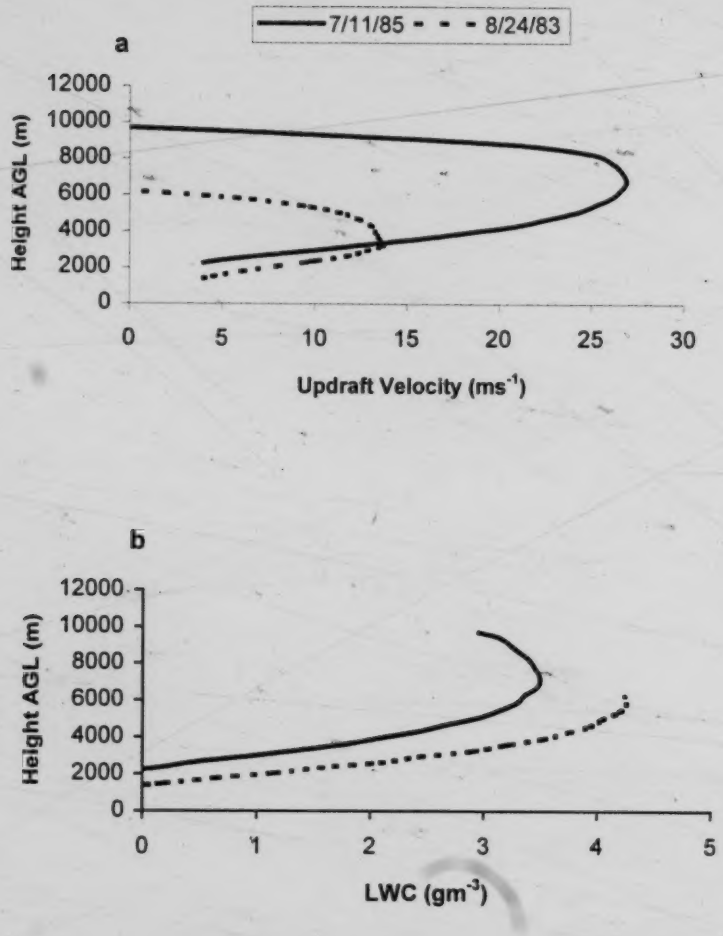

Figure 3.5: Model derived profiles of (a) Updraft velocity and (b) Liquid water content (LWC) for 11 July 1985 (solid lines) and 24 August 1983 (dashed lines).

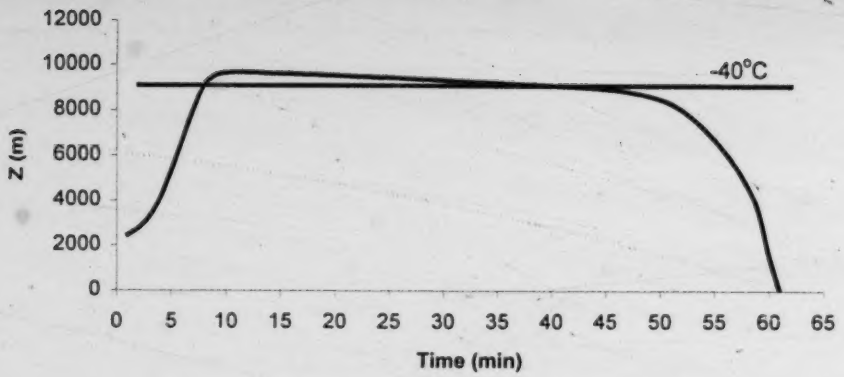

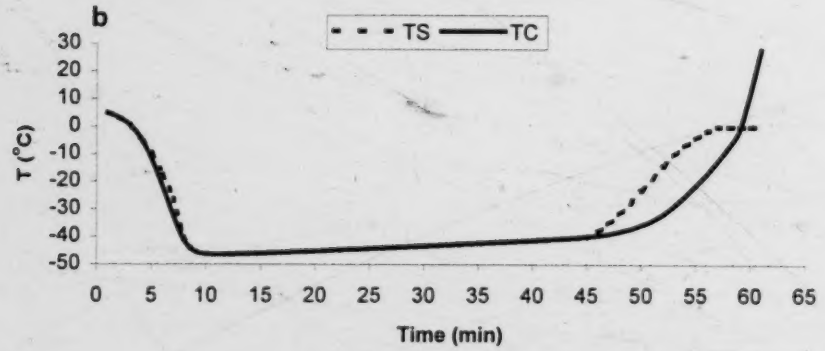

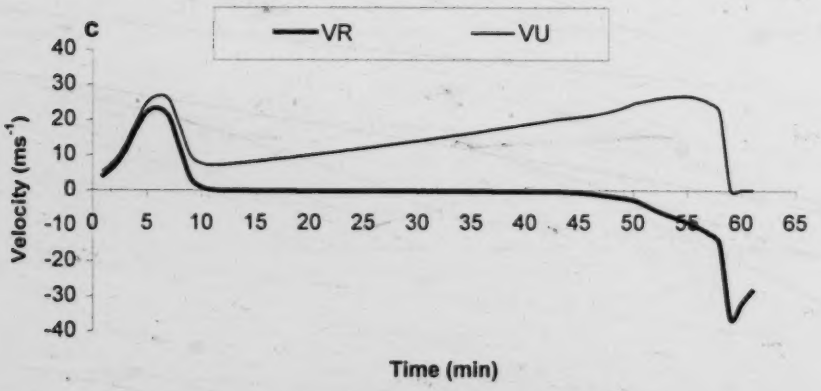

Figure 3.6: Growth time history of a hailstone simulated by HAILCAST for 11 July 1985. Depicted are (a) Height (Z); (b) In-cloud (TC) and hailstone temperature (TS); (c) Ground relative (VR) and updraft velocity (VU); (d) Growth rate (dD/dt); (e) Diameter (D) and (f) Fractional liquid water content (F_w).

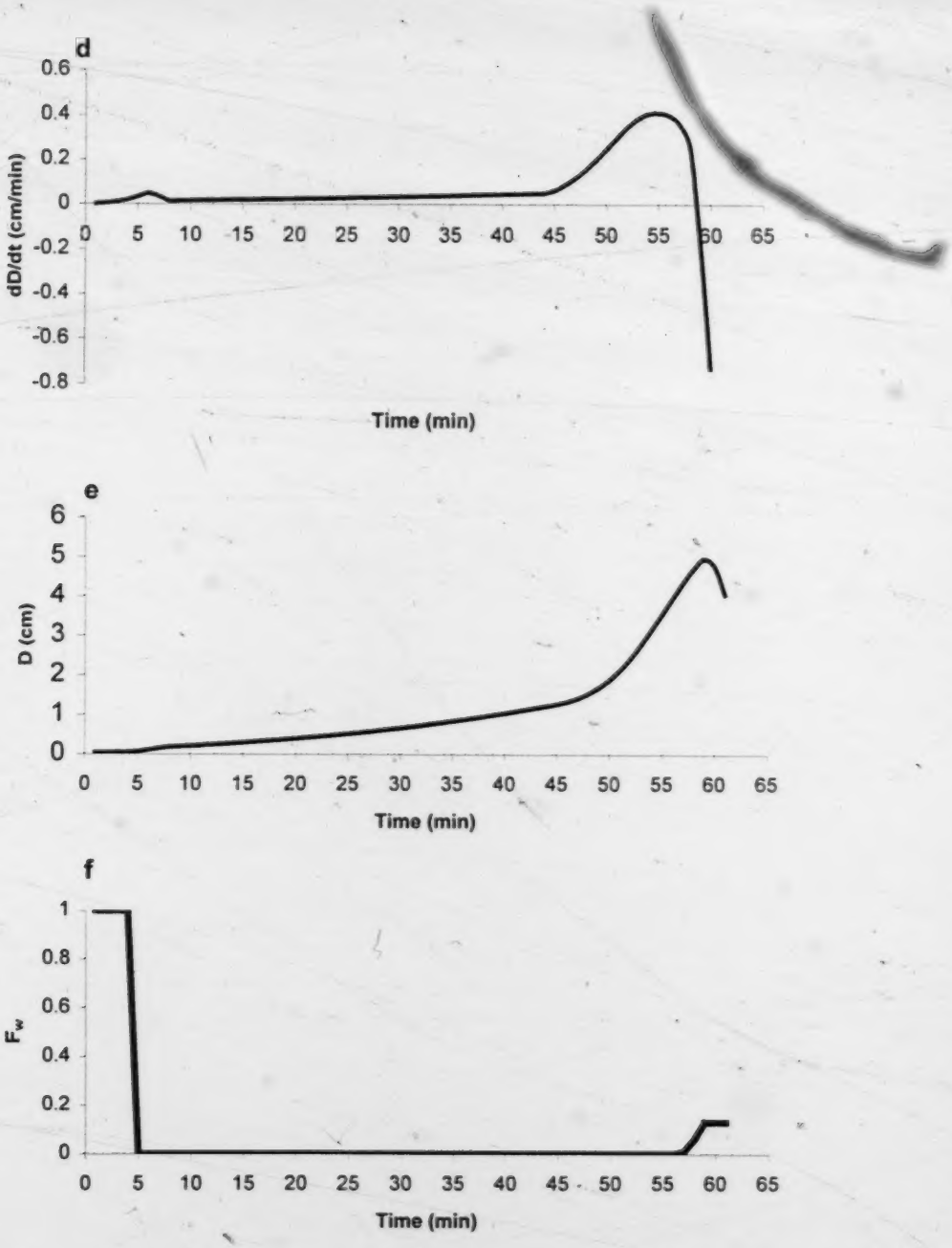

Figure 3.6 (Continued)

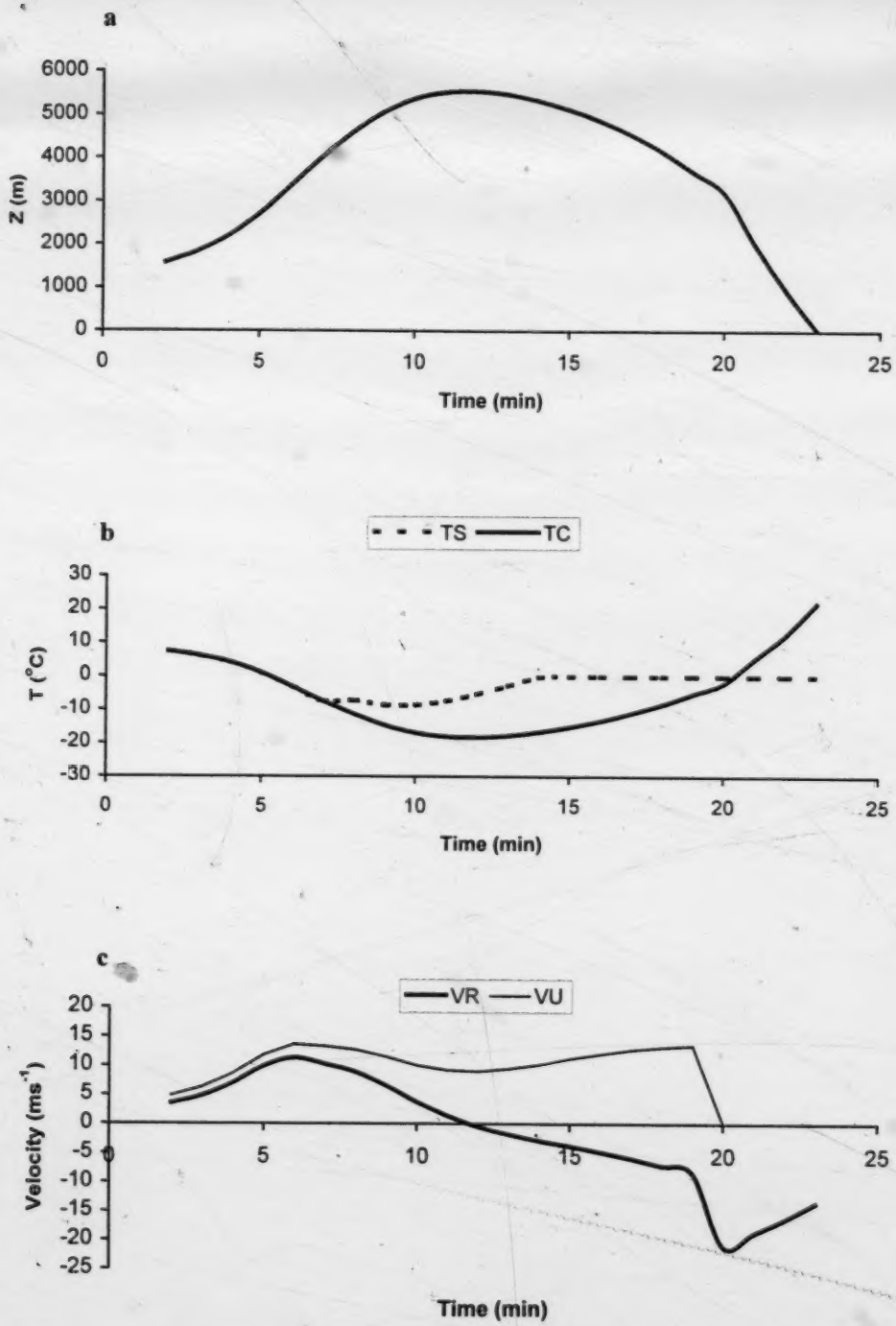

Figure 3.7: Same as Figure 3.6 except for 24 August 1983.

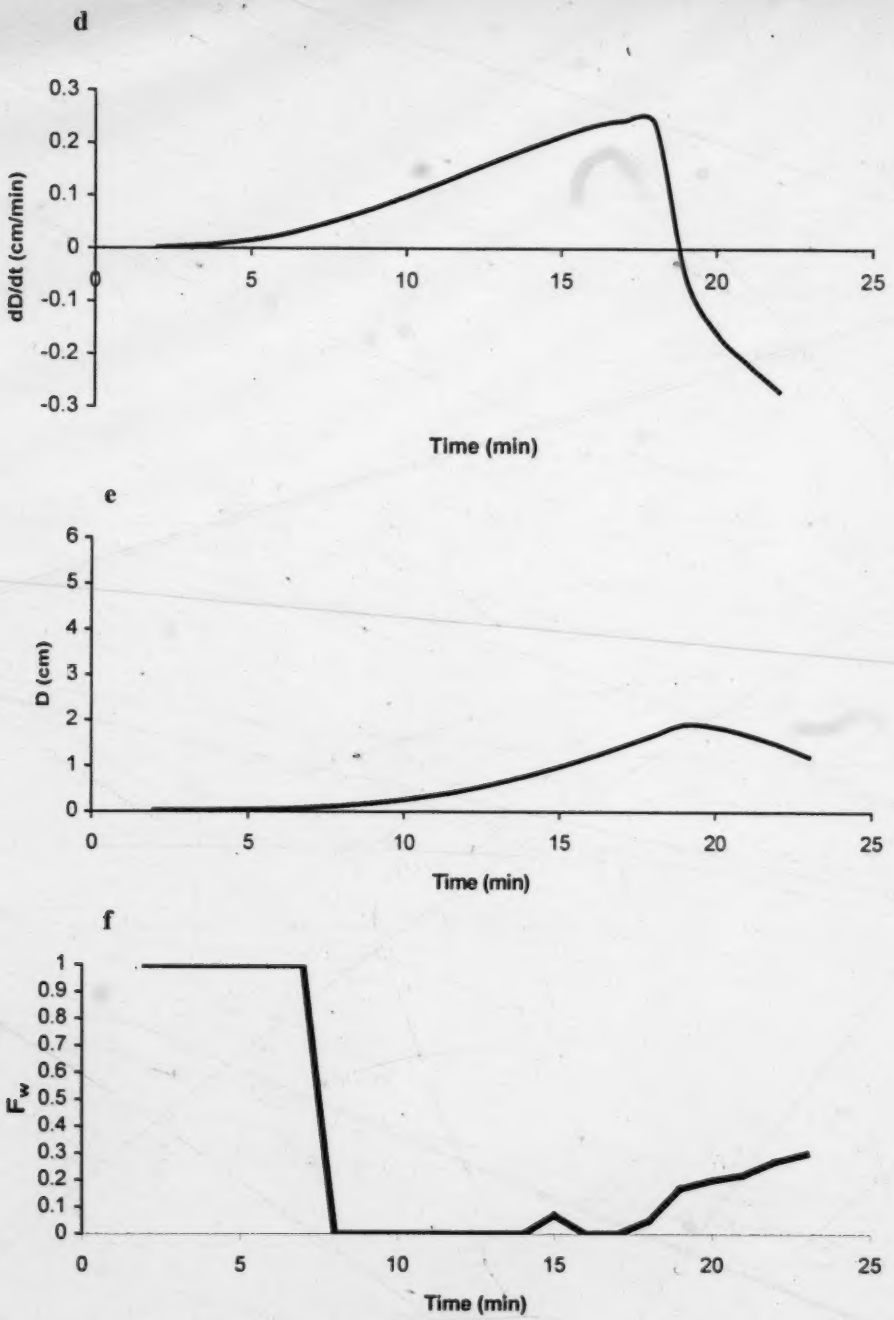

Figure 3.7 (Continued)

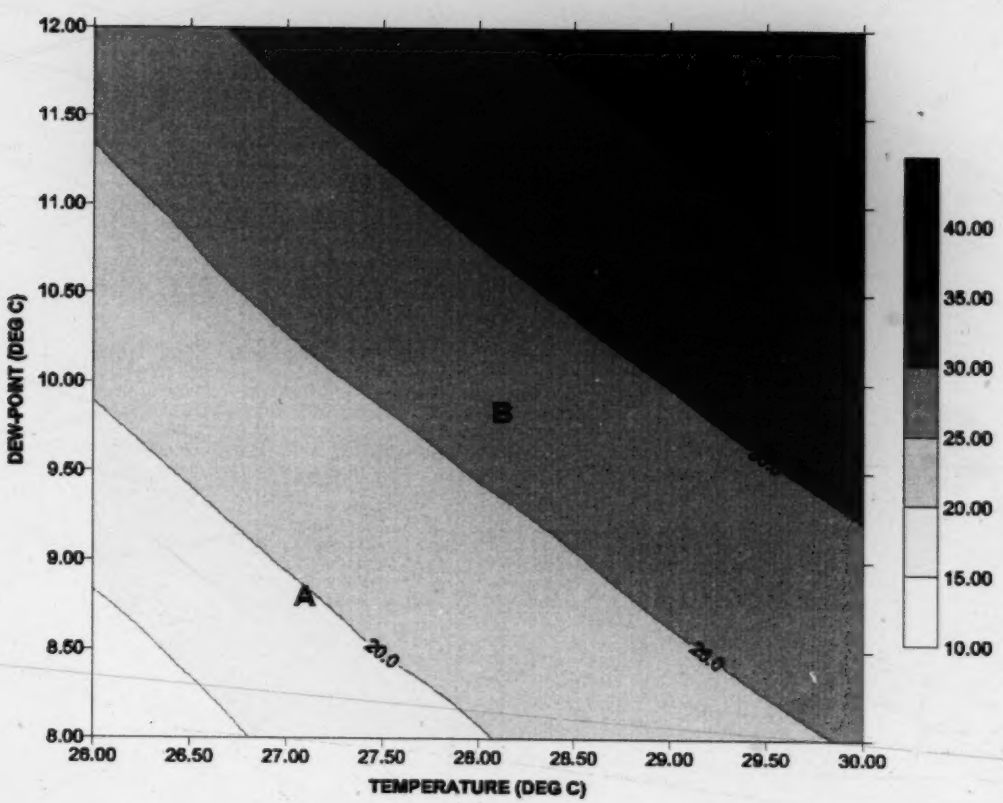

Figure 4.1: Maximum updraft velocity (ms^{-1}) contoured on a surface temperature and surface dew-point diagram. Points A, B and C correspond to sensitivity experiments discussed in section 4.1.1.

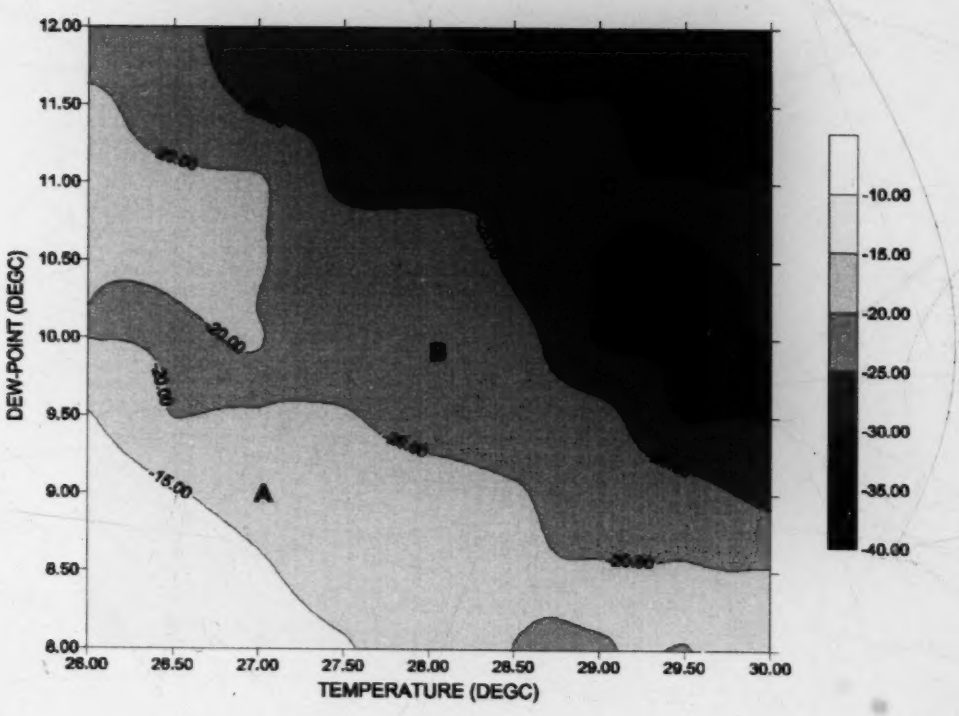

Figure 4.2: Temperature (°C) at the level of maximum updraft velocity contoured on a surface temperature and surface dew-point diagram. Points A, B and C correspond to sensitivity experiments discussed in section 4.1.1.

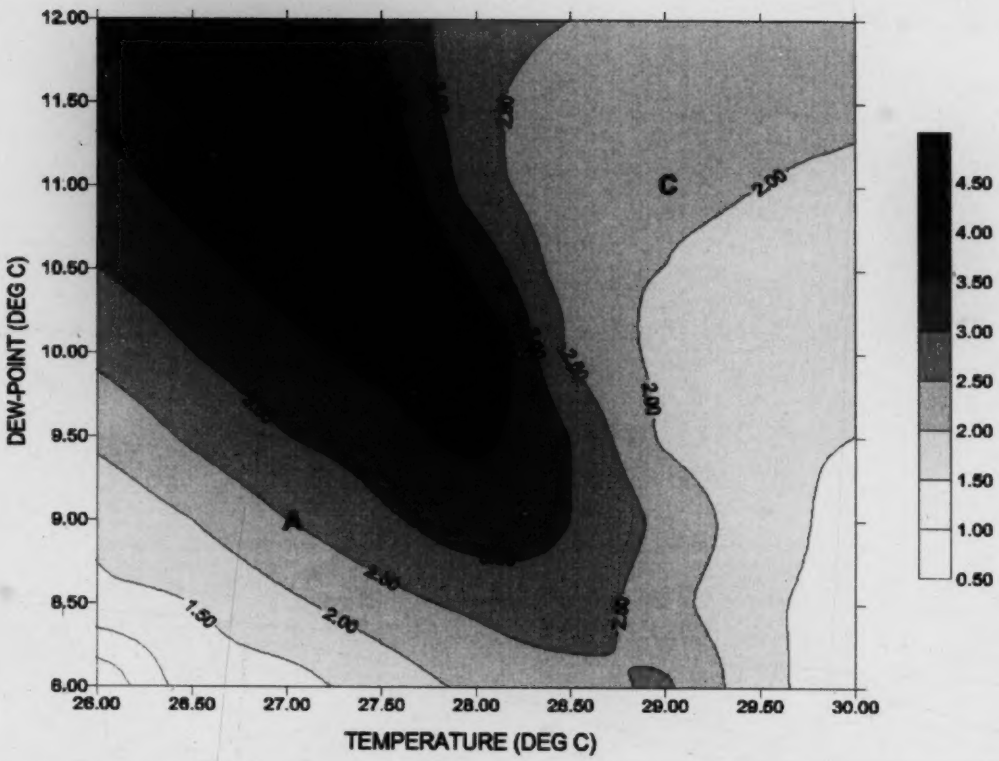

Figure 4.3: Maximum forecast hail diameter at the ground (in cm) contoured on a surface temperature and surface dew-point diagram. Points A, B and C correspond to sensitivity experiments discussed in section 4.1.1.

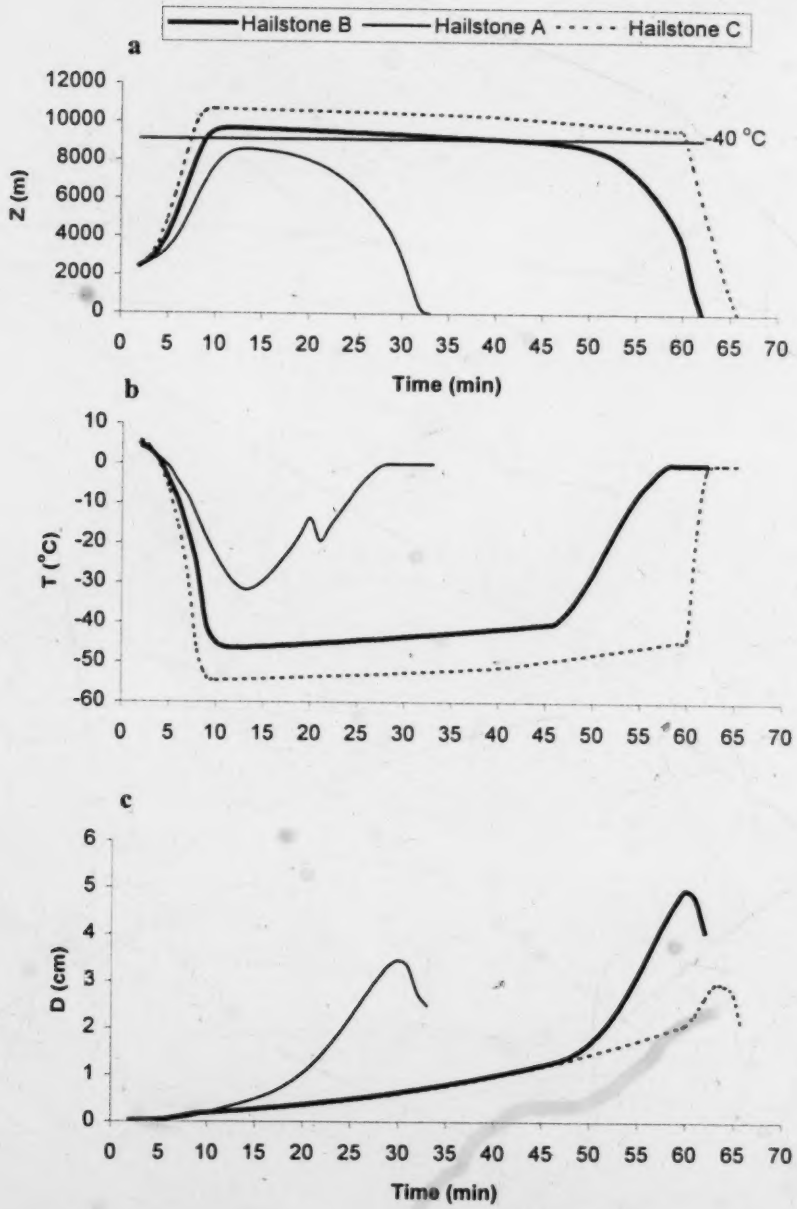

Figure 4.4: Hail growth time series for 3 hailstones A, B and C determined using different surface temperature and dew-points. Hailstone B denotes the control. Depicted are (a) Height (Z), (b) Hailstone temperature (T) and (c) Diameter (D).

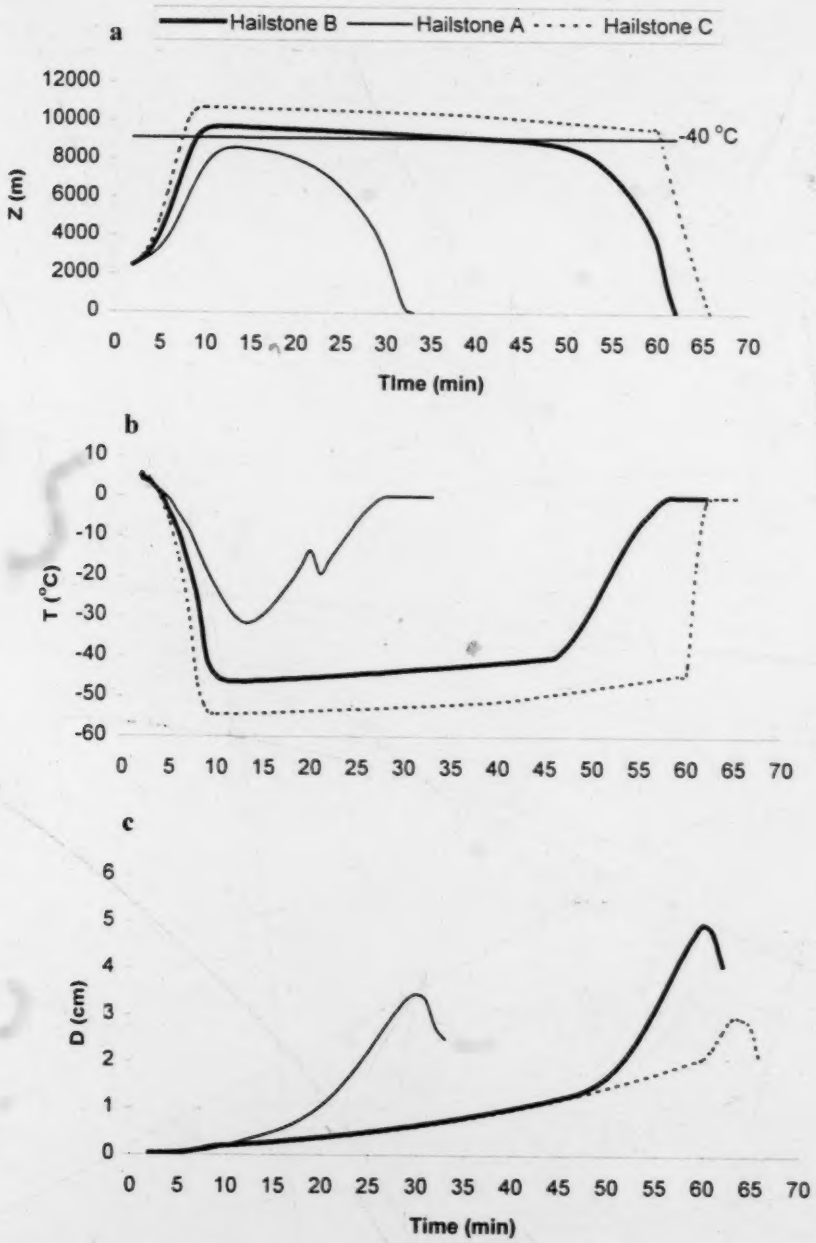

Figure 4.5: Hail growth time series for 3 hailstones A, B and C determined using hail embryo diameters of 100 μm (C), 300 μm (B) and 1000 μm (A). Variables are the same as shown in Figure 4.4.

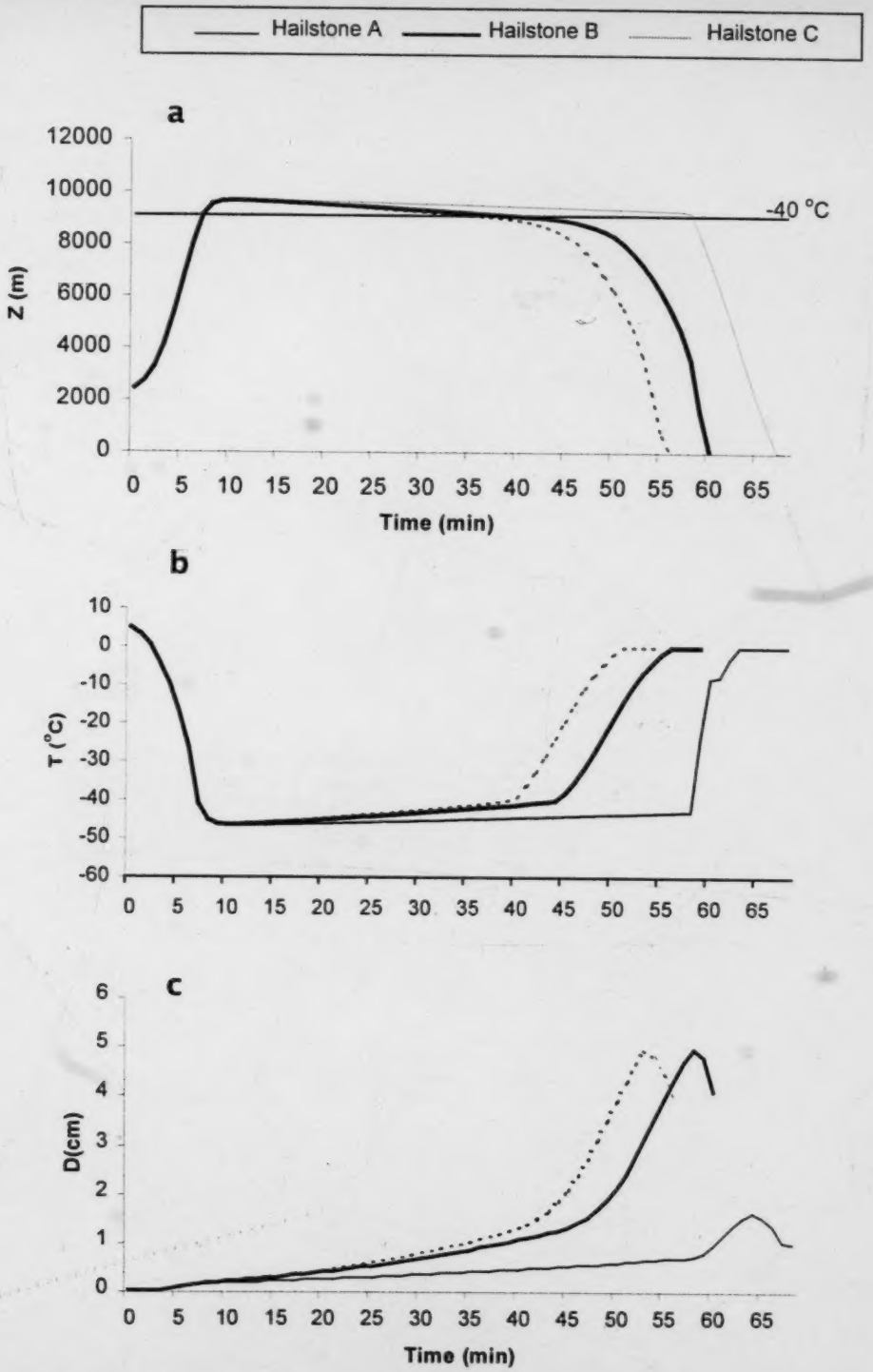

Figure 4.6: Hail growth time series for 3 hailstones using E_i of 0.15 (hailstone A), 0.21 (hailstone B) and 0.25 (hailstone C) respectively.

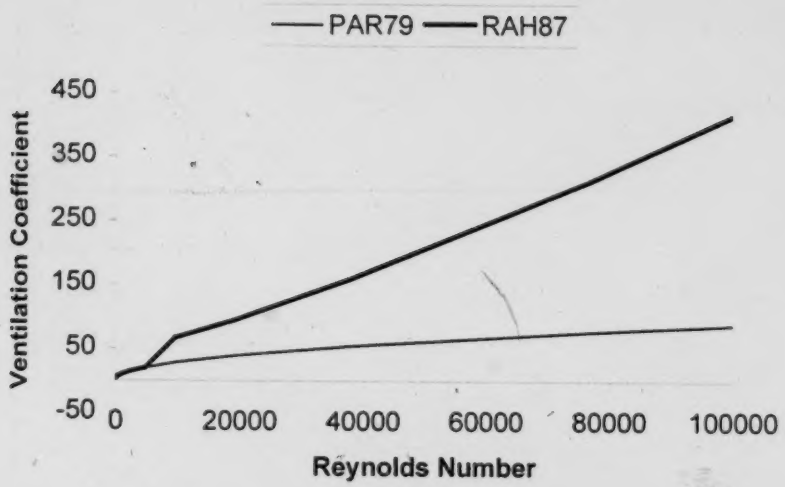

Figure 4.7: Ventilation coefficient versus Reynolds number calculated using the scheme of PAR79 (Pruppacher and Rasmussen, 1979) and that of RAH87 (Rasmussen and Heymsfield, 1987a).

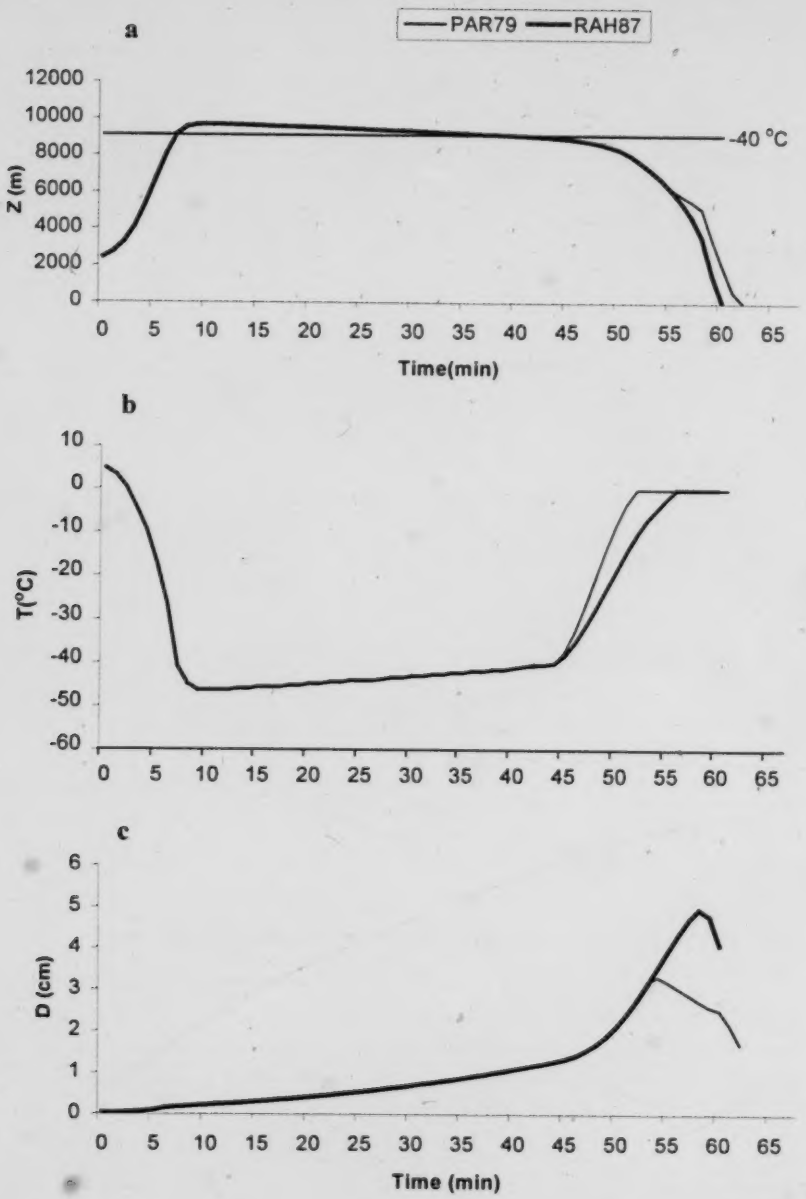

Figure 4.8: Hail growth time series for 2 hailstones using the ventilation coefficient scheme of RAH87 (Rasmussen and Heymsfield, 1987a) and PAR79 (Pruppacher and Rasmussen, 1979).

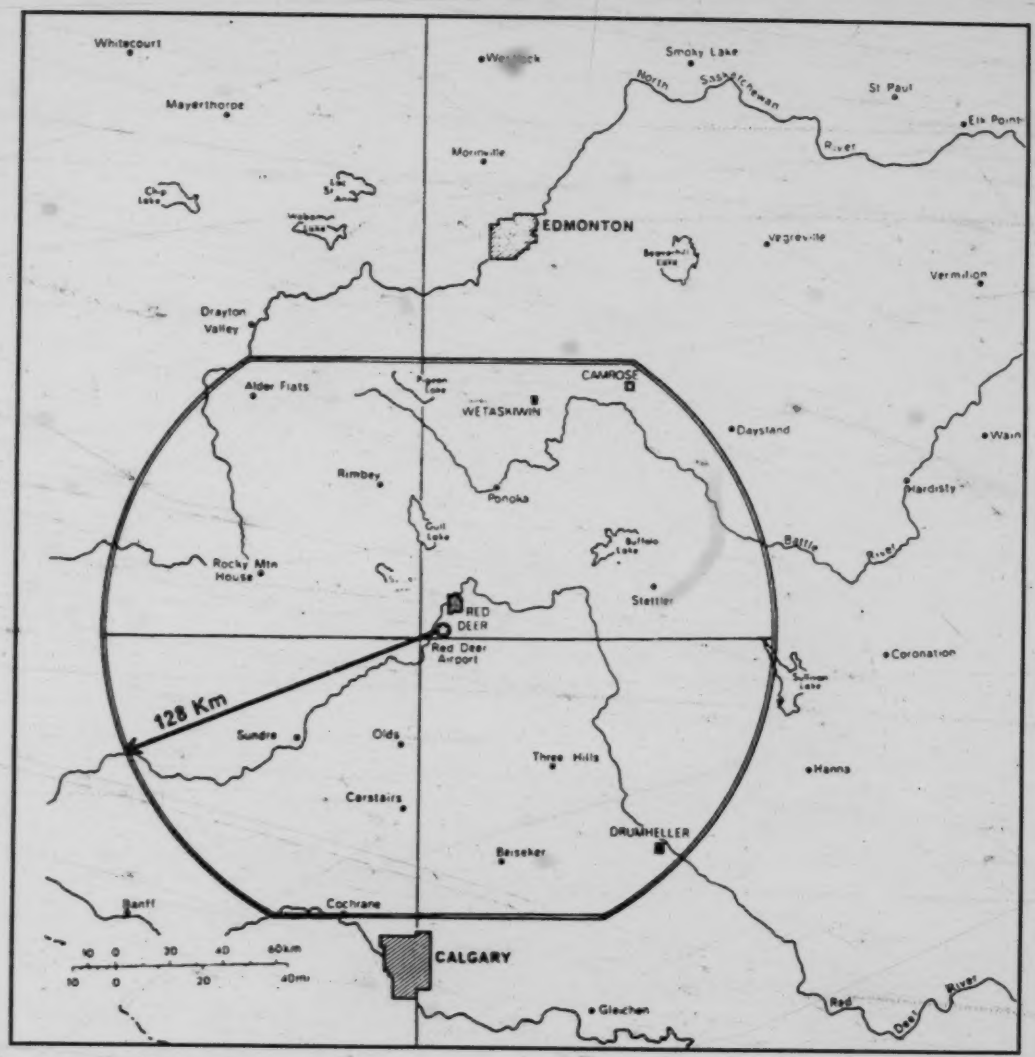

Figure 5.1: The Alberta Hail Project's principal target area between Edmonton and Calgary and centred on the radar site located at the Red Deer Industrial Airport.

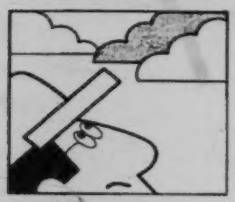

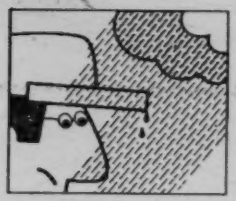

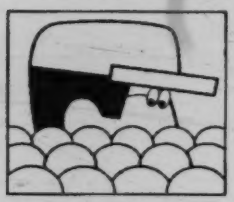

Storm Date: _____ 1984
Day of Week: _____
Location ___ ¼ S ___ T ___ R ___ W of ___

Hail: Began _____ am _____ pm
Lasted for _____ minutes

Rain: Began _____ am _____ pm
Lasted for _____ minutes
Measured _____ mm
Estimated _____ mm

Largest Hailsize:
Shot ☐ Pea ☐ Grape ☐
Walnut ☐ Golfball ☐ Larger ☐

Most Common Hailsize:
Shot ☐ Pea ☐ Grape ☐
Walnut ☐ Golfball ☐ Larger ☐
Average Spacing of Stones
_____ mm
or Depth of Hail _____ mm
or Ground Just Covered ☐

Wind: Light ☐ Moderate ☐
Strong ☐ Severe ☐
Crop: (type) _____
Estimated Damage _____

Remarks _____

Figure 5.2: Example of a hail card completed each summer by volunteer observers within the Alberta Hail Project area. (From Renick, 1984).

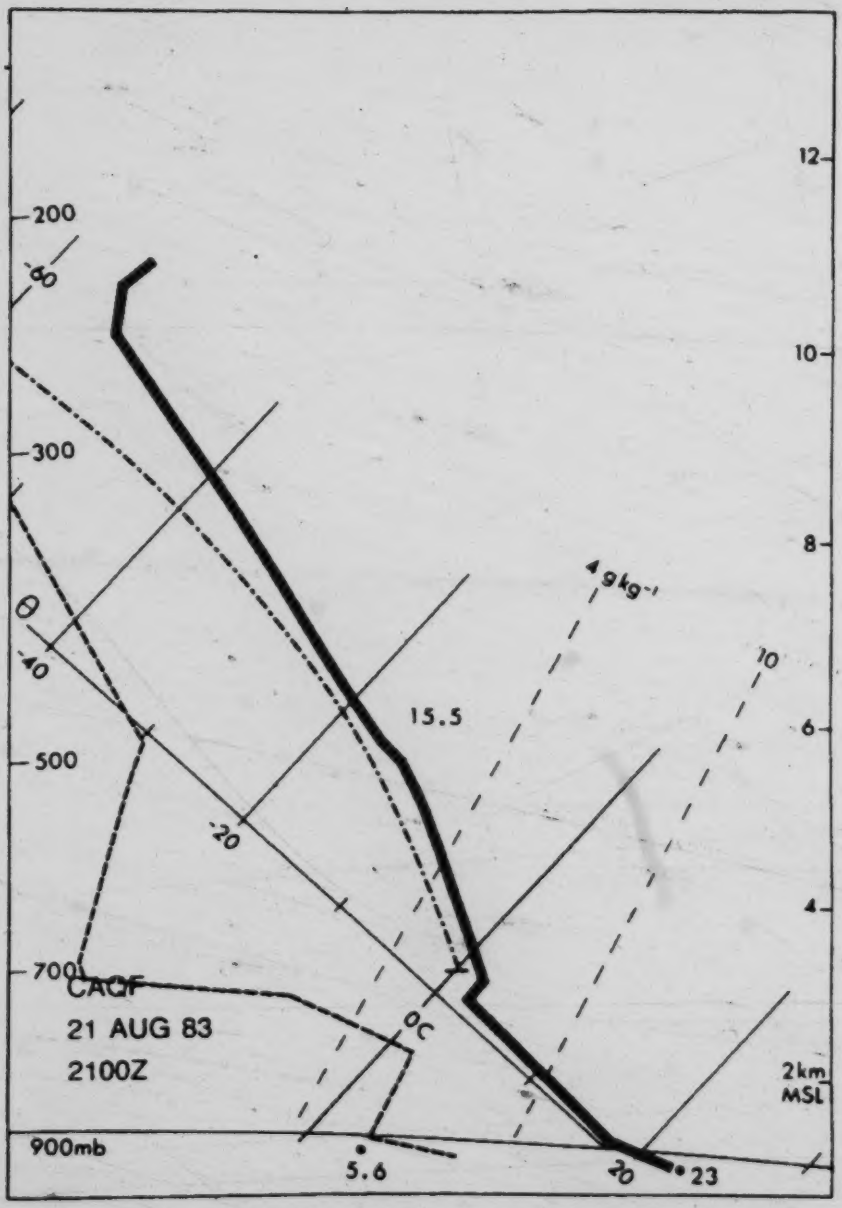

Figure 5.3: Sounding released from Penhold on 21 August 1983. Solid line depicts the environmental temperature profile, dashed line the dew-point and the dot-dashed depicts line the pseudoadiabat. (Adapted from Renick, 1983).

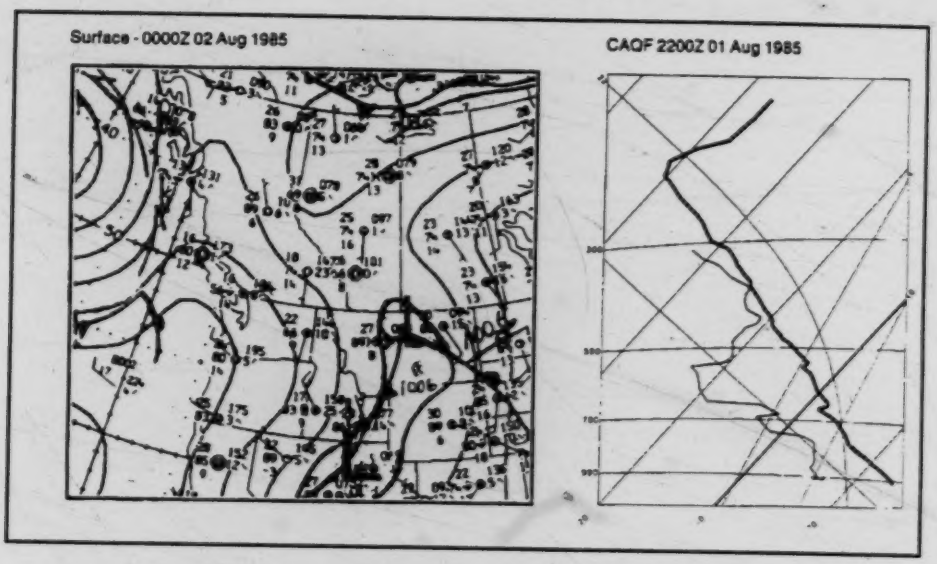

Figure 6.1: 1800 LDT surface analysis and 1400 LDT sounding released from Penhold on 1 August 1985.

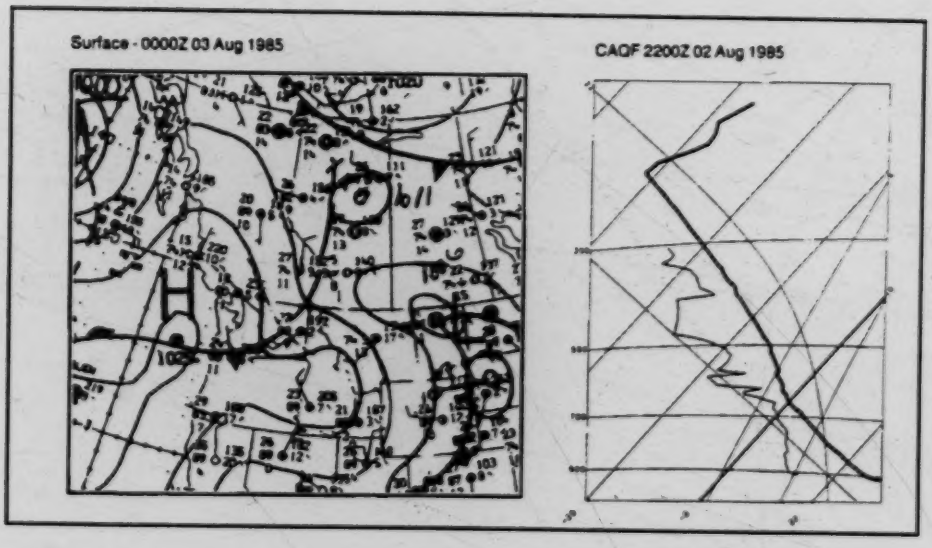

Figure 6.2: Same as for Figure 6.1 except for 2 August 1985.

TABLES

Table 2.1: Entrainment mechanism and amount as determined by the ESI.

ESI (m^2s^{-3})	Entrainment Mechanism	Bett's Entrainment Parameter, β (%)
[0;1]	Lateral	10
(1;3]	Cloud Top	10
(3;5]	Cloud Top	7.5
>5	Cloud Top	5

Table 3.1: Thermodynamic and wind derived parameters calculated using the HAILCAST model for 1800 LDT on 11 July 1985 and 24 August 1983.

	1985-07-11	1983-08-24
Surface temperature (°C)	28	22
Surface dew-point (°C)	10	11
CAPE (Jkg^{-1})	756	1063
Maximum possible updraft (ms^{-1})	38.8	46.1
0.5-6 km AGL shear ($10^{-3}s^{-1}$)	6.5	0.5
ESI (m^2s^{-3})	4.9	0.5

Table 3.2: Environmental and model parameters utilised in model runs for 11 July 1985 and 24 August 1983.

	1985-07-11	1983-08-24
ESI (m^2s^{-3})	4.9	0.5
Forecast thunderstorm type	Strong multi-cell	Weak air-mass
Amount and type of entrainment	7.5%; Cloud Top	10%; Lateral
Forecast W_{max} (ms^{-1})	26.9	13.7
Forecast temperature at W_{max} (°C)	-22.7	-2.8
Updraft duration (s)	3597	1200
Forecast hail size at ground (cm)	4.1	1.2

Table 4.1: Updraft and hail growth statistics for hailstone trajectories A,B and C. Note the time in the supercooled region refers only to the downward pass through the cloud.

	Hailstone B	Hailstone A	Hailstone C
T (°C)	28	27	29
T_d (°C)	10	9	11
W_{max} (ms^{-1})	26.9	20.3	33.9
T_{wmax}(°C)	-22.7	-17.0	-29.6
Time above –40 °C (min)	36	N/A	53
Size descending below –40 °C (cm)	1.3	N/A	2.2
Time in supercooled region (min)	15	15	3
Final diameter at ground (cm)	4.1	2.5	2.1
Time to ground (min)	61.9	32.3	65.8
Maximum hail growth time (min)	60	46	60

Table 4.2: Updraft and hail growth statistics for lateral entrainment sensitivity experiments. D represents the forecast hailstone diameter at the ground and τ the time taken for the hailstone to reach the ground.

Lateral Entrainment (%)	W_{max} (ms^{-1})	T_{wmax} (°C)	D (cm)	τ (min)
0	28.6	-30.2	**2.3**	**61.9**
5	21.9	-14.1	2.5	28.6
10	18.1	-12.4	**1.5**	**26.1**

Table 4.3: Same as Table 4.2, except for cloud top entrainment.

Cloud Top Entrainment (%)	W_{max} (ms^{-1})	T_{wmax} (°C)	D (cm)	τ (min)
0	**28.6**	**-30.2**	**2.3**	**61.9**
5	27.2	-22.6	3.9	62.8
10	26.2	-22.9	**3.7**	**58.3**

Table 4.4: Environmental, updraft and hailstone statistics for vertical wind shear sensitivity experiments. Values in parentheses indicate the updraft duration (maximum hail growth time).

Vertical Wind Shear (10^{-3} s^{-1})	ESI (m^2s^{-3})	W_{max} (ms^{-1})	T_{wmax} (°C)	D (cm)	τ (min)
3.9	2.9	26.2	-22.9	2.3	53.9 (49.2)
5.2	3.9	26.9	-22.7	3.6	60.2 (57.0)
5.9	4.4	26.9	-22.7	4.0	61.4 (59.1)
6.2	4.6	26.9	-22.7	4.1	61.7 (59.7)
6.5	**4.9**	26.9	-22.7	**4.1**	**61.9 (60.0)**
6.9	5.1	27.2	-22.6	3.9	62.8 (60.0)
7.2	5.4	27.2	-22.6	3.9	62.8 (60.0)
7.8	5.9	27.2	-22.6	3.9	62.8 (60.0)
9.1	6.8	27.2	-22.6	3.9	62.8 (60.0)

Table 4.5: Same as Table 4.4, except for 2 August 1985.

Vertical Wind Shear (10^{-3} s^{-1})	ESI (m^2s^{-3})	W_{max} (ms^{-1})	T_{wmax} (°C)	D(cm)	τ (min)
0.4	**1**	**29.6**	**-20.5**	**0.4**	**31.2 (20)**
0.4	1.1	39.1	-35.8	1.6	28.8 (20)
0.5	1.1	39.1	-35.8	1.7	29.2 (21)
0.5	1.2	39.1	-35.8	1.9	30.3 (23)
0.7	1.3	39.1	-35.8	2.1	33.2 (27)

Table 4.6: Hailstone statistics for hail embryo diameter sensitivity experiments.

Embryo Diameter (μm)	D (cm)	τ (min)
100	1.5	66.5
200	3.3	63.4
300	**4.1**	**61.9**
400	3.9	60.0
500	3.9	58.0
600	3.9	56.2
700	3.9	54.7
800	3.9	53.3
900	3.9	52.0
1000	3.9	50.9

Table 4.7: Hailstone diameter (D) and the time taken for the hailstone to reach the ground (τ) for ice collection efficiency sensitivity experiments.

Collection Efficiency	Diameter (cm)	τ (min)
0.10	1.0	69
0.11	1.2	68.5
0.12	1.4	68.1
0.13	1.3	67.7
0.14	1.3	67.3
0.15	1.4	66.9
0.16	1.5	66.4
0.17	1.9	65.5
0.18	2.5	64.5
0.19	3.2	63.6
0.20	3.9	62.7
0.21	**4.1**	**61.9**
0.22	4.0	60.5
0.23	3.9	58.9
0.24	3.9	57.4
0.25	3.9	56.1

Table 4.8: Hailstone diameter (D) and the time taken for the hailstone to reach the ground (τ) for liquid water content (LWC) sensitivity experiments.

Percent of Adiabatic LWC	D (cm)	τ (min)
100	**4.1**	**61.9**
90	2.5	64.7
75	0.9	67.7

Table 4.9: Hailstone diameter (D) and the time taken for the hailstone to reach the ground (τ) for ventilation coefficient sensitivity experiments.

Ventilation Coefficient	D (cm)	τ (min)
RAH87: χ=0.76	**4.1**	**61.9**
RAH87: χ=0.60	4.1	61.9
BAP79	1.7	63.6

Table 4.10: Hailstone diameter (D) and the time taken for the hailstone to reach the ground (τ) for terminal velocity scheme sensitivity experiments.

Terminal Velocity Scheme	D(cm)	τ (min)
Control	**4.1**	**61.9**
RAH 1	3.8	59.7
RAH 2	3.6	58.2
RAH 3	3.8	61.4

Table 5.1: Time frame during which upper-air soundings were conducted at Penhold from 1983-1985.

Year	Begin	End
1983	11 June	31 August
1984	8 June	1 September
1985	20 June	31 August

Table 5.2: Number of no-hail, non-severe and severe hail days from 20 June-31 August (1983-1985) used to validate the hail model forecasts.

Year	No-hail days	Non-severe Hail Days	Severe Hail days	Total
1983	27	16	8	**51**
1984	37	14	6	**57**
1985	34	12	6	**52**
Total	**98**	**42**	**20**	**160**

Table 5.3: Number of hail days and reports recorded in the AHP area from 1 June to 31 August for 1983-1985 compared with the 1974-1985 means.

	1983	1984	1985	Mean 1974-1985
Total hail days	45	42	43	**51**
Non-severe hail days	34	26	35	**31**
Severe hail days	11	16	8	**20**
Total number of hail reports	**1949**	**2330**	**1743**	**2355**

Table 5.4: Categories used to classify hail size during the Alberta Hail Project (AHP).

Class	Interval (cm)	Representative Diameter (cm)
None	[0.0 ;0.1)	0.0
Shot	[0.1 ;0.4)	0.2
Pea	[0.4 ;1.3)	0.8
Grape	[1.3 ;2.1)	1.7
Walnut	[2.1 ;3.3)	2.7
Golfball	[3.3 ;5.3)	4.3
> Golfball	≥ 5.3	6.4

Table 6.1: 2x2 Contingency table used in calculation of forecast skill statistics.

		Forecast	
		Hail	**No Hail**
Observed	**Hail**	**Hit (H)**	**Miss (M)**
	No Hail	**False Alarm (FA)**	**Null Forecast (N)**

Table 6.2: Summary of skill scores used to evaluate hail forecasts.

Score	Measure	Calculation
Probability of Detection (POD)	Measures the ability to detect an event	POD = H/H+M
False Alarm Rate (FAR)	Measures the tendency to "cry wolf"	FAR = FA/FA+H
Heidke Skill Score (HSS)	Measures the true skill of a forecast	HSS= [2*(H*N-M*FA)]/ [M^2+FA^2+2*H*N+ (M+FA)*(H+N)]
Bias (B)	Indicates the degree of under/over-forecasting of an event	B = (H+FA)/(H+M)

Table 6.3: Summary of forecast skill scores for HAILCAST from 1983-1985.

FORECAST SKILL	HAILCAST			
	1983-1985	1983	1984	1985
Hail Forecasts				
POD	0.85	0.88	0.90	0.78
FAR	0.26	0.16	0.36	0.26
HSS	0.64	0.73	0.58	0.62
BIAS	1.16	1.04	1.40	1.06
Severe Hail Forecasts				
POD	0.89	1.00	0.83	0.83
FAR	0.40	0.27	0.55	0.38
HSS	0.67	0.81	0.52	0.67
BIAS	1.50	1.38	1.83	1.33

Table 6.4: HAILCAST Forecast hail size category evaluation.

Forecast Size Category	No-Hail	All Hail	Non-severe Hail	Severe Hail
Correct	81%	38%	37%	39%
Within one size category	83%	81%	74%	94%
One category too small	0%	27%	22%	37%
Two or more categories too small	0%	13%	17%	6%
One category too large	2%	16%	15%	18%
Two or more categories too large	17%	6%	9%	0%

Table 6.5: Summary of hail category forecasts for HAILCAST from 1983-1985.

Percentage Hits	Mean 1983-1985
All days	**64.7**
Within 1 category all days	**82.0**
Within 2 categories all days	**92.3**

Table 6.6: Summary of mean absolute hail diameter errors (cm) for HAILCAST from 1983-1985.

	1983-1985	1983	1984	1985
All days	**0.63**	0.57	0.72	0.63
No-hail days	**0.26**	0.21	0.31	0.25
All hail days	**1.00**	0.92	1.13	1.00
Non-severe hail days	**0.76**	0.74	0.89	0.65
Severe hail days	**1.27**	1.10	1.37	1.35

Table 6.7: Summary of forecast skill scores for HAILCAST, SkyWatch and RAM from 1983-1985.

	HAILCAST	SkyWatch	RAM
Hail Forecasts			
POD	0.85	0.84	0.90
FAR	0.26	0.29	0.33
HSS	0.64	0.62	0.56
BIAS	1.16	1.16	1.39
Severe Hail Forecasts			
POD	0.89	0.32	0.62
FAR	0.40	0.39	0.45
HSS	0.67	0.40	0.54
BIAS	1.50	0.53	1.15

Table 6.8: Forecast hail category evaluation for no-hail days for HAILCAST, SkyWatch and RAM from 1983-1985.

Forecast Size Category	HAILCAST	SkyWatch	RAM
Correct	81%	81.5%	71%
Within one size category	83%	88%	81.5%
One category too small	0%	0%	0%
Two or more categories too small	0%	0%	0%
One category too large	2%	6.5%	10.5%
Two or more categories too large	17%	12%	18.5%

Table 6.9: Forecast hail category evaluation for all hail days for HAILCAST, SkyWatch and RAM from 1983-1985.

Forecast Size Category	HAILCAST	SkyWatch	RAM
Correct	38%	19%	28%
Within one size category	81%	61%	74%
One category too small	27%	32%	29%
Two or more categories too small	13%	39%	23%
One category too large	16%	10%	17%
Two or more categories too large	6%	0%	3%

Table 6.10: Forecast hail category evaluation for non-severe hail days for HAILCAST, SkyWatch and RAM from 1983-1985.

Forecast Size Category	HAILCAST	SkyWatch	RAM
Correct	37%	21%	27%
Within one size category	74%	72%	77%
One category too small	22%	38%	27%
Two or more categories too small	17%	28%	21%
One category too large	15%	13%	23%
Two or more categories too large	9%	0%	2%

Table 6.11: Forecast hail category evaluation for severe hail days for HAILCAST, SkyWatch and RAM from 1983-1985.

Forecast Size Category	HAILCAST	SkyWatch	RAM
Correct	39%	14%	29.5%
Within one size category	94%	37%	68%
One category too small	37%	53%	34.5%
Two or more categories too small	6%	29%	28%
One category too large	18%	4%	4%
Two or more categories too large	0%	0%	4%

Table 6.12: Summary of hail category forecasts for HAILCAST, SkyWatch and RAM from 1983-1985.

Percentage Hits	HAILCAST	SkyWatch	RAM
All days	64.7	56.7	54.0
Within 1 category all days	82.0	76.7	77.7
Within 2 categories all days	92.3	91.2	94.3

Table 6.13: Mean maximum surface temperature, dew-point and CAPE observed at Penhold for severe hail days from 1983-1985.

Year	T (°C)	Td (°C)	CAPE (Jkg^{-1})
1983	23.5	12.6	1542.7
1984	23.0	10.8	1264.4
1985	20.5	9.2	733.9
1983-1985	**22.3**	**10.9**	**1180.3**

Table 6.14: Forecast maximum hail size and upper-air conditions over the AHP area for 19 days when HAILCAST forecast hail and none was observed. UAR denotes upper-air ridge.

Date	Forecast Diameter (cm)	Upper-air (500 hPa) circulation pattern at 1800 LDT	Observed Convection
830704	2.0	UAR	No significant convection
830718	0.8	UAR	No significant convection
830723	1.5	UAR	No significant convection
830809	1.3	UAR	No convection
840623	0.4	UAR	TCU, showers
840627	2.1	UAR	No significant convection
840702	0.9	UAR	TCU
840707	0.4	UAR	TCU, CU
840708	0.9	UAR	TCU, CU
840709	1.2	UAR	Thunderstorms in SE portion of project area
850625	0.3	UAR	TCU
840710	2.6	UAR	TCU
840715	1.2	UAR	No significant convection
840807	1.3	UAR	TCU, CU
840809	0.4	Upper-air trough over S British Columbia	Thunderstorms over foothills
850701	2.1	Weak upper-air perturbation	Thunderstorms over foothills
850729	1.3	UAR	TCU over foothills
850801	3.1	UAR	TCU over foothills
850810	1.6	UAR	No significant convection